THERMAL MODELING OF
EVACUATED TUBULAR SOLAR COLLECTORS

by

ANN LUCILLE BARRETT

A thesis submitted in partial fulfillment of the
requirements for the degree of

MASTER OF SCIENCE

(Mechanical Engineering)

at the

UNIVERSITY OF WISCONSIN - MADISON

1987

THERMAL MODELING OF
EVACUATED TUBULAR SOLAR COLLECTORS

by Ann L. Barrett

Under the supervision of Professors W. A. Beckman and J. A. Duffie

This thesis discusses the simulation of evacuated tubular solar collectors (ETCs) for liquid heating. The application of traditional collector models and parameters for ETC modeling is studied. Specifically, four parameters are examined: collector capacitance, optical efficiency, thermal loss coefficients, and incidence angle modifiers. Each of these parameters is significantly different for ETCs than for flat plate collectors due to the geometry (including that of back reflectors), heat loss characteristics, and large volume of working fluid. The influence of these parameters on simulation results is studied through the use of TRNSYS. Measured data from two large ETC systems are used as inputs and for comparison of predicted and measured results. The systems modeled were at the Cherokee Indian Hospital, NC, and the Gainesville Job Corps Center, FL, both sites from the Solar in Federal Buildings Demonstration Program. From the behavior of the two systems studied, it is shown that it is necessary to include thermal capacitance in the collector model in order to reproduce experimental results. It is also shown that for these two collectors, the dependence of performance on the incidence angle of beam radiation is much less than that predicted by laboratory tests. Furthermore, it is shown that the collector parameters $F_R(\tau\alpha)_n$ and $F_R U_L$ as determined from the ASHRAE test are adequate as simulation input for ETCs modeled in this study. A brief economic comparison of ETCs to flat plate collectors is also given.

Acknowledgements

I'd like to take this opportunity to thank the many people whose assistance and support over the last 17 months have made this thesis possible. Foremost, my appreciation goes to my advisors Professors Jack Duffie and Bill Beckman. These two men were the reason I came to the University of Wisconsin and it has been an honor to work under them.

The financial assistance for this project was provided by the Department of Energy through a grant from ETEC. I'd like to thank them for their support and also for supplying the data which made this project possible.

I'd also like to thank my fellow graduate students who have made the Solar Energy Lab such a great place to study. Special thanks go to Freddie, who helped so much with my adjustment to Madison; Jim, who was always willing to answer questions and give advise; Dawne, for her help proofing this thesis and for joining me in so many distractions from work; Steve, for his good humor and all of his technical help; and Byron, who shared the frustrations of thesis preparation and job searching. I'm very glad I had the opportunity to work with such a special group of people as the Solar Lab staff and I'd like to say to all of them, "Thanks, good luck, and please keep in touch".

Special thanks also go to Mitch, the man who came into my life during all of this. His love and support have given me the motivation I needed these past few months. It's not possible to express here how much his help has meant to me, I can only hope he realizes.

And finally, I'd like to express my appreciation to my family who have been a constant source of support throughout this project. It has been only recently that I've realized that growing up has little to do with independence from them, but rather means learning to better accept and return their love, respect, and support.

Table of Contents

List of Figures

List of Tables

Nomenclature Listing

A_c - collector area (ft^2)

A_n - collector area of one node (ft^2)

b - intercept of a line from linear regression

b_o - constant in incidence angle modifier relationship

Btu - British thermal unit, measure of energy

C_A - cost of a solar heating system per unit of collector area ($/$ft^2$)

C_E - area independent cost of a solar heating system ($)

C_F - cost of energy from fuel ($/Btu)

C_p - specific heat (Btu/lbm F)

C_S - total cost of a solar heating system ($)

CAP_n - capacity of a collector node (Btu/ft^2 F)

CAP_{eff} - effective capacity of a collector (Btu/ft^2 F)

CAP_{emp} - capacity of an empty collector (Btu/ft^2 F)

d - market discount rate (%)

F - degrees Fahrenheit, measure of temperature

F - solar fraction, percentage of solar contribution to total load (%)

F' - collector efficiency factor (%)

F_R - collector heat removal factor (%)

i_f - fuel inflation rate (%)

I - total radiation incident on the horizontal surface (Btu/ft^2 hr)

I_b - beam radiation incident on the horizontal surface (Btu/ft^2 hr)

I_d - diffuse radiation incident on the horizontal surface (Btu/ft^2 hr)

I_o - extraterrestrial radiation (Btu/ft^2 hr)

I_t - total radiation incident on the tilted surface (Btu/ft^2 hr)

G_{sc} - solar constant (Btu/ft^2 hr)

K_T - clearness index (%)

kwh - kilowatt-hour, unit of power

$K_{\tau\alpha}$ - incidence angle modifier

L - total load (Btu)

LCS - life cycle savings ($)

m - slope of a line from linear regression

$\dot{m}$ - mass flow rate (lb$\dot{m}$/hr)

M_s - ratio of first year miscellaneous costs to initial investment for a system

n - number of nodes, number of observations, or day of year

N - number of years for an economic analysis

p - number of independent parameters

Q_u - rate of useful energy gain (Btu/hr)

Q - total energy (Btu)

R - ratio of total radiation on tilted surface to that on the horizontal surface

R^2 - measure of quality of fit of a regression

RS - ratio of resale value at the end of an analysis to the initial investment

R_d - ratio of tilted surface diffuse radiation to that on the horizontal surface

R_b - ratio of tilted surface beam radiation to that on the horizontal surface

S - total absorbed solar radiation (Btu/ft^2 hr)

SR - sum of residuals

T_a - ambient temperature (deg F)

T_i - collector inlet temperature (deg F)

T_o - collector outlet temperature (deg F)

T_n - node temperature (deg F)

T_{env} - temperature of surroundings (deg F)

t - time (hrs)

tx - tax rate (%)

τx - effective tax rate (%)

U_L - overall loss coefficient (Btu/ft^2 F)

(UA) - overall conductance area product loss factor (Btu/F)

$(UA)_n$ - overall conductance area product loss factor for a segment (Btu/F)

$y(i)$ - actual value of a data point

y - predicted value of a data point

$\bar{y}$ - average value value of all data points

β - slope of collector from the horizontal

γ - surface azimuth angle

γ_s - solar azimuth angle

δ - angle of solar declination

η - efficiency (%)

Θ - angle of incidence of beam radiation on the tilted surface

Θ_l - longitudinal angle of incidence of beam radiation on the tilted surface

Θ_t - transversal angle of incidence of beam radiation on the tilted surface

Θ_z - angle of incidence of beam radiation on the horizontal surface

ρ - ground reflectance

σ - standard deviation

$(\tau\alpha)$ - transmittance absorptance product

ϕ - latitude

ω - solar hour angle

CHAPTER I

Introduction

Evacuated tubular solar collectors (ETCs) are devices for converting solar radiation into useful thermal energy in the form of heated water. These collectors have a more complicated geometry than the common flat-plate collector and are designed to operate at higher average thermal conversion efficiencies. ETCs can thus deliver more energy per unit collector area and can achieve greater fluid outlet temperatures. Because of their tubular configuration and large volume of working fluid, they are more expensive to manufacture and presumably more difficult to model. A description of ETCs and the objectives of this thesis will be presented in this chapter.

I.1 ETC Configuration

Evacuated tubular solar collectors are designed to achieve high collector efficiencies by a significant reduction of thermal losses. As a result, they can deliver greater amounts of useful energy per unit area than flat-plate collectors over a day and are more practical for applications where high outlet temperatures (say above 200 deg F) are desired. The relatively high heat loss coefficient of flat-plate collectors is largely due to convection and conduction of heat from the absorber surface through the air gap and cover to the atmosphere.

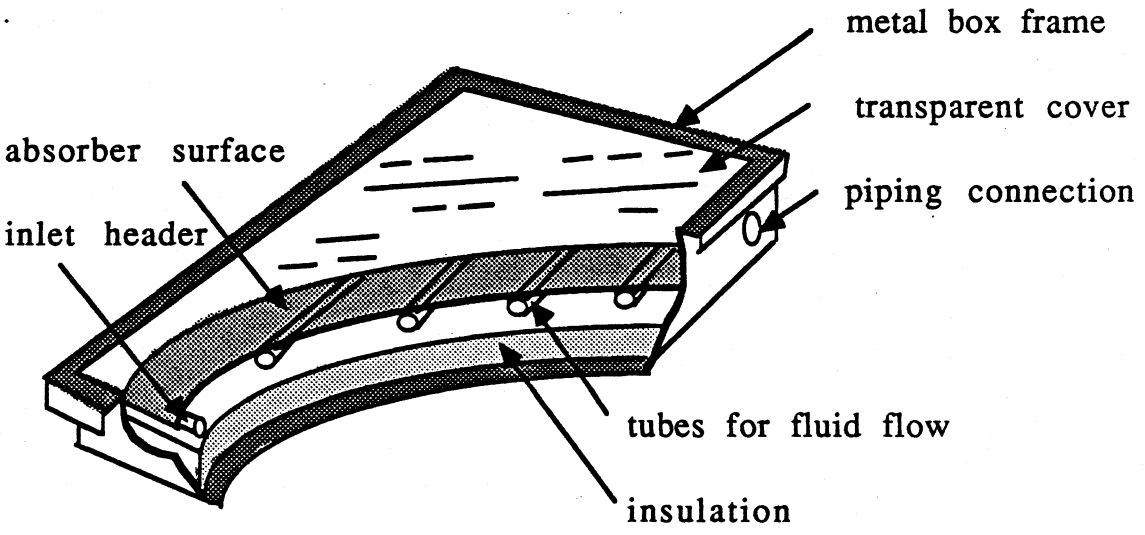

Figure I.1: Typical liquid heating flat-plate collector (from Reference [1]).

The overall heat loss coefficient can be reduced by evacuation of the air gap between the absorber and the cover, thus eliminating convective losses and greatly reducing conduction through this space. Radiation losses can be reduced as well by the use of a selective surface (a surface having high solar absorptance and low long-wave emittance) to coat the absorber. Attempts have been made to evacuate flat-plate collectors but there has been no promise of commercial success due to the large forces exerted on the flat surface. The natural configuration for evacuated collectors is the glass tube which can be made to be very sturdy.

There are a number of ETC designs available, an example being the Owens Illinois (O-I) SUNPACK model shown below which is referred to as a Dewar type collector.

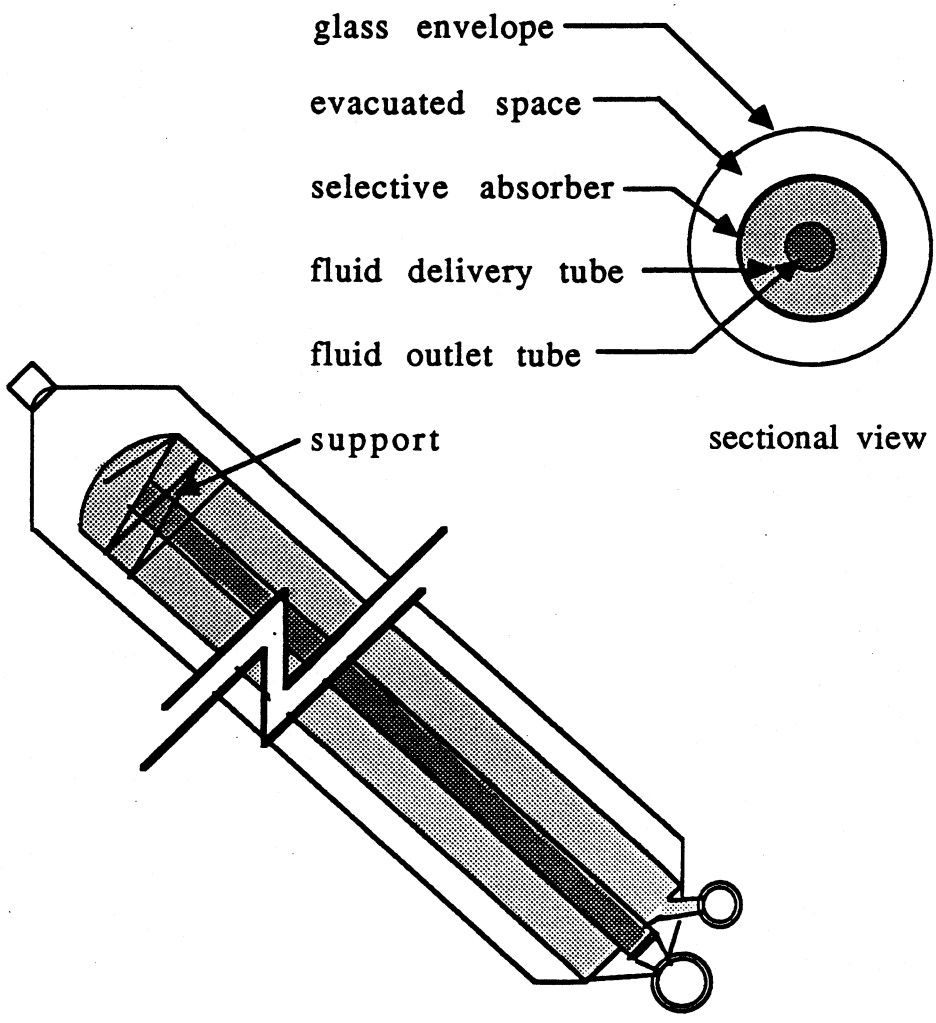

Figure I.2: Owens Illinois SUNPACK ETC (from Reference [2]).

Another common design consists of a single pass fluid tube with a thin fin shaped absorber surface that extends into the vacuum space. Examples of alternate configurations are shown in Figure I.3. There are a number of other configurations available, including a collector which resembles a narrow flat-plate which is backed with copper tubing and encased in the glass tube. All of the designs incorporate the

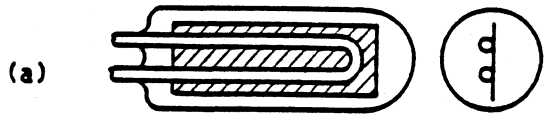

Metal Fin in Vacuum with U-Tube

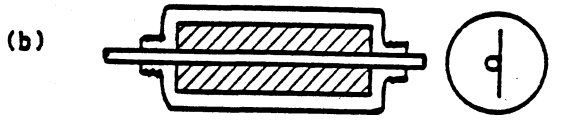

Metal Fin in Vacuum with Straight Through Tube

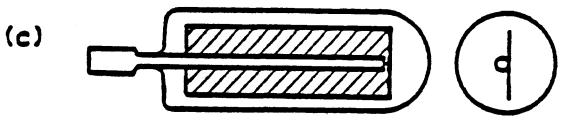

Metal Fin in Vacuum with Heat Pipe

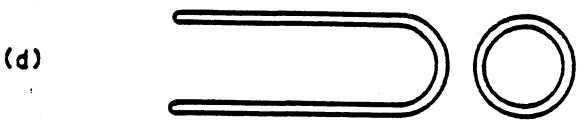

Dewar Flask Construction

Dewar Flask with Metal-in-Vacuum Absorber

Figure I.3: Different configurations of evacuated tubular collectors (Reference [2]).

same principal; a working fluid is in contact with an absorber which is coated with a selective surface and surrounded by a vacuum.

An ETC panel is made up of a parallel or series combination of typically eight to sixteen tubes. The individual tubes are mounted parallel to each other and are joined by a delivery and return pipe for the working fluid. It is common practice to back each tube with a cusp or parabolic reflector to improve the optical efficiency. The collector panels, commonly about 18 ft^2 in gross area, are then connected in parallel to make up the solar array.

I.2 Literature Survey of ETC Studies

Early analysis of ETCs was presented by Speyer in 1965 (Reference [3]). In this paper, the author gives an overview of tubular collector design and stresses the importance of evacuation to minimize thermal losses. Speyer also gives analysis of collector efficiency and comments on temperature dependent loss factors. Although it is outdated, a thorough economic analysis is given.

Further studies of the optical properties of ETCs are presented by McIntire, Reed, and Rabl. McIntire and Reed (References [4], [5], and [6]) present an analysis of biaxial incidence angles which is tthe basis for the discusion in Section III.4.3. Rabl (References [1] and [7]) gives further analysis of ETC optical properties and a discussion of various reflectors available. Ongoing research is being done by Winston, Snail, and O'Gallager in the area of compound concentrating collectors for ETCs. Their studies can be found in References [8], [9], and [10].

A comprehensive study of ETCs was recently completed by the Task VI group

of the International Energy Agency (IEA). The objective of this study was to "further the understanding of evacuated collectors in solar heating, cooling, and hot water systems, and to study, document and compare the performance characteristics of such collectors in different systems and climates" (Reference [11]). The project consisted of analysis of twelve ETC systems used for a variety of applications in ten different countries.

In a detailed IEA report about collector subsystem modeling (Reference [12]), many of the collector parameters which are studied in this thesis were discussed. The IEA states that collector capacitance has a significant effect on the performance of large systems, even for drain back collectors. They also state that the heat loss factor, U_L, should not be considered a constant because of the domination of radiative losses which are highly dependent on temperature. As a results from their study, they conclude that the efficiency curve for ETCs (refer to Section III.4.1) is not well characterized by a straight line. This IEA report also addresses biaxial incidence angle modification. For their analysis, incidence angle modifiers are calculated from data using a procedure similar to that given in Section III.4.5. They also discuss the complexity involved with determining modifiers for diffuse radiation and suggest the approximation of no modification. They also stress that angular dependency varies greatly between systems and that it is difficult to determine general incidence angle modifier curves.

Another IEA Task VI report (Reference [2]) contains results of complete thermal performance measurements over a four year period from all of the systems studies. Detailed information is presented about each of the system components, controls, loads, climate, installations, operation, maintenance, and longevity. In summarizing this report, the IEA states that "ETCs significantly outperformed flat-

plate collectors in every test except the lowest temperature applications." They cited that ETC systems achieved thermal conversion efficiencies of up to 50% which justifies their higher cost. The IEA also asserts that ETC reliability "proved to be excellent, especially considering the relative newness of the technology". Additionally, the ETCs studied needed little maintenance and vacuum loss and breakage were insignificant. The report also stressed that poor system design can negate the high performance of ETCs and cited faulty design or construction problems for the Task VI systems which performed below design expectations.

I.3 Systems Studied

Two large ETC systems (with collector areas over 4,000 square feet) are analyzed in this thesis. One installation is located in Cherokee, North Carolina and provides energy for water and space heating at the Cherokee Indian Hospital. The other system is at the Gainesville Job Corp Center in Florida and is used for water heating and space cooling.

Both were built as part of the Solar in Federal Buildings Demonstration Program (SFBP) which was initiated by congress in 1979 and resulted in the construction of over 700 solar projects across the country. The program's objective was to stimulate growth and improve the efficiency of the solar industry through the demonstrated use of a variety of economical solar systems on federal buildings. The program was administered by the Department of Energy (DOE) with support from the Energy Technology Engineering Center (ETEC) of Rockwell International. ETEC's activities included site surveys, design reviews, acceptance testing, long term monitoring, and redesign when needed.

Eight SFBP systems where chosen to be quality monitoring sites and were extensively instrumented with equipment from the National Solar Data Network (NSDN). The NSDN program was initiated earlier by DOE to monitor various solar energy systems, evaluate performance, and improve the understanding of the technology. The Vitro Corporation of Silver Springs, MD was responsible for the collection and analysis of NSDN data. Data were collected at each site for periods of four months to a year and was used to evaluate the SFBP systems' performance and design. The data were also intended to aid the continued DOE research and development efforts in solar heating.

I.4 Objectives of Study

The objective of this study is to develop an analytical ETC model which accurately predicts collector array performance. Actual data from the Cherokee and Gainesville systems is used as simulation input and to compare predicted results to measured performance. The TRNSYS (TRaNsient SYStem) (Reference [13]) simulation program, which is described in Chapter III, is used and the traditional TRNSYS solar collector model is revised to improve the modeling of ETCs. The first question which is addressed is how well do conventional simulations, using only manufacturer's collector parameters and incidence angle modifiers and no adjustments for unique ETC properties such as high capacitance, predict collector performance. Then, the sensitivity of the ETC model predictions to various parameters is studied. Finally, conclusions are drawn about ETC modeling and generalizations are made about collector design and operations form the study and simulation of the Cherokee and Gainesville systems.

CHAPTER II

Experimental Data

The TRNSYS evacuated tubular collector simulations used in this study are all driven with measured data for ambient and inlet fluid conditions. This chapter describes the collection of the NSDN data, the data available for both the Cherokee and Gainesville systems, its quality, and the problems associated with using real data as simulation input.

II.1 NSDN Data

Each of the SFBP quality sites was extensively instrumented to measure quantities such as temperatures and flow rates throughout the solar and auxiliary energy systems. Sensor locations are shown in each of the system schematics, Figures IV.1 and V.1. All of the site sensors, approximately 64 channels, were read automatically at 5 minute and 20 second intervals by the Site Data Acquisition System (SDAS). The values were converted into digital signals and recorded with the corresponding site number, date, and time. The data were then transmitted over a telephone modem to the Central Data Processing System (CDPS) which was located at Vitro. The CDPS converted the digital information into engineering units and stored it for further processing. Once enough data had been collected, the values were analyzed using site specific equations. The energy flows throughout the

system were analyzed and various performance factors were calculated on an hourly, daily, and monthly basis.

The Vitro data for the SFBP quality sites was saved on magnetic tapes and is now available for ongoing DOE research. The Cherokee and Gainesville tapes were sent to the University of Wisconsin where the information was read and converted to ASCII format. Data records, including the date, time and desired sensor values, were stored for each 5 1/3 minute intervals over the monitoring period. Six months of data is available for the Cherokee system and nine months is recorded for the Gainesville system.

All of the sensors used for data aquisistion were calibrated before the monitoring period, however there is still uncertainty associated with the measured energy flows. Manufacturers' error values used for estimating measurement accuracy are shown below.

pyranometer	+/- 2.5% (Btu/ft^2 hr)
flow meter	+/- 3.0% (gal/min)
temperature sensor	+/- 0.8% (degrees F)

Assuming the above individual errors are uncorrelated, the total expected uncertainty in a given measured energy flow is defined as:

$$\text{uncertainty} = \left[\sum_{i}^{N} \left(\frac{\partial E}{\partial x_i} \Delta x_i \right)^2 \right]^{1/2} \qquad \text{(II.1.1)}$$

where

x_i = the i^{th} term in the equation E

Δx_i = error in each term of the energy equation

E = the equation for the energy flow rate

$\frac{\partial E}{\partial x_i}$ = sensativity of energy calculation to measurement

N = number of terms

For example, the accuracy of the measured collected solar energy is 4 % since the combined error of the flow meter and two temperature sensors is involved.

II.2 Missing Data

A number of data records for the individual time steps were missing on both of the system tapes. This presented a problem when using the data to drive simulations because TRNSYS requires that input values be supplied at constant intervals throughout the simulation period. Overall, approximately 12% of the Cherokee and 5% of the Gainesville data were not available. Many of the longer gaps, i.e. 5 hrs to 3 days in length, were documented in the Vitro monitoring reports as missing for such reasons as maintenance or system failure. There were also many shorter data gaps, usually ranging from one to ten time steps. This happened regularly at about 7 a.m. when data was transmitted to the CDPS, but occurred at many unexpected times as well. One possible explanation was a failure of the SDAS which had to be manually restarted and was not consistently monitored. After screening the data with a program written to list intervals between recording, it was found that most of the gaps were either less than an hour or greater than three hours in length. The shorter gaps were filled with new records using interpolated values for each of the sensors. Days with longer gaps were considered

unsuitable for use as simulation input. While screening the data, an unexpected problem with repeated recordings was also found. On a few occasions, records for a single time step were listed as many as 30 times. These extra recordings were simply hand deleted from the data files.

II.3 Quality of Data

After working with the data gaps, all of the Cherokee and Gainesville simulation input data were plotted and visually screened to look for any obvious problems with the sensor values and also to look at the weather conditions over any given period. Many miscellaneous problems were found including sensor failures which were obvious when a reading would suddenly change from a reasonable value to zero for a number of time steps. Some of the individual sensor failures were documented in the Vitro reports, but others were unexpected. Another problem that appeared occasionally was a malfunction of the internal clock. For example, this was apparent on a day when the peak radiation occurred at 7:00 a.m. Data from days with errors such as these were not used for simulation.

Another problem that was made apparent while screening data was a malfunction of the collector on/off controls. Both of the systems operated using a differential temperature controller which monitored the collector fluid temperature and the temperature at the bottom of the storage tank. This controller was to start collector operation when the collector was 20 F warmer than the storage and shut off the system when the two reached a 5 degree difference. The controller occasionally failed in both of the systems. For instance, there were many clear days when the collector fluid temperature was rising significantly and the collector pump failed to

engage. There were also occasions when the pump did not turn off and continued to operate through the night. Even though these problems were not related to data collection, days with controllers errors were not used for simulation.

After all of the data was screened, six two week periods were chosen as simulation input for each of the two systems. Longer simulations were not feasible because of the various problems noted above. Single days, representative of various weather conditions, were also chosen to more closely examine the system and model behavior. Simulation results from these periods will be referred to throughout this thesis.

CHAPTER III
ETC Simulation and Component Models

Computer simulations are useful tools for design and analysis of solar energy systems. This chapter describes the modular simulation program TRNSYS and the component models used to simulate evacuated tubular collector performance.

III.1 The Simulation Program

The transient system simulation program, TRNSYS, is a versatile modular program which can be adapted to an unlimited number of energy system configurations. The program was originally developed to analyze solar systems, but can be used to model HVAC and power plant systems as well.

One of the advantages of TRNSYS is its modularity. The program is made up of a number of subroutines, referred to as 'types', each of which model the transient thermal behavior of a specific system component. For example, the Type 1 routine models a solar array and the Type 4 routine is used to describe storage tank behavior. TRNSYS also allows the user to add new or modify existing components, as needed.

The subroutines are joined to model a given system through a main execution program which performs the simulation. The main program operates from a 'deck'

which is a computer file where the user defines the system and supplies other needed information such as iteration tolerances or the desired length of the simulation. In the deck, each component is defined by it's parameters, inputs, and outputs. The execution program passes the necessary information, such as flow rates, control signals, or temperatures, between the specific components.

The simulation is driven by forcing functions which usually include meteorological information read from a weather data file. Other forcing functions can be user supplied data files or internally generated time dependent functions. This input is supplied at a predetermined time interval which can range from a few seconds to hours. At each time step, TRNSYS uses the inputs and parameters for each component and solves the set of governing system equations by successive substitution. The resulting outputs are the inputs for the next time step, e.g. the temperature out of a pipe may be the next input into the solar collector. This solution process is ongoing over a user defined simulation period. The results can be presented in a variety of fashions as specified in the simulation deck.

III.2 Configuration of TRNSYS Components for Collector Simulation

The TRNSYS program was used in this study to simulate ETC array performance. A simplified schematic of the collector subsystem represented by its TRNSYS components is shown below. The arrows indicate the flow of information which occurs during simulation.

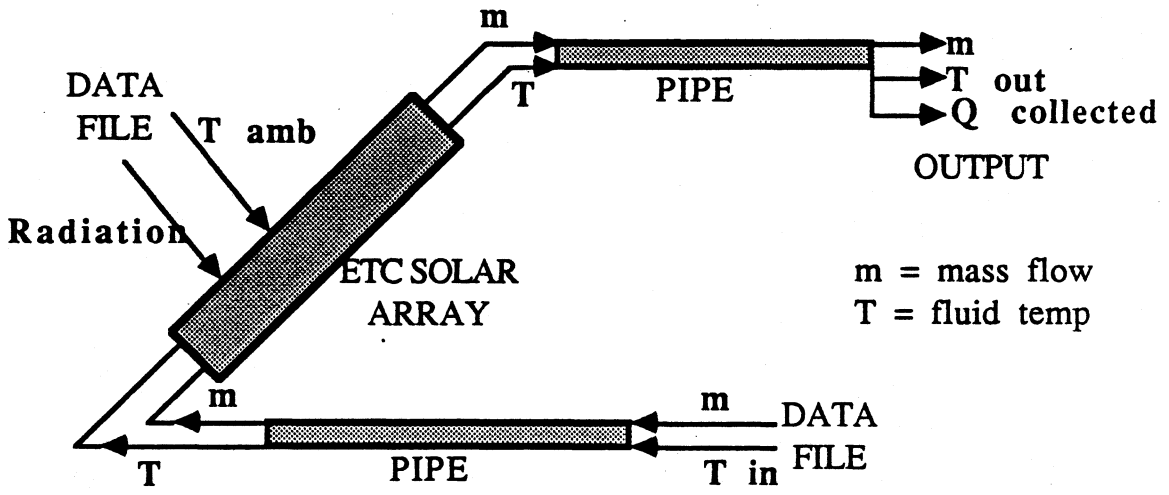

Figure III.1: Simplified collector simulation schematic.

Other components included in the simulation deck were the algebra converter (for unit conversion) and a radiation processor. Each component is defined by a set of parameters shown in the deck listings in Appendices E and F. The input values (ambient temperature, radiation, flow rate, and fluid inlet temperature) are all supplied at 5 1/3 minute intervals from the system data files.

III.3 **Radiation Data**

Radiation data for most of the NSDN sites, including Cherokee and Gainesville, are measured on the tilted collector surface. This value is used as a collector input, but a diffuse radiation component is needed as well. The diffuse value and several other useful quantities are calculated by a TRNSYS subroutine called the solar radiation processor. This processor also calculates needed angles

describing the position of the sun and can estimate insolation on as many as four surfaces of either fixed or variable orientation. The subroutine can also interpolate radiation data if needed, using a non-linear interpolation. One of the inputs required by the radiation processor is the value for horizontal surface radiation which was not measured at the sites studied. This problem was overcome by writing a new TRNSYS component to calculate the horizontal surface radiation from the tilted surface value.

The horizontal surface radiation is calculated using the following relationships. First, the extraterrestrial radiation value is calculated in Btu/ft^2 time step:

$$I_o = \frac{1.067\, G_{sc}}{\pi}\left[1+0.033\cos\left(\frac{360\, n}{365}\right)\right]$$
$$x\left[\cos(\delta)\cos(\phi)\cos(\omega_2-\omega_1)+\frac{2\pi}{360}(\omega_2-\omega_1)\sin(\phi)\sin(\delta)\right] \quad \text{(III.3.1)}$$

where:

G_{sc} = solar constant

n = day of the year

ϕ = latitude

δ = solar declination angle

ω_1 = hour angle at beginning of time step

ω_2 = hour angle at the end of the time step

The radiation value is calculated per 5 1/3 minute time step throughout this calculation procedure, the customary hourly value is not used. Next, an estimate is made for the ratio of tilted surface radiation to the horizontal surface radiation.

$$R = \frac{I_t}{I} \approx R_b = \frac{\cos(\theta)}{\cos(\theta_z)} \qquad \text{(III.3.2)}$$

where:

I_t = total radiation incident on the tilted surface

I = total radiation incident on the horizontal surface

R_b = ratio of beam radiation on the tilted surface to the horizontal beam radiation

Θ = angle of incidence of beam radiation on tilted surface

Θ_z = angle of incidence on the horizontal surface

The angle of incidence is defined as:

$$\begin{aligned}\Theta = &\sin\delta \sin\phi \cos\beta - \sin\delta \cos\phi \cos\gamma \\ &+ \cos\delta \cos\phi \cos\beta \cos\omega \\ &+ \cos\delta \sin\phi \sin\beta \cos\gamma \cos\omega \\ &+ \cos\delta \sin\beta \sin\gamma \sin\omega \end{aligned} \qquad \text{(III.3.3)}$$

where:

γ = surface azimuth angle

β = slope of tilted surface

The assumption that R is approximated by R_b is best on clear days because it

assumes that the diffuse radiation is concentrated from an apparent origin near the sun. The full relationship for R is:

$$R = \frac{I_b}{I} R_b + \frac{I_d}{I} R_d \qquad \text{(III.3.4)}$$

where:

I_d = diffuse component of radiation

I_b = beam component of radiation

R_d = ratio of diffuse radiation of tilted surface to the horizontal diffuse radiation

but equation III.3.2 is useful as a first approximation. With this estimate, I_h and the corresponding clearness index, K_T, are calculated as

$$I = I_t / R_b \qquad \text{(III.3.5)}$$

$$K_T = I / I_o \qquad \text{(III.3.6)}$$

From the value of K_T, the estimate of I_h is distributed into its beam and diffuse components using the Erbs correlation:

$$\begin{aligned} I_d / I &= 1.0 - .09\, K_T && K_T < 0.22 \\ I_d / I &= .951 - 0.160\, K_T + 4.38\, K_T^2 && 0.22 < K_T < 0.80 \\ I_d / I &= 0.165 && K_T > 0.80 \end{aligned} \qquad \text{(III.3.7)}$$

and

$$I_b = I - I_d \tag{III.3.8}$$

With these values, a resulting I_t is calculated using the relation:

$$I_t = I_b R_b + I_d\left(1 + \frac{\cos\beta}{2}\right) + (I_t + I_b)\rho\left(1 - \frac{\cos\beta}{2}\right) \tag{III.3.9}$$

where:

ρ = ground reflectance, assumed to be 0.2

This equation assumes that the diffuse and ground reflected radiation are isentropic. The calculated value of I_t is compared to the actual values to begin an iteration process. K_t is then adjusted by an amount weighted to the error and the calculations are repeated until the new I_t agrees with the actual values within a tolerance of 5 Btu/ft^2 hr. This tolerance was chosen because it is the approximate error range of the radiation measurement. The code for the "radiation converter" subroutine is listed in Appendix A.

The I_h value which results in the correct new I_t is then used as input into the radiation processor. It should be noted that this is used only to calculate the diffuse component. The I_t calculated by the radiation processor is compared to the data as a check, but for precaution and simplicity, the actual value is used as input to the collector. The flow of radiation data is shown in Figure III.2.

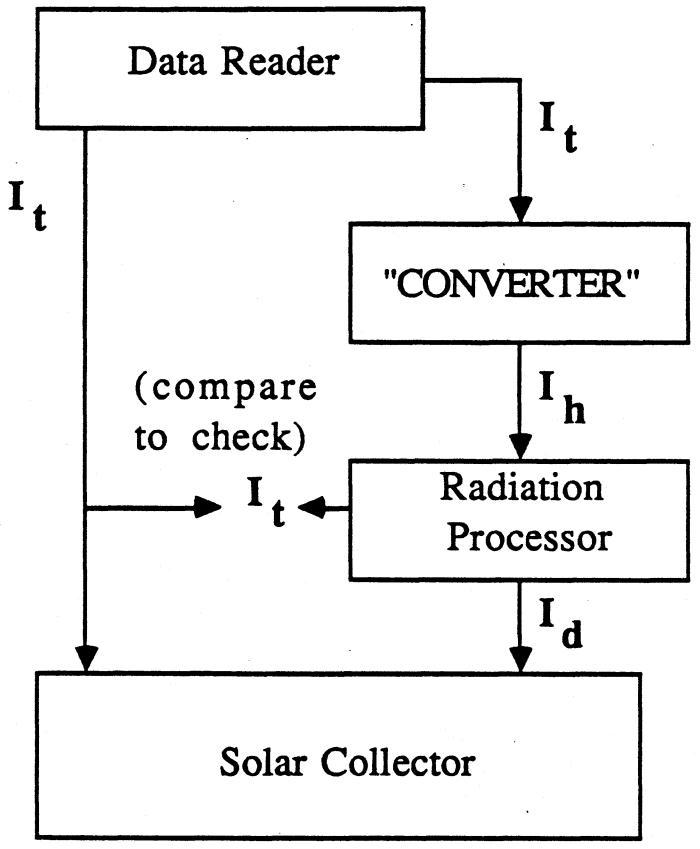

Figure III.2: Flow of radiation data using the converter component.

III.4 **Solar Collector Models**

The steady state performance of a solar collector can be expressed by the Hottel-Whillier equation:

$$\dot{Q}_u = A_c F_R \left[I_T (\tau\alpha)_n K_{\tau\alpha} - U_L (T_i - T_a) \right] \qquad \text{(III.4.1)}$$

where:

Q_u = rate of useful energy gain

A_c = collector area

F_R = collector heat removal factor, the ratio of actual useful energy gain to the maximum gain if the whole collector is at the inlet temperature

I_t = solar radiation incident on the tilted surface

$(\tau\alpha)_n$ = the transmittance absorptance product incorporating the collector optical properties at normal incidence, the ratio of the total absorbed to the incident radiation

$K_{\tau\alpha}$= incidence angle modifier, accounts for the dependence of $(\tau\alpha)$ on the angle of incidence

U_L = overall collector heat loss coefficient (per unit area)

T_i = inlet fluid temperature

T_a = ambient temperature

The useful energy gain is also given by the energy balance equation:

$$\dot{Q}_u = \dot{m} c_p (T_o - T_i) \qquad \text{(III.4.2)}$$

where:

$\dot{m}$ = mass flow rate

c_p = specific heat of the working fluid

$(T_o - T_{i)}$ = change in temperature of the working fluid

The existing collector model in TRNSYS uses these two equations, the supplied collector parameters, and the inlet and ambient conditions, to predict the total energy gain and the outlet fluid temperature. When there is no flow into the collector, a steady state stagnation temperature is found by setting Q_u equal to zero and assuming a uniform collector fluid temperature. This yields the equation:

$$T_o = \frac{S}{U_L} + T_a \qquad \text{(III.4.3)}$$

where:

$$S = I_t(\tau\alpha)_n K_{\tau\alpha}$$

The model neglects capacitance effects and assumes the steady state conditions are reached instantaneously. This assumption and the determination of the collector parameters needed for simulation are discussed in the following subsections.

III.4.1 Performance Parameters $F_R U_L$ and $F_R(\tau\alpha)_n$

Analysis of collector performance can be performed using the Hottel-Whillier equation, combing the terms F_R, U_L, and $(\tau\alpha)_n$ and substituting the definition of efficiency to obtain the following equation:

$$\eta = \frac{\dot{Q}_u}{A_c I_t} = F_R K_{\tau\alpha} (\tau\alpha)_n - F_R U_L \frac{(T_i - T_a)}{I_t} \qquad \text{(III.4.4)}$$

The variables in this equation which are not directly measurable are the performance parameters $F_R(\tau\alpha)_n$ and $F_R U_L$. These values are used to rate collectors and are determined by the standardized ASHRAE (American Society of Heating, Refrigeration and Air-conditioning Engineers) 93-77 test (Reference [14]). In this test, the collector is exposed to a measured amount of radiation at normal incidence and operated at a constant known flow rate. The temperature measurements of the ambient air and inlet and outlet fluid flows are taken at predetermined time intervals. The experimental useful energy gain is calculated using equation III.4.2 while running the test with a varying collector inlet temperature. From the values of the instantaneous rate of energy gain, collector efficiencies, η, are calculated using equation III.4.4 . These values are plotted as a function of $(T_i - T_a)/I_t$, referred to as the operating point. When the testing is done at normal incidence, the value of $K_{\tau\alpha}$ is unity. If F_R, U_L, and $(\tau\alpha)_n$ were constants, it is clear that plots of η vs. $(T_i - T_a)/I_t$ would form a straight line with the intercept $F_R(\tau\alpha)_n$ and the slope - $F_R U_L$. These values, however, are not strictly constant and some scattering of the data is expected. For instance, U_L is a function of temperature and F_R is a weak function of U_L. In spite of these difficulties, long term collector performance can be characterized by the collector parameters as defined by the line which best fits the efficiency vs. operating point test data.

In general, ETC test curves have a lower intercept and flatter slope than do curves for flat plate collectors. For instance, the reported performance parameter values for the SUNPACK ETC system in operation in Gainesville are $F_R(\tau\alpha)_n$ =

0.57 and $F_R U_L$ = 0.21 Btu/ft^2 deg F. A typical flat plate collector might have the values of 0.75 and 0.70 for the intercept and slope, respectively.

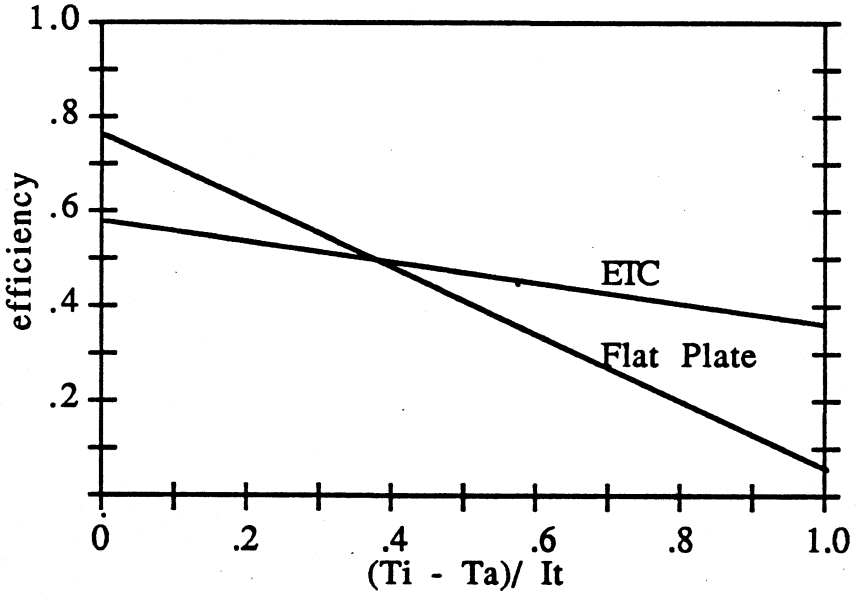

Figure III.3: Typical collector test curves.

As shown in Figure III.3, the efficiency of the flat plate collector is greater at operating points below about 0.37. Typically, however, operating points are typically scattered over the day from about 0.2 to 1.0 and therefore the ETC curve represents a greater potential for total energy collection. The performance comparison of the two collectors is discussed further in Chapter VI.

The reported ASHRAE values of the test parameters $F_R(\tau\alpha)_n$ and $F_R U_L$ are traditionally used and trusted in the design and simulation of solar collectors.

However, there is some uncertainty as to how well these parameters, calculated under controlled laboratory conditions, represent the performance of operating collectors. In the field, collectors are exposed to unpredictable environmental influences, such as a partial covering by snow or dust, which may degrade efficiency. For example, in a DOE study (Reference [15]) of 25 various solar systems from the NSDN project (ranging in size from 50 to 5,000 square feet of collector area), two-thirds of the collectors performed below design predictions. As stated earlier, the question addressed in this thesis is: 'How well do TRNSYS simulations using the ASHRAE test parameters predict the performance of the collectors studied ?' Also addressed is the sensitivity of the simulated performance to the supplied values of the test parameters.

The existing TRNSYS collector model used in this research requires that test values for $F_R(\tau\alpha)_n$ and $F_R U_L$ be supplied as collector parameters and assumes a linear behavior for the efficiency as previously described. Other parameters are required so that the model can account for deviation from test conditions. Analytical corrections are applied to the performance parameters to account for operation at flow rates other than the value used in testing, the number of collectors mounted in series, and the presence of heat exchangers (for further detail, refer to Reference [17]). The simulation program uses these corrected parameters and the input conditions to predict the collector performance.

To compare the measured versus design performance of the Cherokee and Gainesville systems, the actual values for the performance parameters were derived from the system data. Plots of the instantaneous efficiency vs. $(T_i - T_a) / I_t$ (see equation III.4.4) were generated from the actual data taken over the two week monitoring periods used for simulation. The program used to generate these points

is listed in Appendix B. Only data from time steps at near normal incidence, i.e. Θ_t < 10 degrees, were used. (refer to Figure III.12) Data was also eliminated if the collector pump had not been running continuously for the previous hour to minimize errors due to non-steady state effects. A regression analysis was performed on the points generated to find the best linear fit and thus the slope and intercept values, $F_R(\tau\alpha)_n$ and $F_R U_L$ respectively. In some cases, extraneous errors where evident when the instantaneous efficiencies were calculated. This was possibly due to sensor error or a radiation value that fluxuated considerably over the 5 1/3 minute time step. When these errors were apparent, points lying beyond three standard deviations from the predicted curve fit (which defines a 95% confidence interval) were filtered and the regression repeated.

The regression analysis used was a linear least squares fit which minimizes SR, the sum of the residuals squared.

$$SR = \sum_{i=1}^{n} \left(y_{i,\,\text{actual}} - y_{i,\,\text{fitted}}\right)^2 \qquad \text{(III.4.5)}$$

where:

n = number of observations

The resulting equations for the slope, m, and the intercept, b, are:

$$m = \frac{n\sum_{i=1}^{n} x_i y_i - \sum_{i=1}^{n} x_i \sum_{i=1}^{n} y_i}{n\sum_{i=1}^{n} x_i^2 - \sum_{i=1}^{n} (x_i)^2} \qquad \text{(III.4.6)}$$

and:

$$b = \frac{\sum_{i=1}^{n} y_i \sum_{i=1}^{n} x_i^2 - \sum_{i=1}^{n} x_i \sum_{i=1}^{n} x_i y_i}{n\sum_{i=1}^{n} x_i^2 - \sum_{i=1}^{n} (x_i)^2} \qquad \text{(III.4.7)}$$

where:

x = independent axis values, $(T_i - T_a)/I_t$

y = dependent axis variables, η

The quality of the fit is characterized by the standard deviation value σ, which is proportional to the sum of the residuals. A standard deviation of zero is thus a perfect fit.

$$\sigma = \left(\frac{SR}{n-1}\right)^{1/2} \qquad \text{(III.4.8)}$$

The fit is also characterized by the parameter R^2 which is called the coefficient of determination. This value is related to the ratio of the variance of residuals to the variance of the data and is defined as:

$$R^2 = 1 - \frac{\sum_{i=1}^{n} (y(i) - y)^2 \Big/ (n - p)}{\sum_{i=1}^{n} (y(i) - \bar{y})^2 \Big/ (n - 1)} \qquad \text{(III.4.9)}$$

where:

y(i) = actual value of data point

y = predicted value

$\bar{y}$ = average value of data points

n = number of data points

p = number of independent variables

The value of R^2 varies from 0 to 1 with 1 being a perfect fit.

Figure III.5 is an example of a calculated 'test' curve for the Cherokee data on the day of April 1. This day was chosen because of the clear weather conditions as are shown in the input data plot, Figure III.4. Performance parameter values for single days were not used in this study, but are presented here for clarity. The ASHRAE test curve for this collector, with $F_R(\tau\alpha)_n = 0.391$ and $F_R U_L = 0.224$, is shown compared to the curve obtained from the linear regression with $F_R(\tau\alpha)_n = 0.321$ and $F_R U_L = 0.057$ Btu/ft^2 F. The standard deviation for this fit is 0.012 and the R^2 parameter is 0.022. This value is so low because the mean value of y is very near the predicted curve, i.e. the slope is almost 0. This is a relatively good fit for this type of plot, but the fit parameters will have more meaning when compared to values for other fits as will be shown in later chapters.

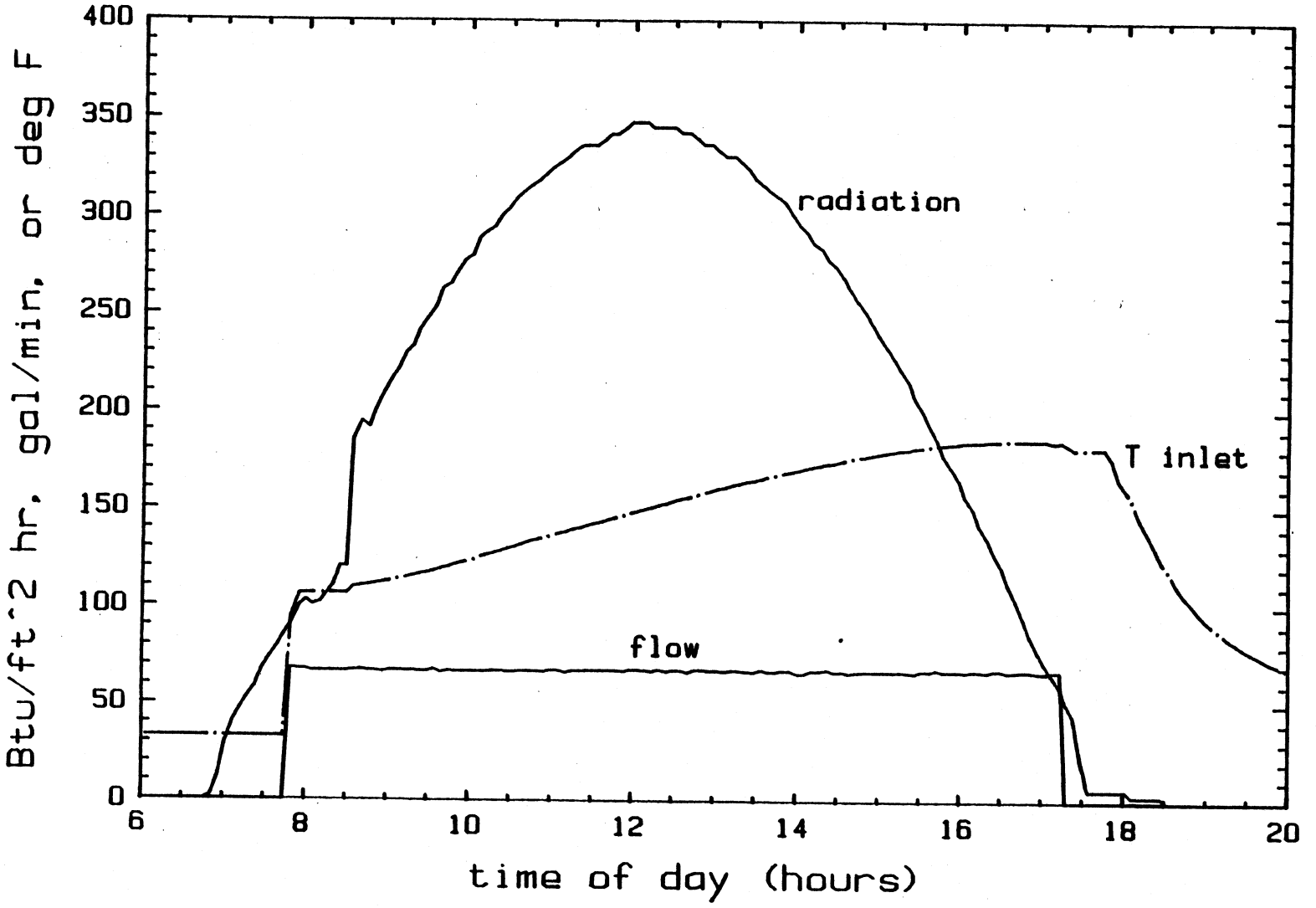

Figure III.4: TRNSYS input data for Cherokee, April 1.

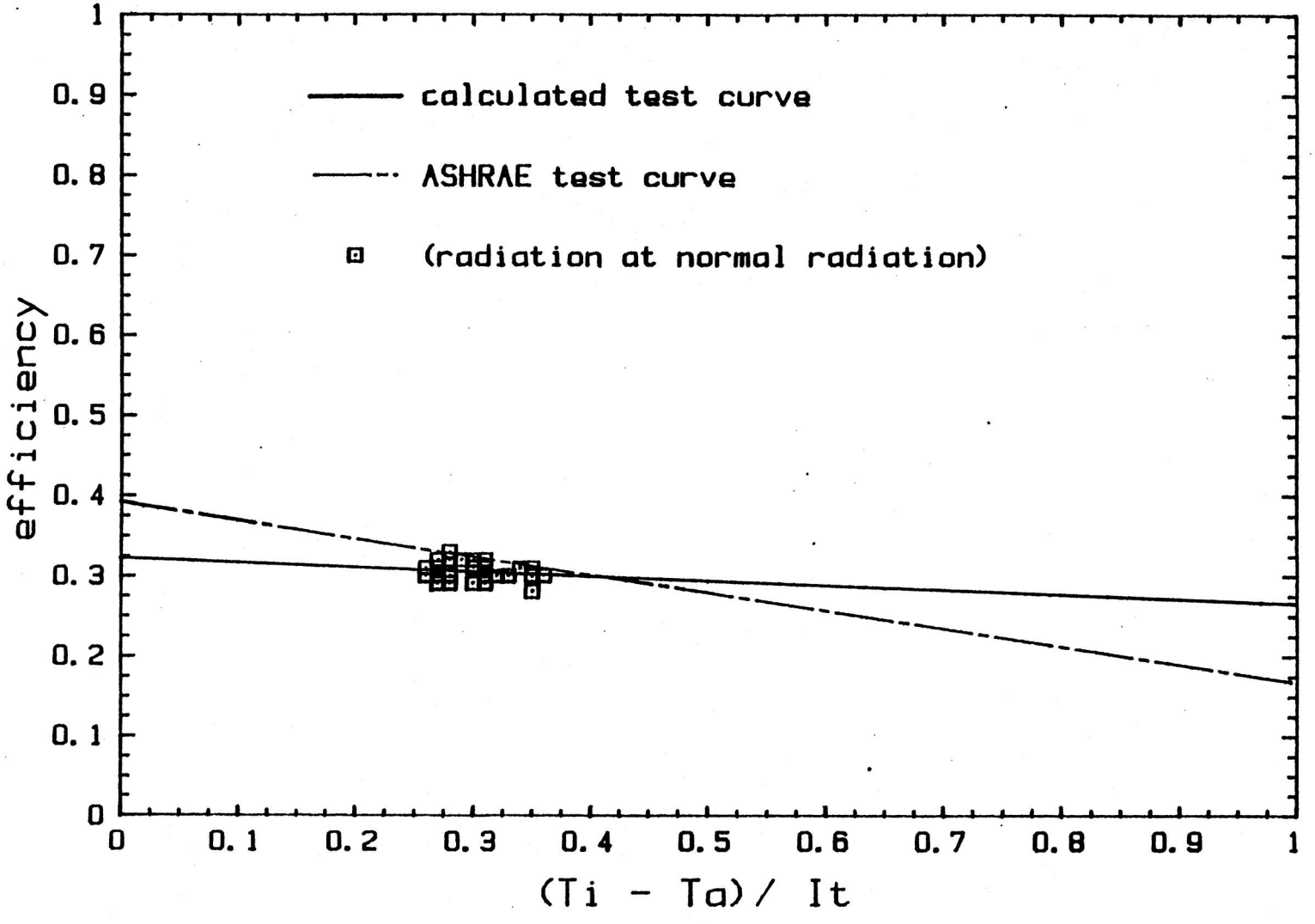

Figure III.5: Generated collector test curve for Cherokee, April 1.

Similar results generated from the two week periods of data are presented in Sections IV.3.2 and V.3.2. The monthly values of the same performance parameters calculated by the Vitro corporation are also presented for both systems and the discrepancies explained. These results and their relevance to simulation performance are discussed.

III.4.2 Collector Capacitance

Most ETCs have a significantly higher capacitance than do flat-plate collectors due to their large volume of working fluid. The SUNPACK model studied in this thesis holds about two and a half gallons of water in each collector, or about 1.5 lbs of fluid per square foot of collector area. This is about 5 times the typical value for a flat-plate collector.

The effect of this capacitance is a dampening of the system's response to changes in input. This behavior is characterized by a parameters called the time constant, τ, which is defined as the time required for a collector outlet fluid to attain .632 of the total change from its initial temperature to its ultimate steady state value after experiencing a step change in radiation or inlet temperature. Mathematically, τ is the time when the following equality if reached:

$$\frac{T_{o,\tau} - T_{in}}{T_{o,i} - T_{in}} = \frac{1}{e} = .368 \qquad \text{(III.4.10)}$$

where:

$T_{o,\tau}$ = outlet temperature at time τ

$T_{o,i}$ = outlet temperature when the step change in introduced

The value of the time constant is determined experimentally by a standard ASHRAE collector test which monitors the outlet temperature response to a step change in either radiation or inlet temperature. Typical values for a flat-plate collector time constant are on the order of 1 to 2 minutes; the reported value for the SUNPACK ETC is 21.07 minutes..

To study the effects of capacitance through simulation, the existing TRNSYS collector subroutine was modified. A new capacitance model was developed based on earlier work done by Kummer (Reference [17]). The TRNSYS subroutine FORTRAN code for this model is listed in Appendix C. The new model is a combination of a lumped parameter and a finite difference analysis. The collector is broken into a user specified number of nodes in the flow direction with each node having a fraction of the overall collector capacitance. The overall capacitance is determined by lumping the effects of the working fluid and the collector materials.

An energy balance on a single node, n, results in the following equations:

$$CAP_{eff}\frac{dT_n}{dt} = F'\left[S - U_L(T_n - T_a)\right] - \frac{\dot{m}C_p}{A_n}(T_{o,n} - T_{i,n}) \qquad \text{(III.4.11)}$$

and:

$$T_{o,n} = T_n \qquad \text{(III.4.12)}$$

where:

CAP_{eff} = effective capacitance per unit area

T_n = temperature of node

F' = collector efficiency factor

A_n = node collector area, A_c / total number of nodes

$T_{o,n}$ = fluid temperature leaving node n

$T_{i,n}$ = fluid temperature entering node n

The collector parameters in this equation are assumed to be constant. It is also assumed that the collector materials are at the same temperature as the local fluid, i.e. there is infinite heat transfer. Note that this equation uses F', the collector efficiency factor rather than the heat removal factor, F_R. This is because the nodal model approximates the temperature distribution through the collector and the node temperature rather than the inlet temperature can be used in the loss term. The two values are related by the following equations:

$$F' U_L = - \frac{\dot{m} C_p}{A_c} \ln \left(1 - \frac{F_R U_L A_c}{\dot{m} C_p} \right) \qquad \text{(III.4.13)}$$

By performing energy balances on each node, a system of coupled, first order differential equations results. These equations are solved sequentially using the solution for the average temperature of node T_n as the inlet temperature for node T_{n+1}.

The effective capacitance value needed in the equation is determined experimentally and then compared to hand calculations. This was done by

comparing the simulated ETC response to a step change in radiation to the known capacitance behavior from the time constant test. Different values for the effective capacitance were substituted into the collector model until the system responded with the appropriate time constant for a 63.2% change from initial to steady state conditions. The results of the experiment are shown in Figure III.6 and an effective capacitance of 1.7 Btu/ft^2 F was determined. This compared favorably with the value expected due to the water alone calculated as:

$$CAP = \frac{\dot{m} C_p}{A} = 1.47 \text{ Btu/ft}^2 \text{ F}$$

For this experiment and all of the simulations run using the capacitance model, a 50 node collector and 5 1/3 minute time step was used. For more information on appropriate time steps and nodes numbers, refer to Kummer (Reference [17]).

Also included in the new model were the effects of filling and draining. This is needed to simulate the Cherokee collector system which has a drain back feature. Each night, the collector fluid is drained into a storage tank to prevent overnight heat loss and also as a freeze protection measure. When collector operation initiates in the morning, the tubes fill up gradually over about fifteen minutes which results in a time dependent capacitance.

A simplified model is used which divides the entering fluid equally between the number of nodes chosen. Realistically, the orientation of the collector is such that the nodes fill up one at a time. This could be modeled, but would add unnecessary computational effort. The simplified model exhibits the same thermal behavior although it is dynamically incorrect. Each node thus has the same capacitance which is defined as the capacity of the empty collector plus the fluid

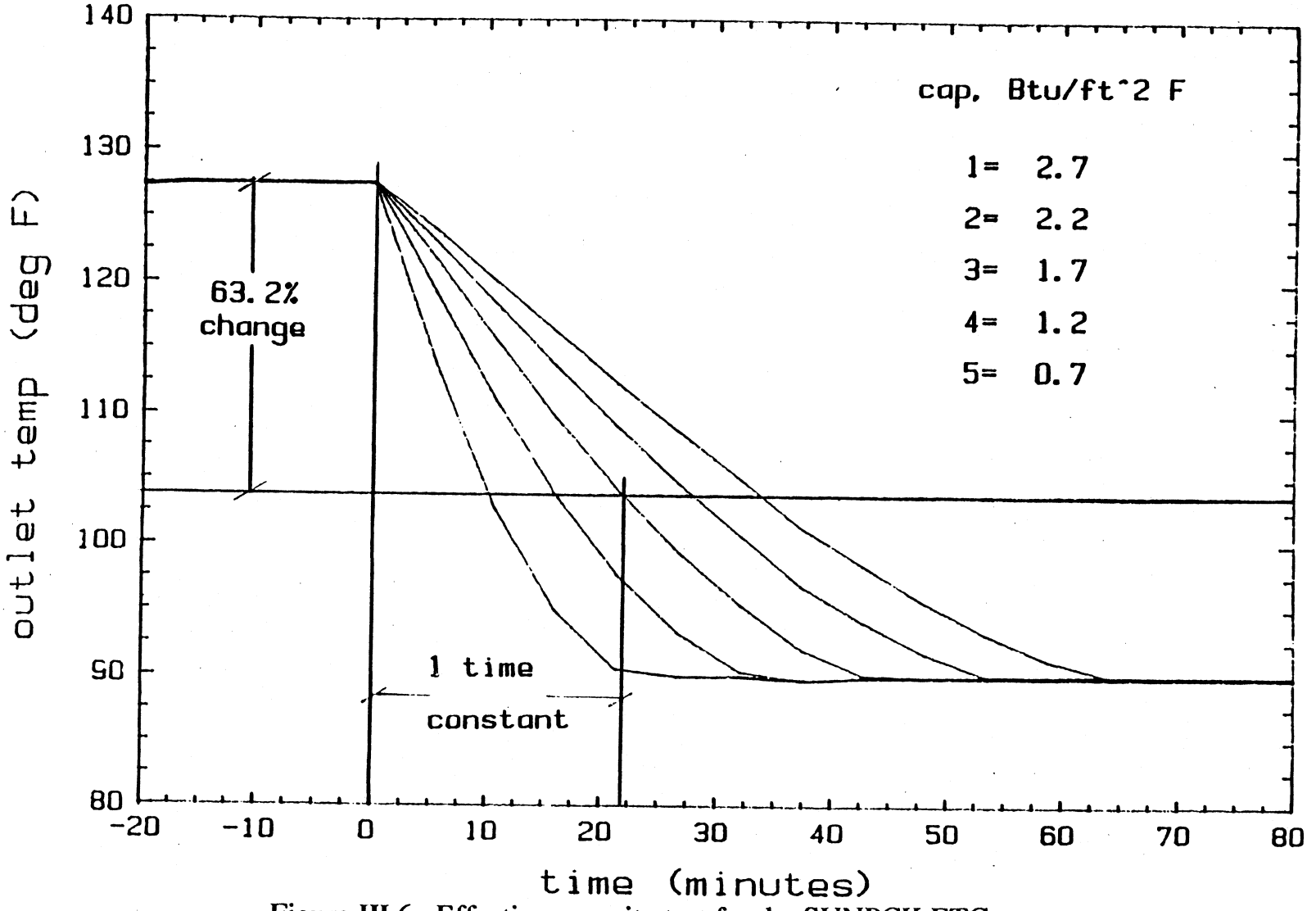

Figure III.6: Effective capacity test for the SUNPCK ETC, outlet temperature response to a step change in radiation.

added during each time step while filling.

$$CAP_n = CAP_{emp} + \frac{\dot{m}C_p \Delta t}{A_c} \qquad \text{(III.4.14)}$$

where:

$$CAP_{emp} = CAP_{eff} - \left(\frac{\dot{m}C_p}{A_c}\right)_{fluid} \qquad \text{(III.4.15)}$$

The energy collected during the filling is thus governed by a time variant mass and the resulting transient effective capacity.

The use of the capacitance model improves the simulation results of both systems. The new model accounts for the long time constant of ETCs and the resulting delay of response to changes in input. Also, the model accounts for the morning filling of the Cherokee collectors and the morning heating of the non-draining Gainesville collector before operation is initiated. None of these effects can be seen with the traditional TRNSYS steady state calculations.

Examples of these improvements when using the model which account for capacitance are shown in Figures III.7 through III.9 which are all taken from daily simulation results. The simulations were run using calculated values for $F_R U_L$ and $F_R(\tau\alpha)_n$ to better isolate the errors in the original model due to the capacitance effects. Figure III.7 shows the outlet temperature response for a two hour simulation of the Cherokee collector. The radiation over the period was fluctuating and the flow and inlet temperature were constant. This example shows how the

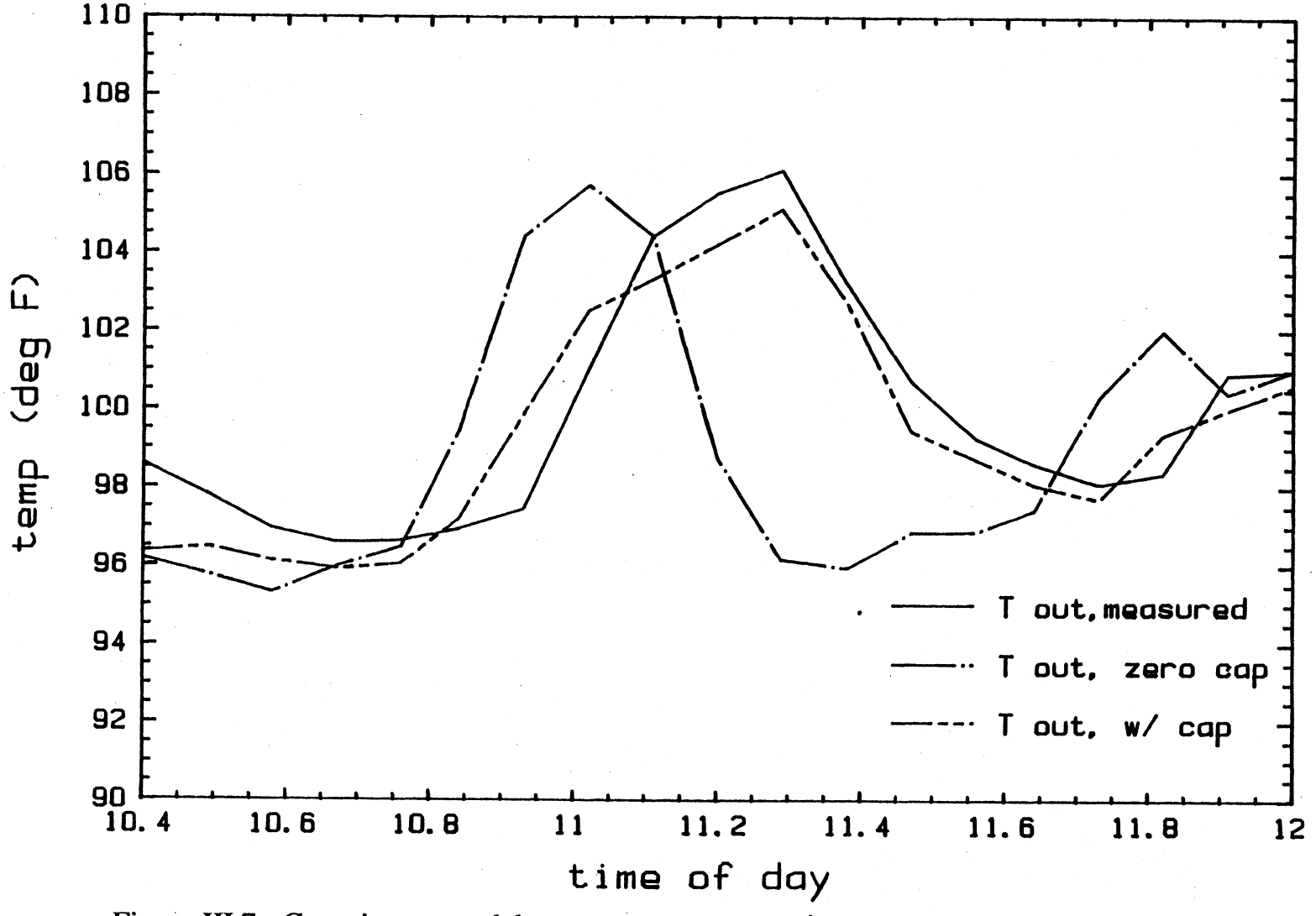

Figure III.7: Capacitance model temperature response improvements, Cherokee, Feb. 6.

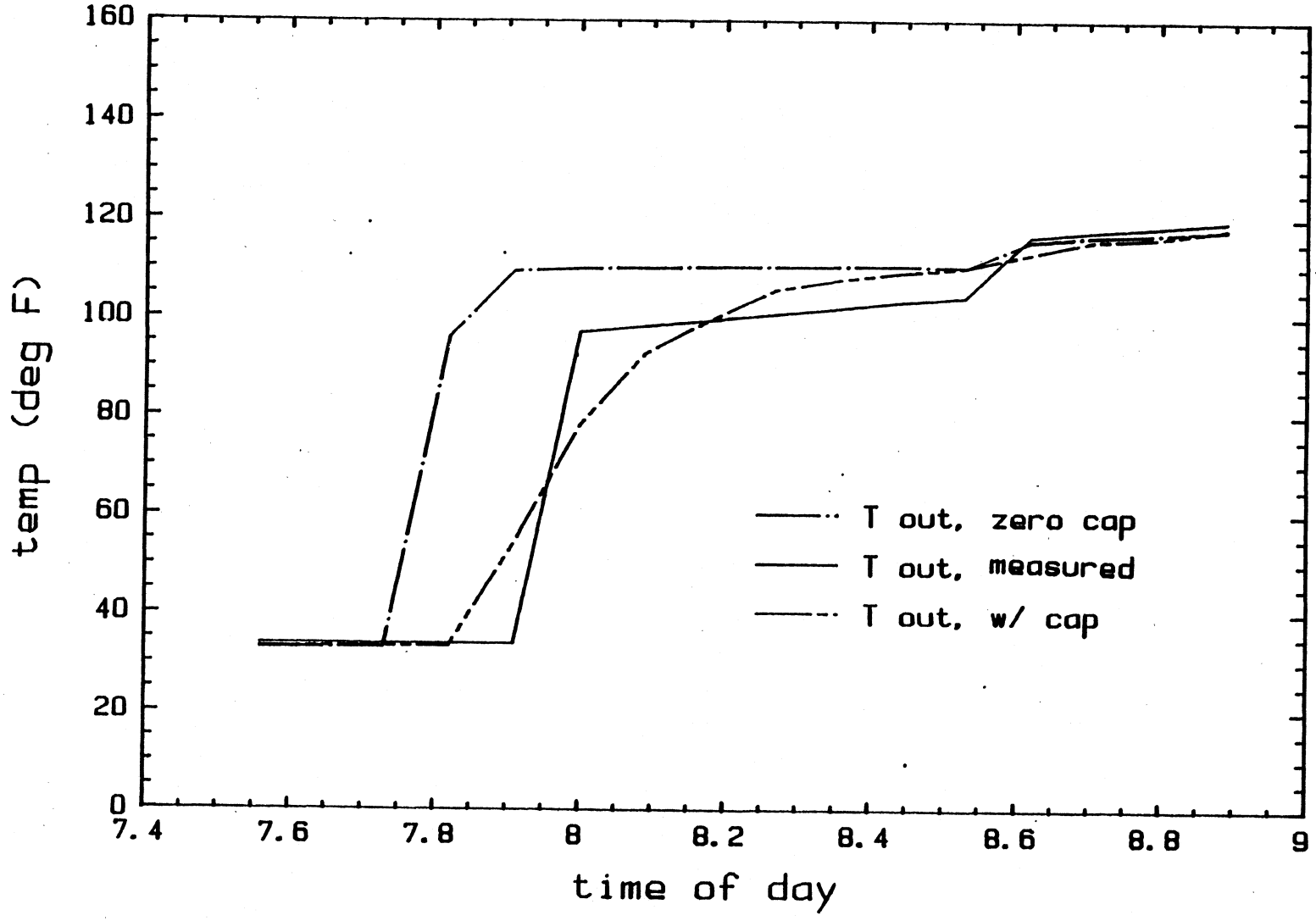

Figure III.8: Capacitance model filling improvement, Cherokee, April 1.

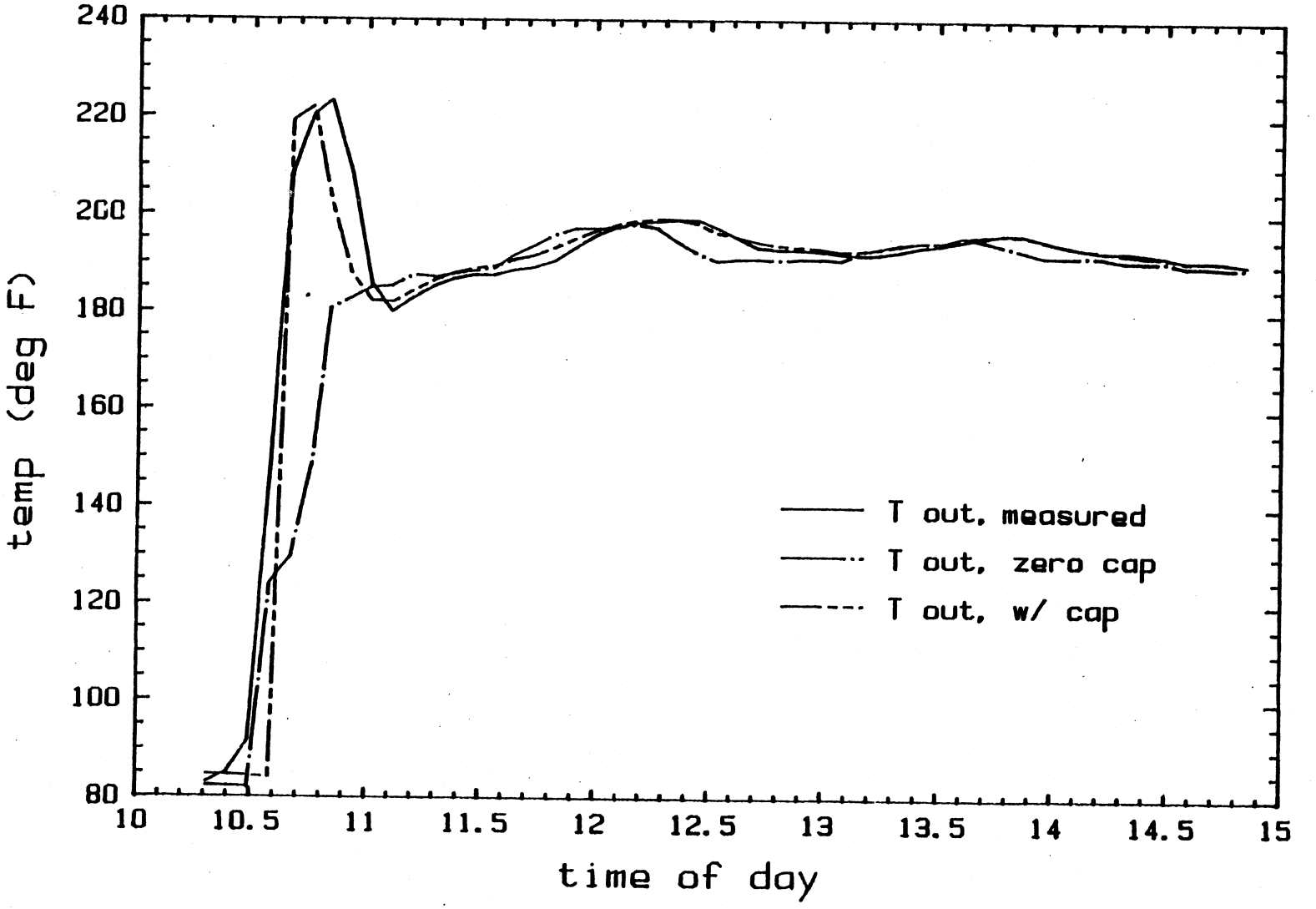

Figure III.9: Capacitance model temperature response improvement, Gainesville, April 3.

heating and cooling of the fluid is dampened by its capacitance. Figure III.8 is of another two hour Cherokee simulation and is an example of the improvements by modeling the morning filling of this drain back collector. The non filling case is shown in Figure III.9 which is of results from a five hour Gainesville simulation. Here, it is shown that the capacitance model is needed to simulate the heating of the collector fluid in the morning before operation begins. Improvements of response to fluctuation in radiation is also apparent. These plots are meant to show improvements in temperature tracking only. Comparisons of energy collected and longer term simulation results are presented and discussed in Chapters 4 and 5.

III.4.3 Incidence Angle Modifiers

The incidence angle modifier, $K_{\tau\alpha}$, as used in equation III.4.1, describes the dependence of the transmittance absorptance product on the angle of incidence. By definition,

$$K_{\tau\alpha} = \frac{(\tau\alpha)}{(\tau\alpha)_n} \qquad \text{(III.4.16)}$$

For flat-plate collectors, the incidence angle modifier is traditionally written as:

$$K_{\tau\alpha} = 1 - b_o\left(\frac{1}{\cos\Theta} - 1\right) \qquad \text{(III.4.17)}$$

where:

b_o = incidence angle modifier constant, determined by an ASHRAE test

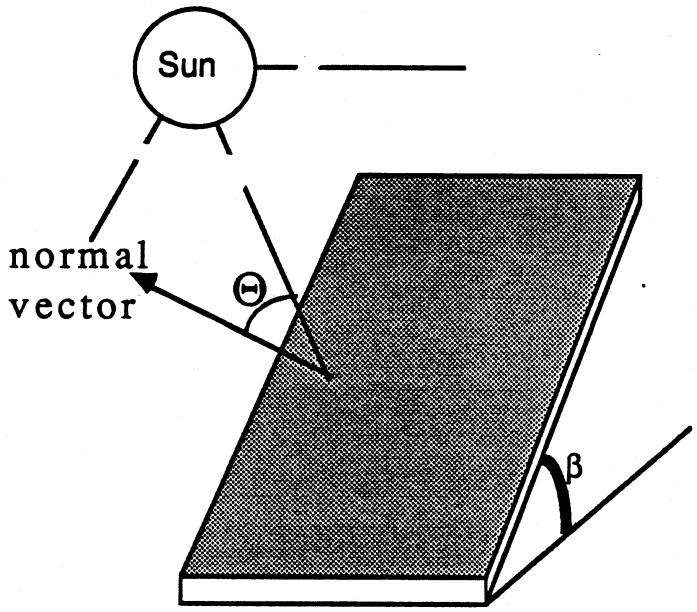

Figure III.10: Incidence angle on a flat-plate collector.

Equation III.4.17 applies to values of theta less than 60 degrees. A linear fit is assumed from the value at 60 to a value of 0 at 90 degrees. A typical value for b_o might be -0.1, resulting in a $K_{\tau\alpha}$ curve shown in Figure III.11.

Incidence angle modification is more complicated for ETCs because of their tubular geometry and the use of reflectors. As shown in Figure III.12, both a longitudinal and a transversal angle of incidence are involved.

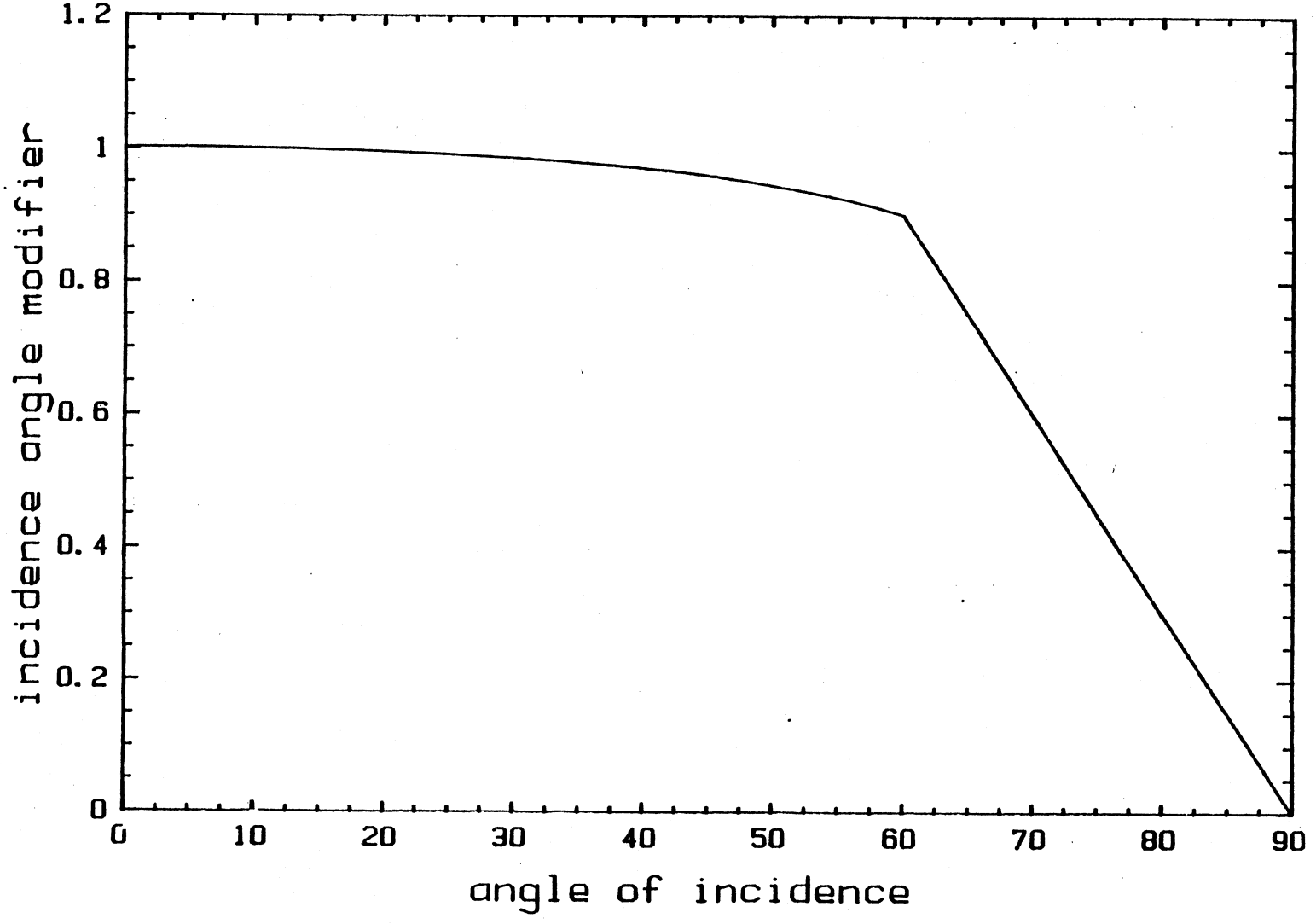

Figure III.11: Typical incidence angle modifier curve for a flat-plate collector.

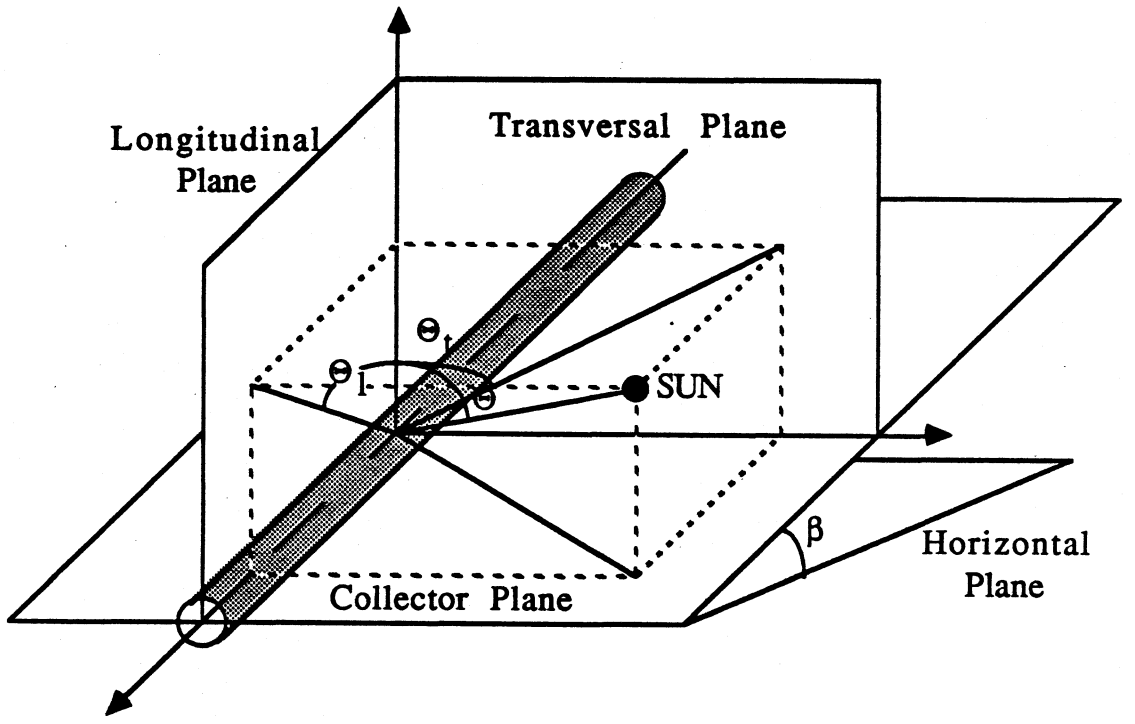

Figure III.12: Biaxial incidence angles for ETCs.

The two angles are defined as:

$$\Theta_t = \arctan\left(\tan\Theta_z\left(\gamma - \gamma_s\right)\right) - \beta \qquad \text{(III.4.18)}$$

$$\Theta_l = \arctan\left(\frac{\sin\Theta_z \sin\left(\gamma - \gamma_s\right)}{\cos\Theta}\right) \qquad \text{(III.4.19)}$$

Both sets of $K_{\tau\alpha}$ values are defined in TRNSYS in a user supplied data file containing between two and ten values of the incidence angle and the corresponding

modifiers. These values are read from the input file by a TRNSYS subroutine and the intermediate $K_{\tau\alpha}$ values are obtained from linear interpolation. The values for Θ_l are similar to typical $K_{\tau\alpha}$ values for flat-plate collectors, however $K_{\tau\alpha}(\Theta_t)$ is more dependent on the angle of incidence and can rise above unity if reflectors are used.

The combined effect of both incidence angle modifiers can be approximated by factoring it into two components:

$$K_{\tau\alpha}(\Theta_l, \Theta_t) \approx K_{\tau\alpha}(\Theta_l, 0)\ K_{\tau\alpha}(0, \Theta_t) \qquad \text{(III.4.20)}$$

The accuracy of this approximation is shown by McIntire (Reference [4]) through ray tracing calculations of the various optical effects which shows that the percent error is less than 3.5%.

The DSET (Desert Sunshine Exposure Testing) Laboratories of Phoenix, AZ completed incidence angle testing of the O-I SUNPACK ETC used in both the Cherokee and Gainesville systems (Reference [18]). Figure III.13 shows the laboratory values for the transversal and longitudinal incidence angle modifiers which are reproduced from the DSET report.

These $K_{\tau\alpha}$ values were used in TRNSYS for initial collector simulations, however their accuracy was questionable. For instance, the magnitude of the transversal modifiers appeared to be too high at large angles, even considering that cusp reflectors were used. It is also intuitively clear that this value should approach zero at perpendicular incidence, i.e. Θ = 90 degrees.

As a check, the collector outlet temperature error, defined as the difference

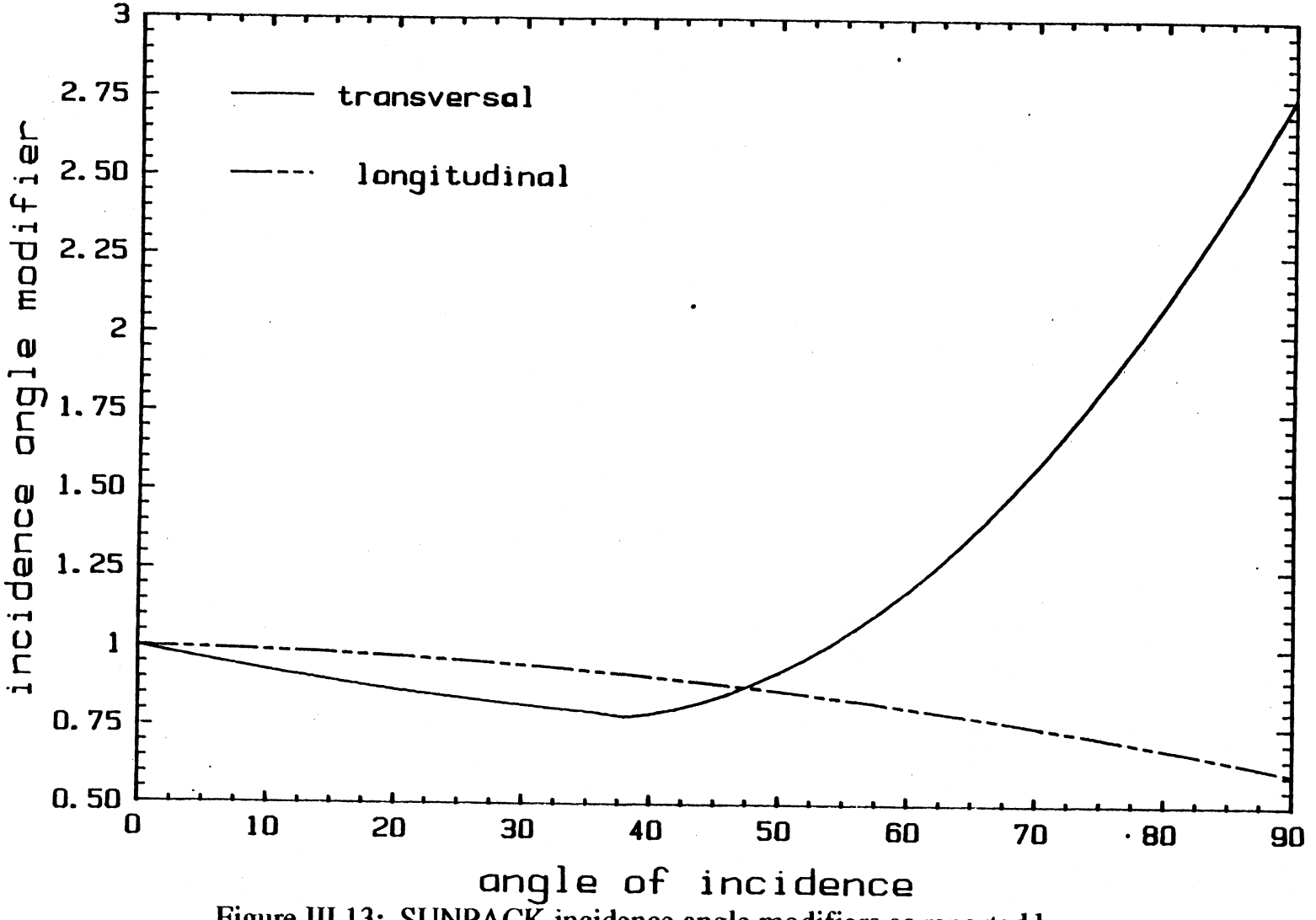

Figure III.13: SUNPACK incidence angle modifiers as reported by DSET Laboratories (from Ref [18]).

between the simulated and measured value, was plotted as a function of transversal incidence angle for each time step over various days. The Θ_l dependence is not significant because large angles are never reached during daylight hours due to the orientation; both collectors studied are south facing and mounted at a slope of about 30 degrees (refer to Figure III.12). Although the longitudinal angle of incidence varies seasonally, no modification is needed because the longitudinal $K_{\tau\alpha}$ is very near unity for all angles encountered during operation. $K_{\tau\alpha}$ (Θ_l) is assumed to be 1.0 through out this discussion.

In general, there was a tendency of over prediction for angles above 70 degrees and under prediction in the 30 to 60 degree range for both of the systems. An example of this trend is shown in Figure III.14 which is generated from TRNSYS results using the Cherokee system data taken on April 1. The calculated collector parameters $F_R(\tau\alpha)_n$ and F_RU_L are used to try to isolate the error due to incidence angle modification. These values are the best representation of measured perfromance at normal incidence. Again, results from a single day are presented here and longer term studies are shown in Chapters 4 and 5.

This difficulty with incidence angle modifier raises two questions: 1) How do lab test values predict the actual tau-alpha dependence of collectors in operation? 2) How sensitive are simulation results to the values used, i.e. how greatly is the predicted performance affected by using a poor set of modifiers?

To determine the actual angular behavior, $K_{\tau\alpha}$ can be calculated using the Hottel-Whillier equation and substituting the ASHRAE collector perfromance factors (experimentally determined from normal data) and the measured collector data. The instantaneous value of $K_{\tau\alpha}$ is defined by rearranging equation III.4.4 and substituting equation III.4.2 to get:

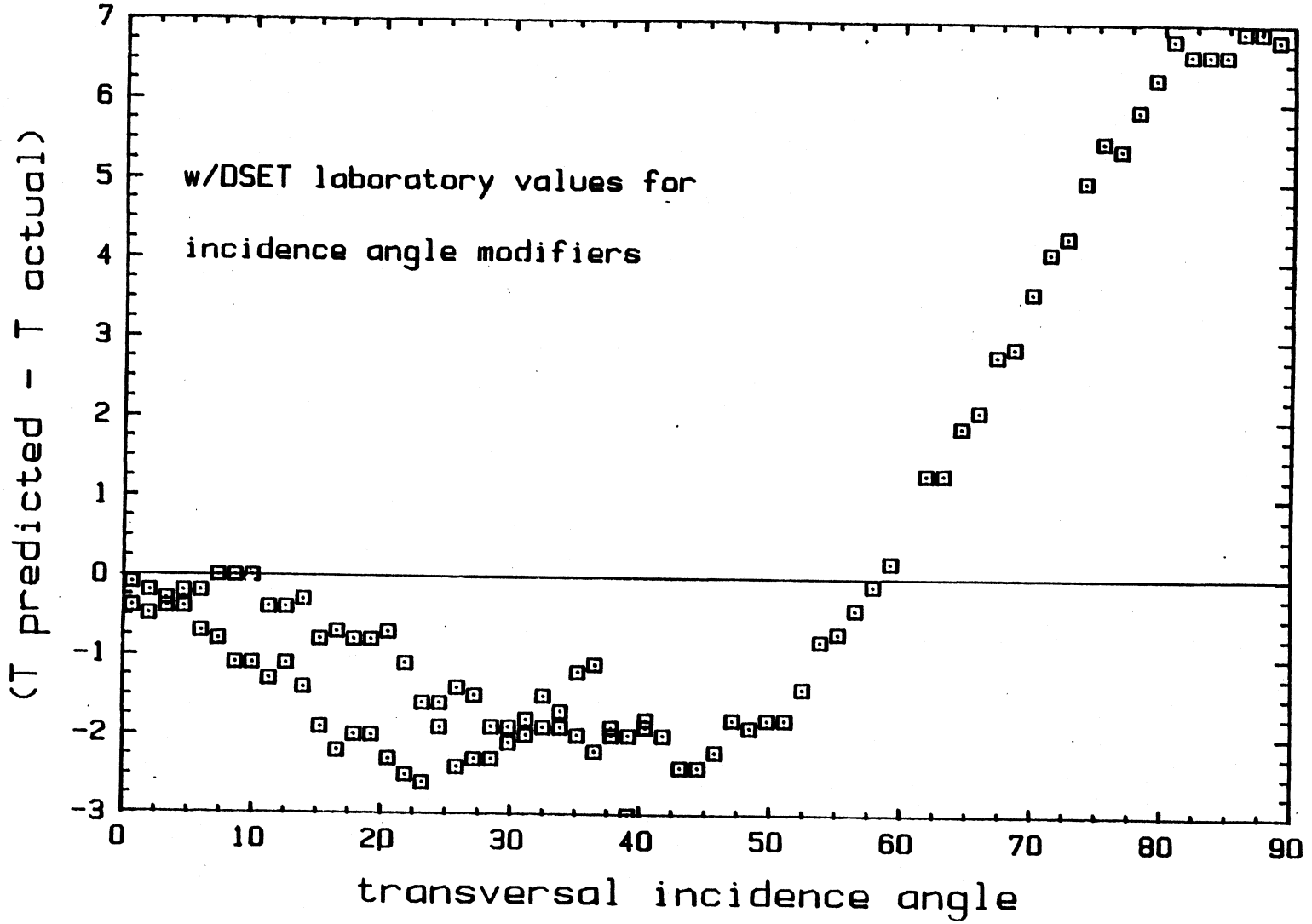

Figure III.14: Outlet temperature error versus incidence angle for Cherokee, April 1.

$$K_{\tau\alpha} = \frac{\left[\frac{\dot{m}C_p(T_o - T_i)}{A_c I_t} + \frac{F_R U_L (T_i - T_a)}{A_c I_t}\right]}{F_R(\tau\alpha)_n} \qquad \text{(III.4.21)}$$

$K_{\tau\alpha}$ was calulated at each time step and the corresponding incidence angles were found knowing the time of day, location, and the collector orientation. Implicit in this calculation procudure is the assumption of linear behavior for the collector efficiency curve. The program used to calculate $K_{\tau\alpha}$ is listed in Appendix D.

The values of $K_{\tau\alpha}$ were then plotted as a function of transversal incidence angle and fit with a third order regression routine. As explained earlier, the longitudinal angle dependence is not significant for this collector orientation. Again, the results for April 1 for the Cherokee system are shown in Figure III.15. The values shown in this figure are listed below and compared to the lab report values for each angle.

Θ_t	0	10	20	30	40	50	60	70	80	90
$K_{\tau\alpha}$ Calculated from Data	1.0	.98	.99	1.04	1.10	1.15	1.16	1.09	.90	.70
$K_{\tau\alpha}$ DSET Lab Test	1.1	.92	.86	.81	.80	.92	1.18	1.58	2.10	2.76

Table III.1: Transversal incidence angle modifier comparison for Cherokee, April 1 .

Here, the reasons are apparent for the overprediction of collector performance in the

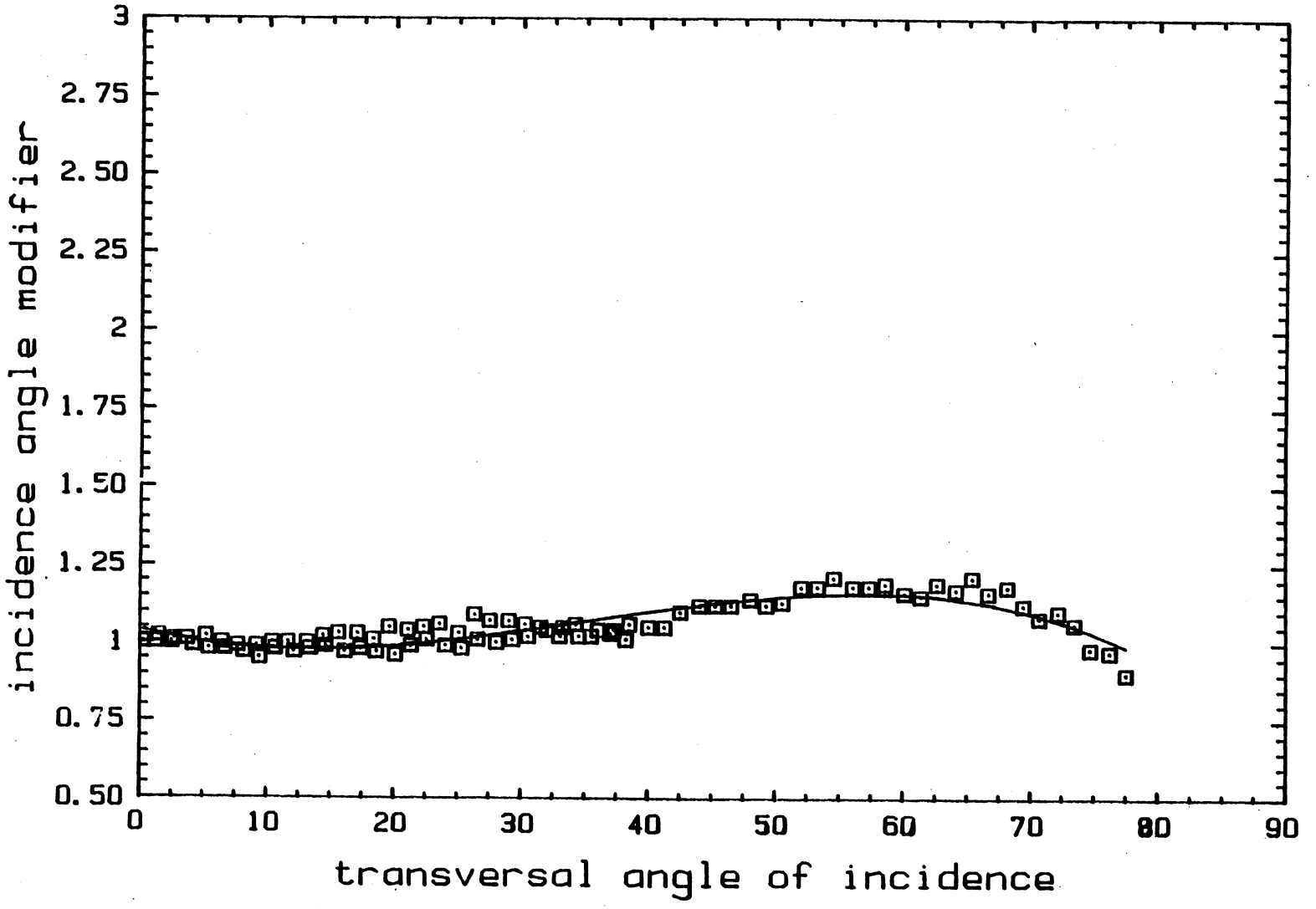

Figure III.15: Incidence angle modifiers determined from data for Cherokee, April 1.

30 to 50 degree range and under prediction above 60 degrees. The effect on TRNSYS results is shown in Figure III.16. The predicted vs. actual collector outlet temperature (again for Cherokee, April 1) is plotted for simulations run using both sets of incidence angle modifiers.

Similar calculations and comparisons are shown in section IV.3 and V.3 and include longer periods of data and conclusions drawn about the discrepancies. Also studied is the sensitivity of the simulation accuracy to the use of different sets of incidence angle modifiers including lab test values, calculated values, and no modification.

III.5 **Pipe Component**

In both of the systems studied, the collector outlet and inlet fluid temperature sensors are located in pipes at an unknown distance from the array. No specific information about their location was available, but it was estimated to be about 20 to 50 feet from the collector [REF]. As a result, there was some difference between the actual collector inlet and outlet conditions and the measured data. This difference was due to time delays for flow through the pipes and cooling from pipe heat losses. This discrepancy was accounted for in the simulation by addition of pipe lengths to the ETC model.

The pipe model used in TRNSYS is a plug flow model which assumes no conduction through the fluid in the direction of flow. This assumption is reasonable for the working fluids used in ETCs. The pipe is considered to be divided into fluid segments of uniform temperature but not necessarily of uniform size. Temperature fronts moving through the pipe are simulated by tracking the temperature and the

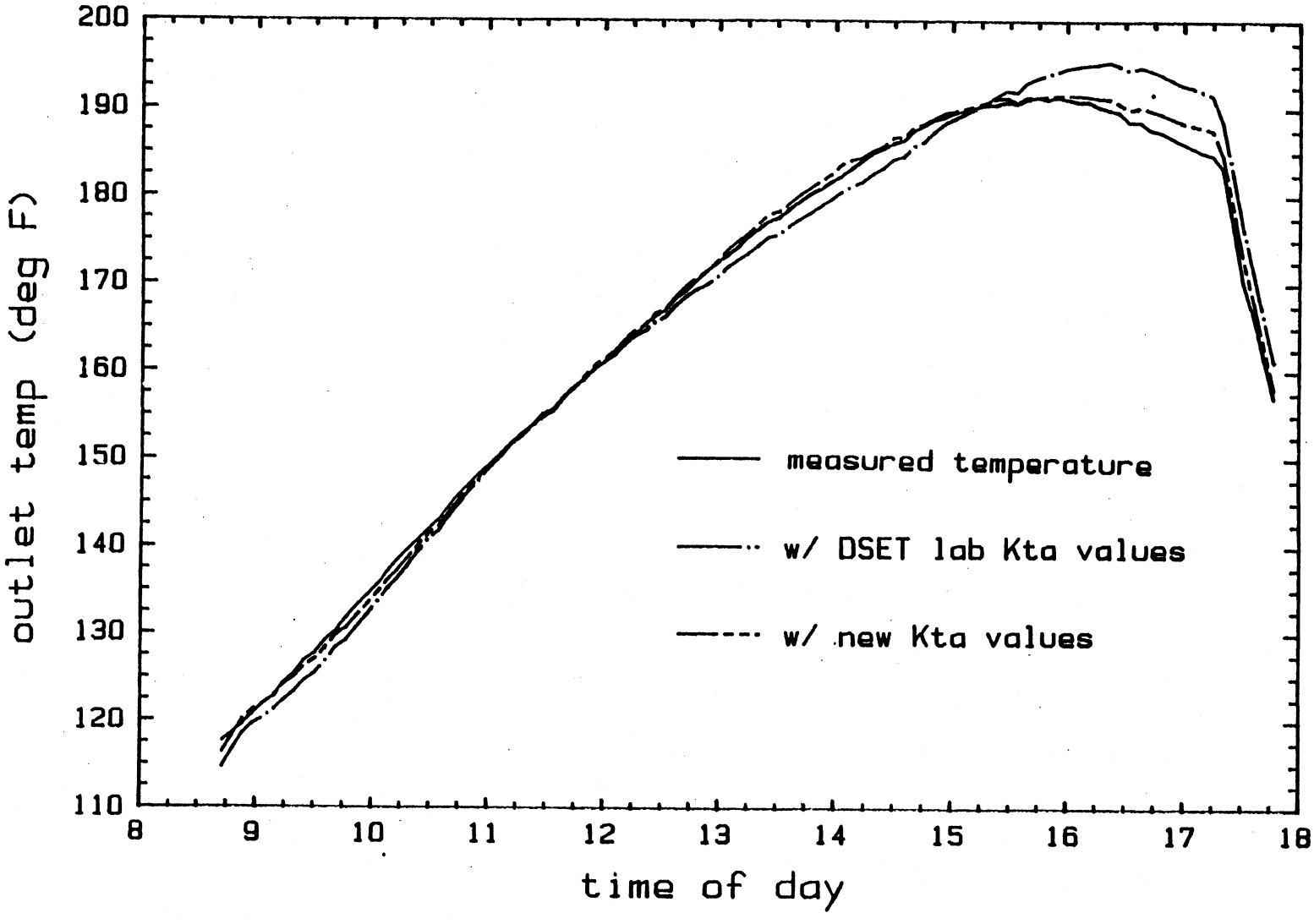

Figure III.16: Simulated collector outlet temperature comparison for Cherokee, April 1.

location of the individual fluid segments. As flow enters the pipe at each time step, an equal mass is displaced at the exit. The outlet temperature is determined by a mass weighted average of the displaced segments. Heat loss is calculated from each segment by solution to the governing first order differential equation:

$$m_n C_p \frac{dT_n}{dt} = (UA)_n (T_n - T_{env}) \qquad \text{(III.5.1)}$$

where:

m_n = mass of fluid in the segment

T_n = temperature of fluid in the segment

C_p = specific heat of working fluid

$(UA)_n$ = overall conductance - area product of the segment

T_{env} = temperature of the surroundings

t = time

An artificially long pipe length was added before the collector array to account for the long fluid dwell time though the collector. The TRNSYS model assumes that the inlet fluid passes though the collector in one time step, but this is not always the case for collectors with large volumes of fluid or when short time steps are used. Given the flow rate and the size of the collector tubes, it takes approximately 12 minutes for the fluid to pass through the tube. This dwell was accounted for by addition of a very long pipe (with no losses) at the collector inlet. It thus takes the correct amount of time for the fluid to flow from inlet to outlet, but energy is only collected during the last time step. Again, this is not a dynamically accurate

description of the system, but the model exhibits the proper thermal behavior because the amount of energy collected is the same.

Piping was also added to the exit of the collector to account for losses which were evident when the data was screened. Since none of the pipe lengths were known, estimates were made and the corresponding UA was determined experimentally from the data. For example, for the outlet of the Cherokee collector, a reasonable length of 20 ft was chosen. The loss coefficient, U, was then found by solving equation III.5.1 using the actual data from the cooling of the pipe fluid after the collector pump shut off for the day. A UA value of 13 Btu/ deg F was found which corresponds to a R values of 2 hr ft^2 F/Btu. The pipe was described as having 1 1/2 inches of foam insulation which would correspond to an R value closer to 6. The lower value calculated for both of the systems was probably due to poorly fitted insulation or missing insulation at the pipe joints. This and other discrepancies between designed and actual performance are addressed later in the conclusions to this thesis.

CHAPTER IV
The ETC System at the Cherokee Indian Hospital

This chapter describes the Cherokee solar heating system and its performance over the six month period monitored. Results are presented from simulations using both the capacitance and zero capacitance collector models. Various values for the performance parameters $F_R(\tau\alpha)_n$ and $F_R U_L$, and transversal incidence angle modifiers are used. Comparisons are made between laboratory test values for these parameters and values calculated from measured data collected during field operation. The predicted TRNSYS results are then compared to measured performance for all cases to show the sensitivity of the simulation accuracy to the variation of the above parameters and choice of collector models.

IV.1 Overview of System

The ETC solar heating system at the Cherokee Indian Hospital is a retrofit which was installed as part of the Solar in Federal Buildings Program. The system is designed to supply the energy needed for hot water heating and for part of the space heating requirements of the facility. The system schematic is shown in Figure IV.1 and includes flow loops for the collector, water heating, space heating, and auxiliary energy subsystems. The drain back solar array consists of 320 evacuated

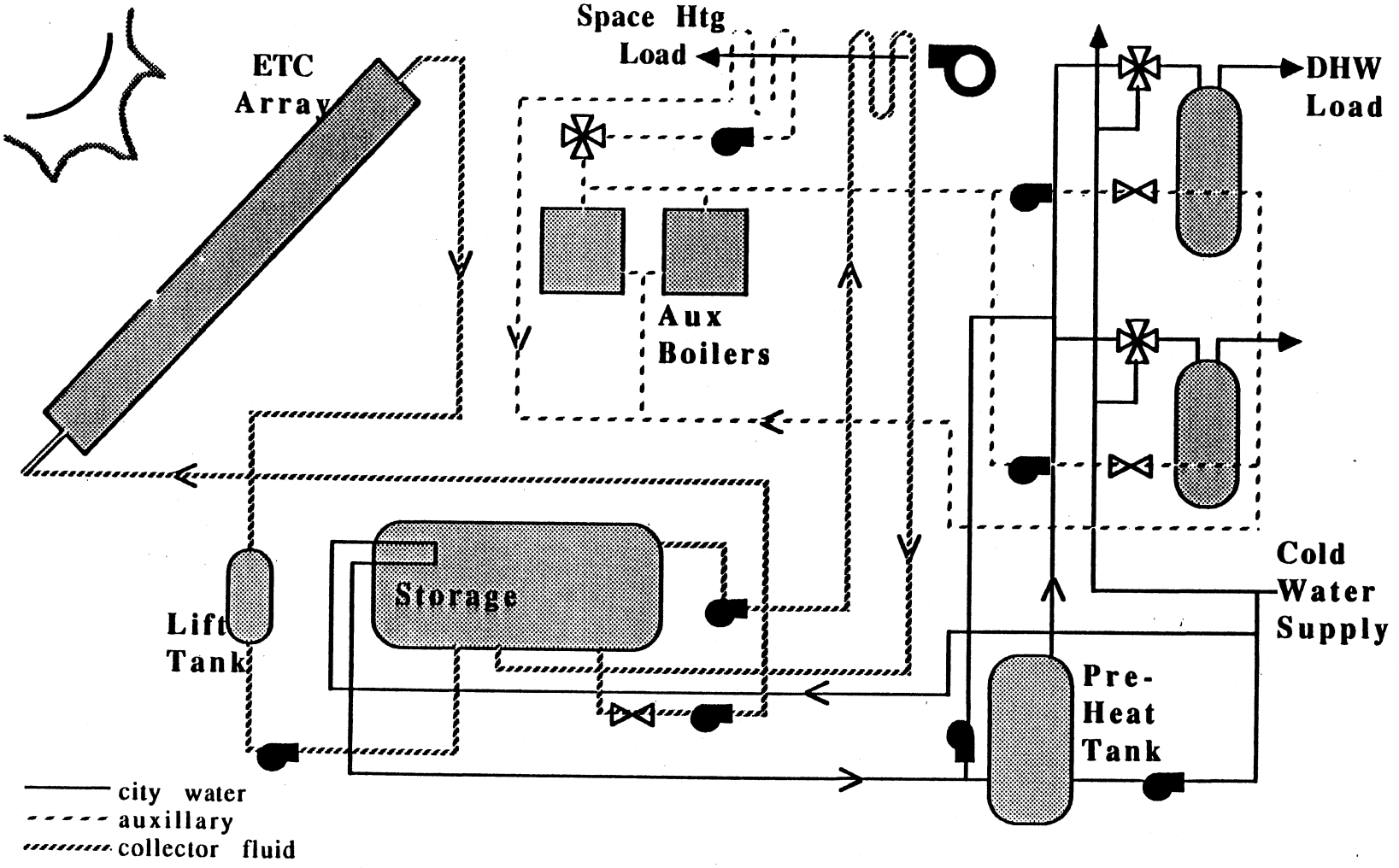

Figure IV.1: Cherokee hospital solar system schematic (from Reference [19]).

tubular collectors totaling a gross area of 5517 square feet. Solar energy is stored in a 6335 gallon tank and supplied to a 700 gallon domestic hot water heating (DHW) preheat tank through an internal heat exchanger in the main storage tank. Solar energy is supplied directly to the space heating load by circulation of water from the main storage tank through heat exchangers in the air handlers. Auxiliary energy is provided to both loads by two large oil fired boilers.

The collectors used at Cherokee are the Owens Illinois SUNPACK Model 1104 Each collector panel consists of eight evacuated tubes connected in a parallel flow arrangement. Specular reflectors are used behind each tube. The array is made up of eight rows of forty collectors which are mounted on a roof top steel structure. The array is oriented eight degrees east of south and tilted at an angle of 34 degrees from the horizontal. The total flow rate through the collector is 68 gallons per minute (gpm), or 0.213 gpm per collector. The ASHRAE 93-77 test for this collector gave the results: $F_R(\tau\alpha)_n = 0.391$ and $F_R U_L = 0.224$ Btu/ft^2 F based on a gross area of 17.17 square feet and a flow of 5.96 lbm/hr ft^2. The collector time constant was determined to be 22.07 minutes. The collector fluid is drained each night into a lift tank to protect against freezing and reduce overnight losses.

Collector operation is controlled by a differential temperature sensor. This control monitors the fluid temperature at the outlet of the array and the bottom of the storage tank. Flow is initiated when the array temperature is 20 degrees greater than the storage temperature and turned off when a 5 degree difference is reached. To protect against overheating, operation is also stopped and the array is drained if the collector fluid gets hotter than 205 deg F.

For more detailed information about the Cherokee solar heating system and its components, consult Reference [19].

IV.2 System Performance

The performance of the Cherokee system was monitored over the six month period from January through June 1985. The total solar insolation for this period was 6% below the long term average and the number of heating degree days was 4% lower. The total energy flows through the system over the period of January through May are shown in Figure IV.2. As shown, a overall collector efficiency of 23% was achieved and 72% of the collected energy was delivered to the loads. This represented a solar contribution of 83% to the hot water heating and 3% to the space heating requirements. Vitro estimated the resulting fuel savings over the period to be $1751 but at an operating cost of $317, based on current reasonable price estimated of $0.846 per gallon of fuel and $0.067 per kwh.

In general, the Cherokee system performed below design expectations. Losses in the storage tank and pipes were greater than predicted. For instance, the effective R value of the storage tank was calculated to be 3.1 (using the method discussed in section III.5) compared to a design value of 14. This was due to loosely fitting insulation and poorly covered tank supports. There was also a problem with unnecessary consumption of parasitic power when the pumps in the DHW auxiliary loop ran continuously due to controller failure. This consumed more than 9 million Btu over the six month monitoring period month and no explanation was given in the Cherokee system reports about why repairs were not made. Other problems were encountered because the DHW load was only 11% of the design prediction due to low occupancy of the hospital. For the small hot water draws needed, the preheat loop was not necessary and only increased thermal losses while

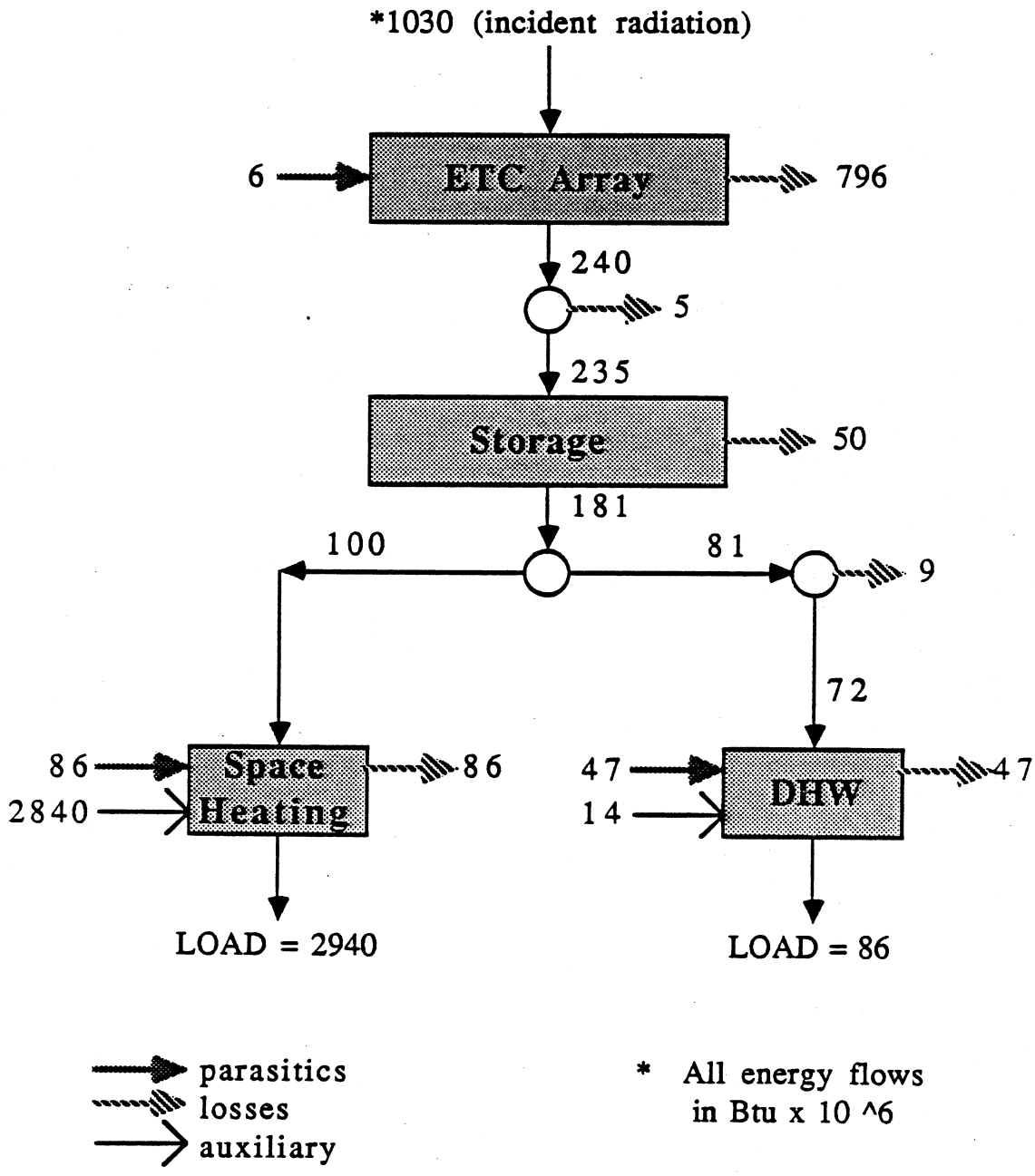

Figure IV.2: Cherokee system measured energy flows from Jan - May 1985 (from Reference [19]).

consuming parasitic power. It was also found that the pump for the preheat loop operated at a flow rate that was too high for the internal tank heat exchanger. The resulting effectiveness as calculated from the system data was only 0.07. Overall, however, there was little problem with the dependability of the system. Although data were not always successfully recorded, Vitro reported that the system was available 98% of the time over the period monitored.

IV.3 Collector Subsystem Simulation

For the purposes of this thesis, only the ETC subsystem performance is studied. The deck configuration for the simulation is discussed in Section III.2 and listed in Appendix E. The following sections describe the inputs and results for various simulations performed.

The accuracy of each simulation is shown by the percent difference between the actual and predicted energy collected over the period. This is defined as:

$$\text{percent dif} = \frac{Q_{TRNSYS} - Q_{measured}}{Q_{measured}} \times 100\% \qquad \text{(IV.3.1)}$$

The bias error is also given which measures the average difference between the estimated and actual values of the outlet temperature at every time step. As the name implies, it represents an offset for the predicted results and it is usually an indication of a systematic problem with the model. The bias error between modeled and measured performance is given by:

$$\text{bias error} = \frac{\sum_{i=1}^{n} \left(Y_{i,\,\text{measured}} - Y_{i,\,\text{predicted}} \right)}{n} \qquad \text{(IV.3.2)}$$

The bias error measurement is a better indication of the capacitance model corrections than is the percent difference value. This is because the outlet temperature tracking improves but the total energy collected is not always greatly affected. An example of this is given in the simulation results shown in Figure III.7. The following errors are calculated from the simulation results from 10:40 to 11:40 that are presented for this period.

	percent dif	bias error
CAP MODEL	-3.8	.99
ZERO CAP	-7.2	4.2

Throughout the next two chapters, the accuracy of each simulation is evaluated by the percent difference and bias error deviation from the actual data. It should be stressed that some measurement error is associated with the 'actual' values as is discussed in Section II.1. These uncertainties should be considered when evaluating the simulation results.

All simulations are run for six two week time periods which were chosen after the monthly data were screened as described in Chapter II. Each of these periods is made up of a combination of clear and cloudy days and is representative of the weather conditions over each month.

IV.3.1 Initial Simulation

Initial simulations were run for each period using the origonal zero capacitance TRNSYS collector model and the following design conditions: ASHRAE collector test parameters $F_R(\tau\alpha)_n$ and F_RU_L, DSET values for incidence angle modifiers, and and R value of 6 hr ft^2 F/Btu for the insulation of the pipe running from the collector outlet to the location of the sensor. The results are shown in Table IV.1.

Month	Q measured (total Btu x 10^6)	Q TRNSYS	Bias Error (deg F)	Percent Dif (%)
JAN	31.55	27.61	4.6	-12.5
FEB	33.76	32.55	5.0	-3.6
MAR	43.89	40.38	5.1	-8.0
APR	42.72	36.41	6.4	-14.8
MAY	38.72	33.14	6.0	-14.4
JUN	26.57	21.72	7.4	-18.2
SUM	217.21	191.81	---	-11.7

Mean Bias Error = 5.6

Table IV.1: Cherokee simulation results using origonal collector model and design values for $F_R(\tau\alpha)_n$, F_RU_L, $K_{\tau\alpha}$, and pipe losses.

The simulations were then repeated with the effective piping insulation values of R=2 hr ft^2 F/Btu. All of the other TRNSYS inputs remained the same. There was an insignificant change in the results as is shown below.

Month	Q measured (total Btu x 10^6)	Q TRNSYS	Bias Error (deg F)	Percent Dif (%)
JAN	31.55	27.51	4.7	-12.8
FEB	33.76	32.54	5.0	-3.6
MAR	43.89	40.10	5.1	-8.6
APR	42.72	36.41	6.4	-14.8
MAY	38.72	33.18	6.0	-14.3
JUN	26.57	21.72	7.4	-18.3
SUM	217.21	191.46	---	-11.8

Mean Bias Error = 5.7

Table IV.2: Cherokee simulation results using origonal collector model, design values for $F_R(\tau\alpha)_n$, F_RU_L, $K_{\tau\alpha}$, and calculated pipe loss factors.

IV.3.2 Simulation with New $F_R(\tau\alpha)_n$ and F_RU_L Values

As described in section III.4.1, the collector parameters $F_R(\tau\alpha)_n$ and F_RU_L can be calculated from the collector data measured while the beam radiation is at normal incidence. Values for these two parameters were calculated for each two week period of data using the algorithm and regression method given in section III.4. The results are shown in Table IV.3 which includes σ, the standard deviation and the R^2 value for the fit.

month	$F_R(\tau\alpha)_n$	$F_R U_L$	σ	R^2
JAN	0.359	-0.087	0.041	0.017
FEB	0.410	-0.201	0.097	0.098
MAR	0.398	-0.102	0.043	0.083
APR	0.381	-0.121	0.069	0.058
MAY	0.411	-0.113	0.075	0.107
JUN	0.367	-0.147	0.051	0.143
AVE	0.388	-0.127	0.067	0.111
ASHRAE Test Values	0.391	-0.224	-----	-----

Table IV.3 Calculated values for $F_R(\tau\alpha)_n$ and $F_R U_L$ for each simulation period.

Three trends are obvious from these results: 1) $F_R(\tau\alpha)_n$ values do not vary much from the test results. 2) the loss coefficients are in generally less than the value predicted by the ASHRAE test. 3) While the standard deviation from the fit is small, the R^2 values are extremely low. Recall the R^2 is defined as unity minus the ratio of the variance of the residuals to the variance of the data. (Eqn III.4.9) Because this number is consistently very small, this indicates that the two variances are about the same. This means that the curve fit of the data is very close to the horizontal line that runs through the average y value of the points regressed. While the low R^2 values would seem to indicate a poor fit, it is expected in this case because the slope of the predicted test curve line is so low. The small standard deviation values are better indications of the quality of the fit. These results indicate, however, that using an average value for the collector efficiency would be as

reasonable of an approximation as the more complicated method of regression of the η vs $(T_i - T_a)/I_t$ points. An example of this behavior is shown in Figure IV.3 which is the calculated test curve from the January data.

The new values of $F_R(\tau\alpha)_n$ and F_RU_L (shown in Table IV.3) were then used in simulations for each month to study the difference between using the ASHRAE test values and those calculated from actual performance data. The new simulation results are presented in Table IV.4 and compared to the initial case results in Figure IV.4.

Month	Q actual (total Btu x 10^6)	Q TRNSYS	Bias Error (deg F)	Percent Dif (%)
JAN	31.55	28.67	4.5	-9.1
FEB	33.76	34.16	4.7	1.2
MAR	43.89	41.59	4.4	-5.4
APR	42.72	39.61	6.1	-7.3
MAY	38.72	37.17	5.2	-4.0
JUN	26.57	24.58	7.0	-7.5
SUM	217.21	205.78	---	-5.3

Mean Bias Error = 5.3

Table IV.4: Cherokee simulation results using origonal collector model, design $K_{\tau\alpha}$ values, and calculated $F_R(\tau\alpha)_n$ and F_RU_L.

The predicted values for Q collected were on the average six percentage points closer to the actual value and the average bias error improved 0.5 degrees F. This is

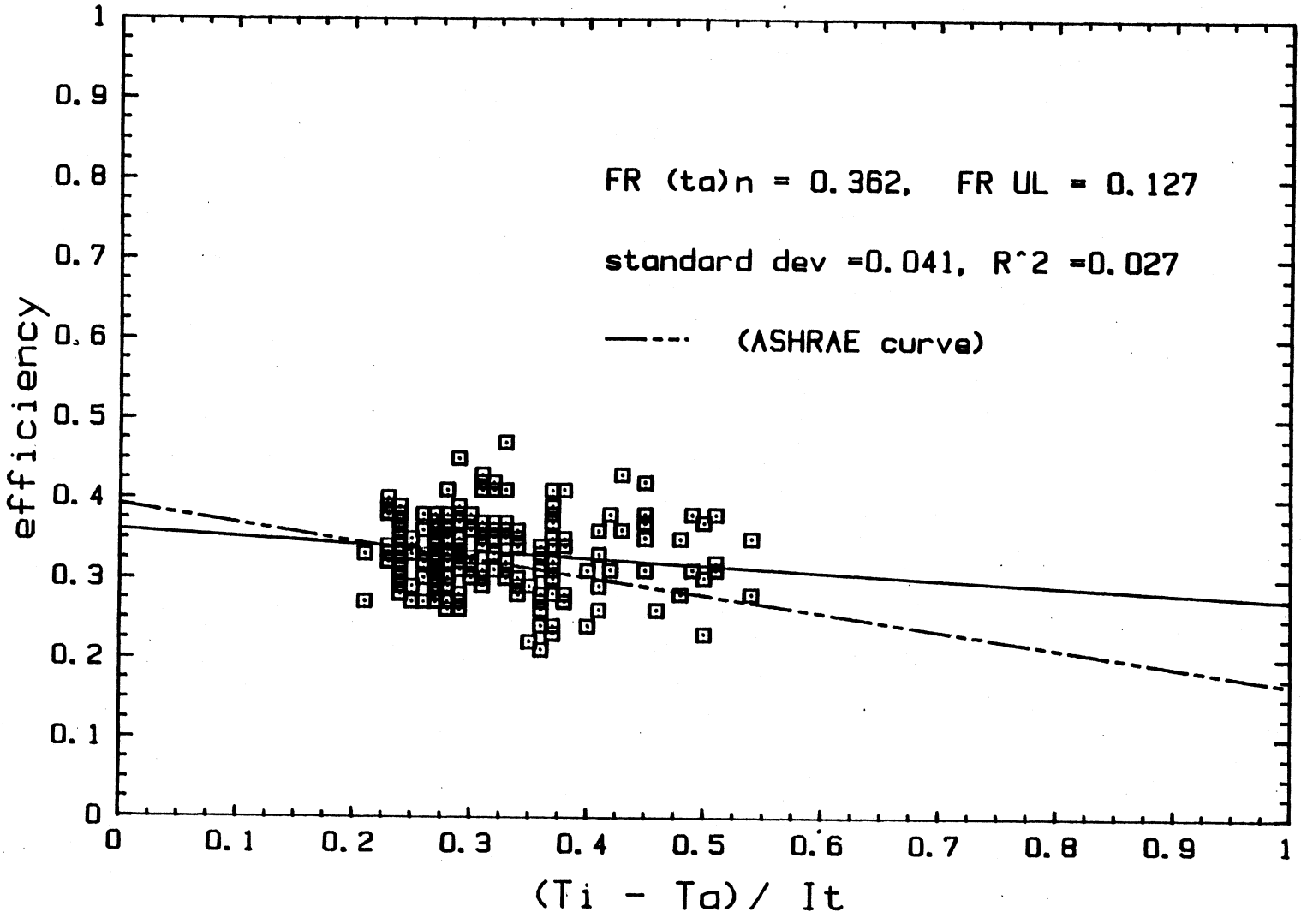

Figure IV.3: Generated test curve using actual data for January.

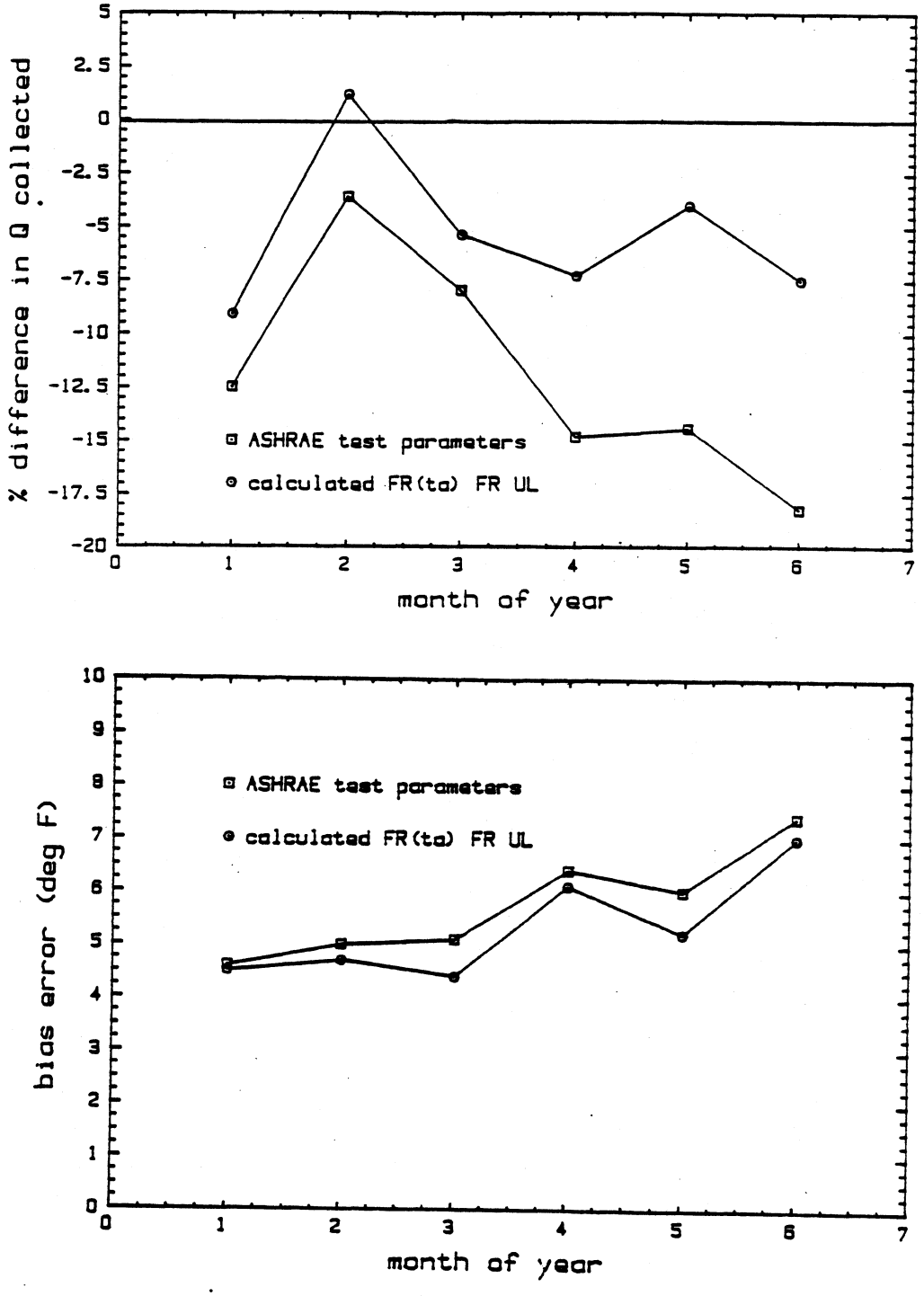

Figure IV.4: TRNSYS simulation results using calculated and ASHRAE test parameters.

not a very significant improvement in results, especially considering the 4% uncertainty in the measured energy collected and the 2 degree uncertainty in the temperature measurement due to sensor limitations. (refer to Section II.1) Significant differences in the results were not expected because of the lack a good fit of the reproduced test curve data from any of the months. Also, the average calculated value of the test curve intercept was less than 1% different than the ASHRAE value for $F_R(\tau\alpha)_n$. This indicates that the efficiency does not behave in a strictly linear fashion, but is uniformly scattered around an average value which, for this collector, is accurately predicted by the laboratory test. The deviation in field performance from that in a controlled laboratory environment is expected due to the uncertainty in measurements and uncontrollable influences such as wind or the fluctuation of radiation over a time step. For this case, however, it is concluded that the ASHRAE values are suitable for simulation input.

The best pair of values for $F_R(\tau\alpha)_n$ and F_RU_L to represent all of the data would be the average values listed in Table IV.3. Note that the optical efficiency is very close to the ASHRAE parameter, but the loss factor is significantly lower. Using these values as TRNSYS input would increase the average Q predicted value for each period about 5%, bringing the simulation results closer to measured performance.

IV.3.3 Simulation with New $K_{\tau\alpha}$ Values

The next TRNSYS input studied was the transversal incidence angle modifier $K_{\tau\alpha}$. As explained in section III.4.3, using the DSET test values for this parameters to describe the behavior of the collector in operation at Cherokee is

questionable. To study the actual dependence of performance on the incidence angle of beam radiation for this collector, new instantaneous values of $K_{\tau\alpha}$ were calculated and plotted as a function of transversal incidence angle. This was done using eqn. III.4.22, the ASHRAE test values for $F_R(\tau\alpha)_n$ and F_RU_L, and all the data for each of the six two week periods used for simulation. Data from every time step after the first hour of operation was used, totalling over 5,600 points. A third order regression was performed and the resulting fit is given in equations IV.3.1.

$$K_{\tau\alpha} = 1.055506 - 0.006242\,\Theta + 0.000305\,\Theta^2 - 0.000002\,\Theta^3 \qquad \text{(IV.3.1)}$$

The standard deviation for this fit is 0.153 and the R^2 value os .139. The corresponding curve is shown in Figure IV.5 with the DSET Laboratory curve also presented for comparison. Values for both sets of incidence angle modifiers are given in Table IV.5.

Θt	0	10	20	30	40	50	60	70	80	90
$K_{\tau\alpha}$ Calculated from Data	1.0	1.02	1.04	1.09	1.17	1.26	1.35	1.43	1.48	1.50
$K_{\tau\alpha}$ DSET Lab Test	1.1	.92	.86	.81	.80	.92	1.18	1.58	2.10	2.76

Table IV.5: Transversal incidence angle modifier comparison.

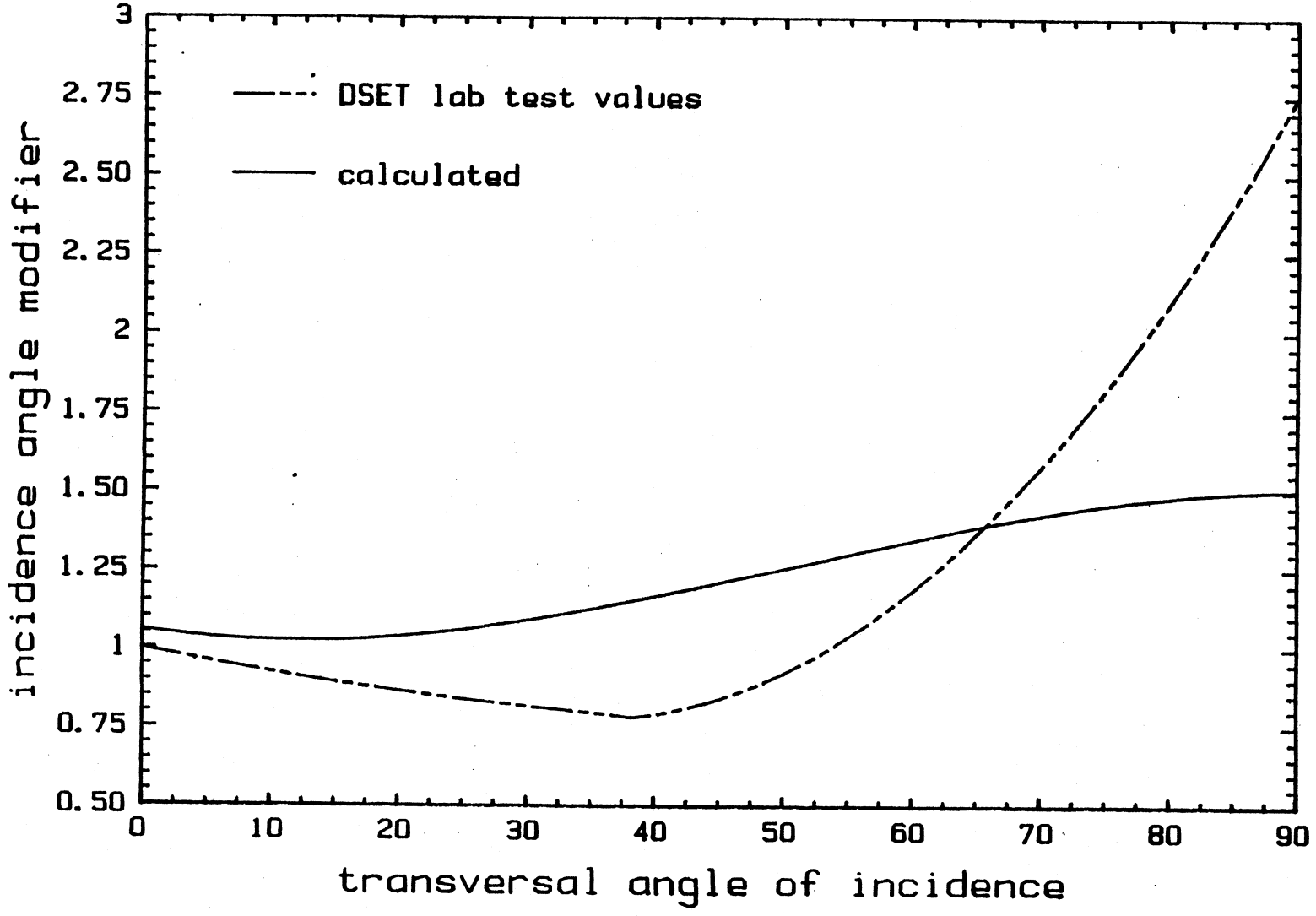

Figure IV.5: Transversal incidence angle modifer calculated from all data.

The fitted value of 1.0 at $\Theta = 0$ indicates that the ASHRAE $F_R(\tau\alpha)_n$ and F_RU_L values used in the calculation procedure are indicative of the collector performance at normal incidence.

The six simulations were again repeated but with the new incidence angles modifiers. Design values were used for the other inputs. The results from these simulations are presented in Table IV.6.

Month	Q measured (total Btu x 10^6)	Q TRNSYS	Bias Error (deg F)	Percent Dif (%)
JAN	31.55	32.94	3.8	4.4
FEB	33.76	34.97	4.3	3.4
MAR	43.89	42.78	3.6	-2.5
APR	42.72	42.84	4.9	0.3
MAY	38.72	39.02	4.8	0.8
JUN	26.57	26.11	6.6	-1.7
SUM	217.21	218.66	---	.67

Mean Bias Error = 4.6

Table IV.6: Cherokee simulation results with origonal collector model, design $F_R(\tau\alpha)_n$ and F_RU_L values, and calculated $K_{\tau\alpha}$.

Simulation results are significantly improved by use of the new $K_{\tau\alpha}$ values for input. The percent difference of energy collected comparisons is better by an average of 10 percentage points for each simulation and was only 0.67% over the entire period. The average bias error is improved as well.

These results show that the laboratory predictions for the incidence angle modifiers do not represent the behavior of the Cherokee system as installed. The low $K_{\tau\alpha}$ values for incidence angles in the 30 - 40 degree range resulted in a net under prediction of performance in the initial simulations. Figure IV.5 shows that there is, in general, less angular dependence than expected. This difference could be due to deviation in reflector configuration for the laboratory and field collectors. Although it was specified that the same diffuse reflectors were used for both cases, it is possible that there was some difference in the tube spacing or height of the cusp reflectors. Also, it is evident that the reflectors were not as effective at large angles as predicted by the laboratory test. Also, the $K_{\tau\alpha}$ curve did not rise as sharply at angles greater than 60 degrees as expected. However, this did not have much influence on the simulation results because most of the energy collection is during mid-day while the incidence angle is less than 40 degrees.

For comparison, the simulation were also run with no incidence angle modification, i.e. $K_{\tau\alpha}$ =1.0 for all Θ_t. Results from these simulations are listed in Table IV.7. Figure IV.6 shows the comparison of simulation accuracy for different incidence angle modifiers using laboratory values, calculated values, and no modification.

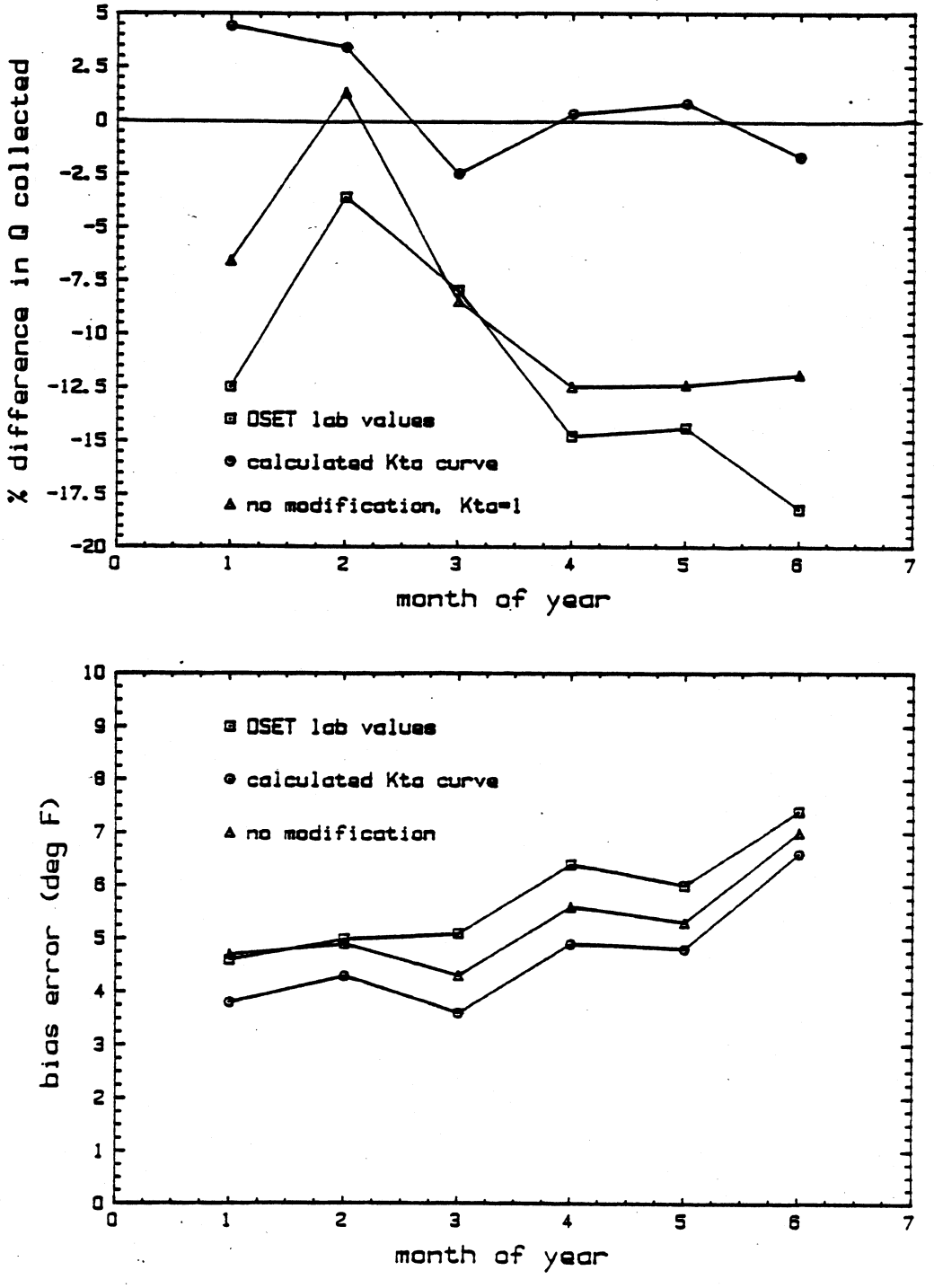

Figure IV.6: TRNSYS simulation results using calculated and laboratory test values for $K_{\tau\alpha}$ and also no modification.

Month	Q measured (total Btu x 10^6)	Q TRNSYS	Bias Error (deg F)	Percent Dif (%)
JAN	31.55	29.46	4.7	-6.6
FEB	33.76	34.21	4.9	1.3
MAR	43.89	40.14	4.3	-8.5
APR	42.72	37.39	5.6	-12.5
MAY	38.72	33.91	5.3	-12.4
JUN	26.57	23.41	7.0	-11.9
SUM	217.21	198.53	---	-8.3

Mean Bias Error = 5.3

Table IV.7: Cherokee simulation results with with origonal collector model, design $F_R(\tau\alpha)_n$ and F_RU_L values, and $K_{\tau\alpha} = 1.0$ for all angles.

Figure IV.6a shows once again the magnitude of the simulation error when using the laboratory test values for $K_{\tau\alpha}$ as TRNSYS input. As expected, the best results are obtained when using the calculated values. In general, better results are obtained when using no modification than when using the laboratory test values. These trend is also seen in the bias error curves, Figure IV.6b.

IV.3.4 Simulation with ETC Capacitance Model

Each of the six simulation was again repeated using the new collector model which accounts for capacitance effects. The capacitance model is explained in

section III.4.2 and requires additional parameters to describe the drainback characteristics of the subsystem, the mass of the fluid in the filled array, and the effective capacitance of the collector. As described earlier, the effective capacitance of the SUNPACK collector was determined to be 1.7 Btu/ft^2 F. The results obtained from simulations using the new model are given in Table IV.8. Design values were used for the input parameters $F_R(\tau\alpha)_n$, F_RU_L and $K_{\tau\alpha}$.

Month	Q measured (total Btu x 10^6)	Q TRNSYS	Bias Error (deg F)	Percent Dif (%)
JAN	31.55	30.03	3.4	-4.8
FEB	33.76	32.62	3.8	-3.7
MAR	43.89	42.01	4.5	-4.3
APR	42.72	40.16	5.3	-6.0
MAY	38.72	37.31	4.2	-3.6
JUN	26.57	24.32	5.5	-8.5
SUM	217.21	206.45	---	-4.9

Mean Bias Error = 4.5

Table IV.8: Cherokee simulation results using new capacitance model and design $F_R(\tau\alpha)_n$, F_RU_L, and $K_{\tau\alpha}$ values.

Accounting for the effects of capacitance and the filling of the collector improves simulation results by an average of seven percentage points. Much of the remaining error in these simulation results is again due to using the design values for incidence angle modifiers. To isolate this problem, the simulations were repeated using the calculated $K_{\tau\alpha}$ curve as input. ASHRAE test values were used for the

parameters $F_R(\tau\alpha)_n$ and F_RU_L. These simulation results are listed in Table IV.9.

Month	Q measured (total Btu x 10^6)	Q TRNSYS	Bias Error (deg F)	Percent Dif (%)
JAN	31.55	30.91	2.1	-2.0
FEB	33.76	33.05	2.7	-2.1
MAR	43.89	42.71	2.7	-2.7
APR	42.72	40.23	3.8	-5.8
MAY	38.72	37.31	3.0	-3.6
JUN	26.57	25.32	4.6	-4.7
SUM	217.21	209.56 3	---	-3.5

Mean Bias Error = 3.1

Table IV.9: Cherokee simulation results using new capacitance model, design $F_R(\tau\alpha)_n$ and F_RU_L values, and calculated $K_{\tau\alpha}$ values.

The simulation accuracy of these cases is shown in Figure IV.7. Here, the results from initial simulations and simulations using the new capacitance model both with original and calculated sets of incidence angle modifiers are compared. As expected, the greatest improvement are seen in the bias error. Figure IV.7b shows that the outlet temperature prediction of the capacitance model is consistently about three degrees better than the prediction of standard TRNSYS model. This difference is significant because good temperature predictions are needed to simulate collector control. Note that the predicted values of energy collected are also improved but they are still consistently low.

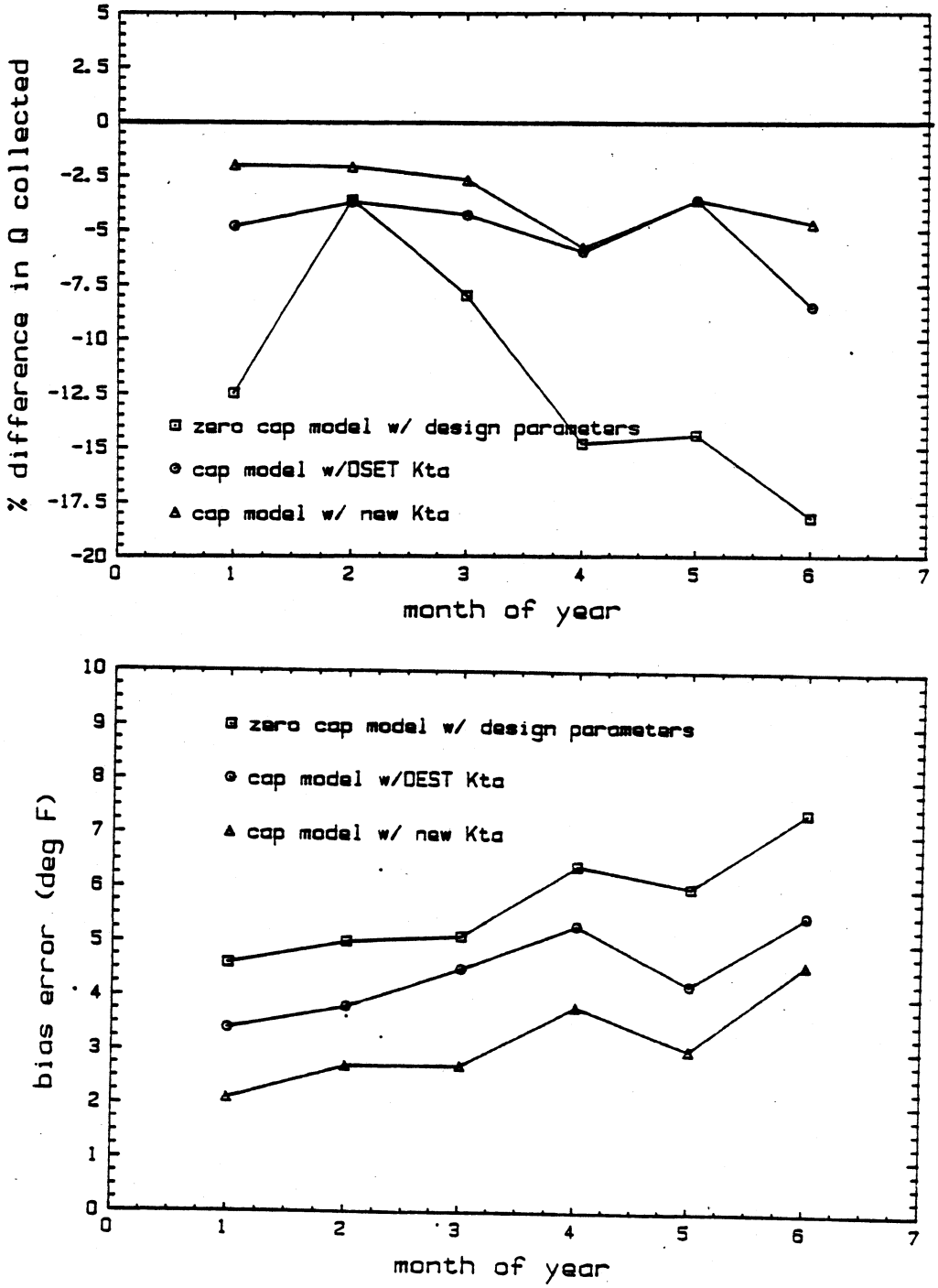

Figure IV.7: TRNSYS simulation results using the origonal and capacitance collector models.

Some of the under prediction in these simulations is a results of using the ASHRAE $F_R(\tau\alpha)_n$ and F_RU_L values that are slightly low as shown in Table IV.3. As a final comparison, the monthly calculated values for these parameters were used in simulation with the capacitance collector model and the calculated $K_{\tau\alpha}$ curve. These results are given in Table IV.10.

Month	Q measured (total Btu x 10^6)	Q TRNSYS	Bias Error (deg F)	Percent Dif (%)
JAN	31.55	31.97	1.9	1.3
FEB	33.76	32.80	2.1	2.7
MAR	43.89	44.21	1.9	0.7
APR	42.72	43.43	3.2	1.7
MAY	38.72	37.33	2.9	-3.5
JUN	26.57	26.25	2.5	-1.2
SUM	217.21	215.99	---	-.06

Mean Bias Error = 2.4

Table IV.10: Cherokee simulation results using new capacitance model and calculated $F_R(\tau\alpha)_n$, F_RU_L, and $K_{\tau\alpha}$ values.

The last comparison is shown in Figure IV.8 which shows simulation results for the final and initial cases. The improvements are obvious, but it is important to note that the final case uses calculated parameters that are only obtainable from data of the system in field operation. This information is obviously not available when design simulations of a system are run. The results presented, however, are helpful in

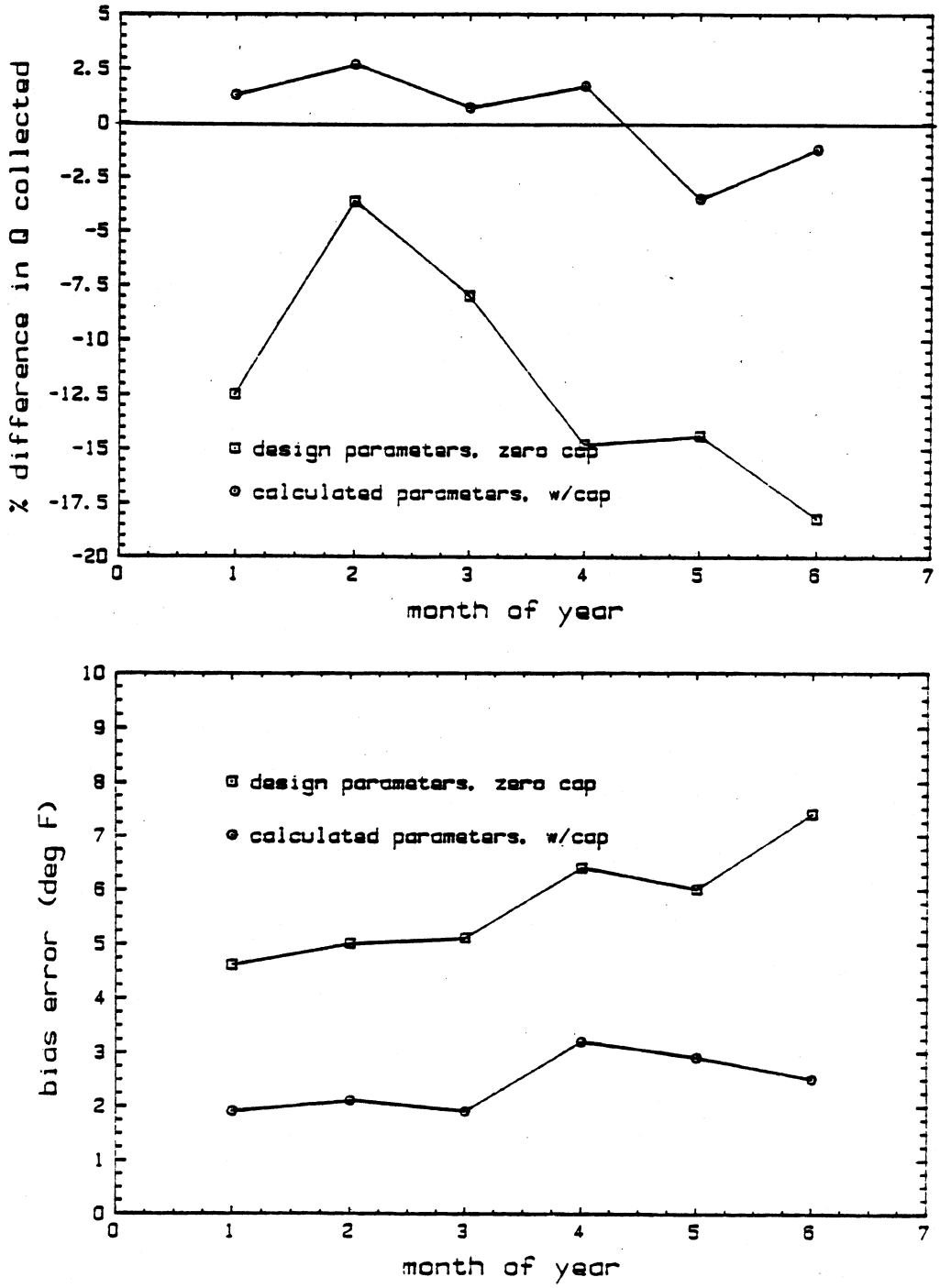

Figure IV.8: TRNSYS simulation results for initial and final case simulations.

understanding the difference between designed and actual performance and the influence of the parameters studied on the simulation results. The important improvements result from including the capacitance effects in the collector model. These and other conclusions are discussed in Chapter VII.

CHAPTER V

The ETC System at the Gainesville Job Corps Center

This chapter describes the solar ETC system at the Gainesville Job Corps Center. The overall performance of the system is described and problems associated with its design and operation are discussed. Simulation results and comparisons with measured performance are also presented.

V.1 Overview of the System

The Gainesville ETC system is a retrofit which was designed to contribute solar energy to the hot water and space cooling loads of a 18,000 square foot cafeteria building. Figure V.1 shows the schematic of the system which includes flow loops for the collector, space cooling, and water heating subsystems. The solar array consists of 192 non-draining ETCs with a total gross area of 6,144 square feet. Heated collector fluid flows into a 3,000 gallon main storage tank which supplies energy to a DHW preheat tank through an internal heat exchanger. Energy is supplied directly to a 25 ton Arkla LiBr absorption chiller. Auxiliary energy for water heating is provided by a liquid propane gas burner and an electric chiller is the auxiliary supply for space cooling.

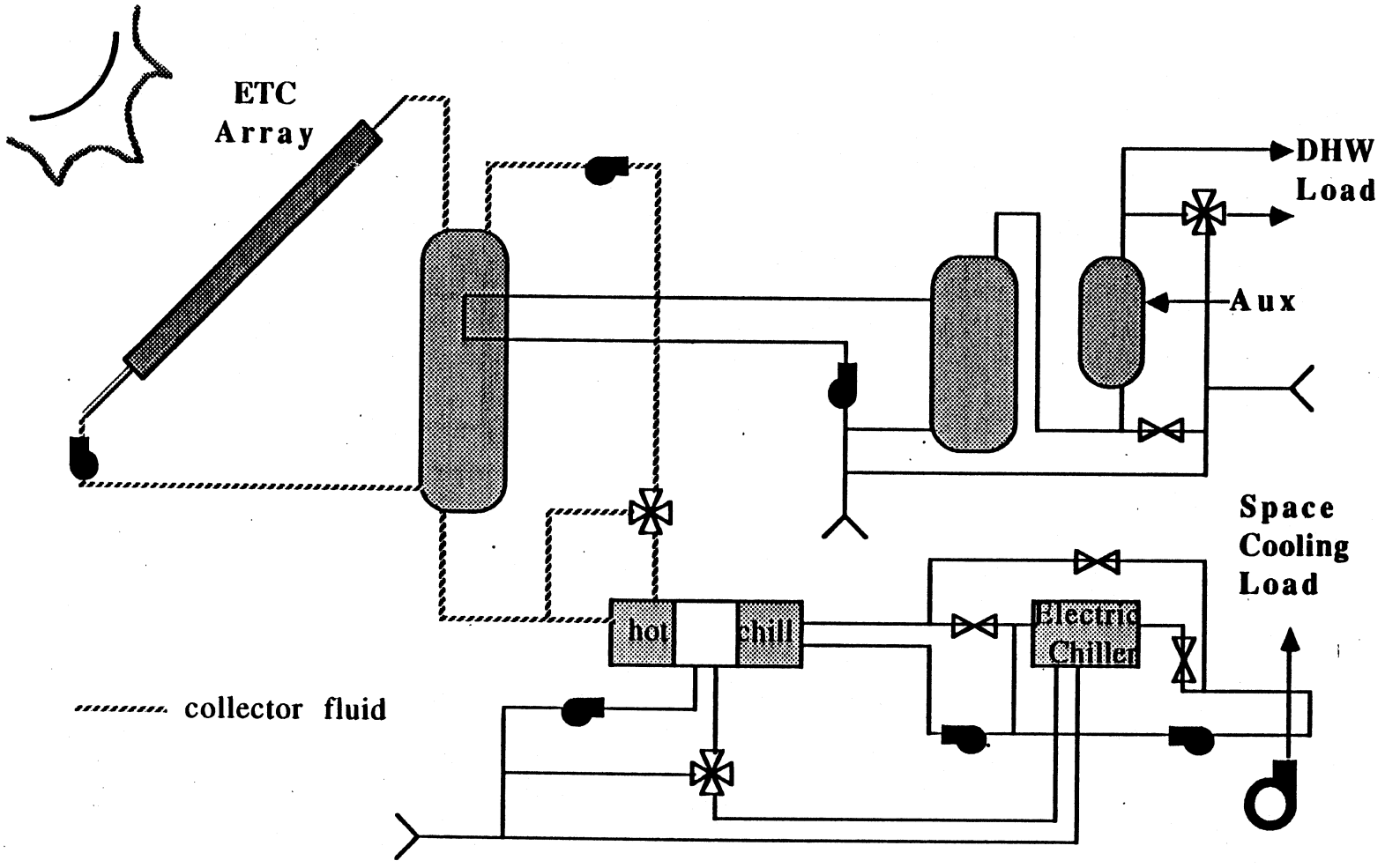

Figure V.1: Gainesville Job Corps Center solar system schematic (from Reference [20]).

The ETCs in this system are the Owens Illinois SUNPACK Model 1004. This model consists of 24 tubes in a series flow arrangement which are located on both sides of a center manifold. Specular cusp reflectors are used behind each tube. The array is oriented due south and is tilted at an angle of 25 degrees from the horizontal. The flow rate though the collector is 79 gpm (6.43 lbm/hr ft2). The values of $FR(\tau\alpha)n$= 0.496 and FRUL=0.240 Btu/hr ft2 F were determined from DSET Laboratories using the ASHRAE 93-77 test procedures and a flow rate of 10.93 lbm/hr ft^2.

The collector array is controlled by a differential temperature sensor which activates flow through the array when the collector fluid is 18 degrees F warmer than the fluid temperature at the bottom of the storage tank. The pump is turned off when a 3 degree temperature difference is reached or when the tank temperature rises above 210 degrees F to protect against boiling. If the array temperature rises above 240 degrees, cold water is circulated through the collector and drained onto the ground. City water is also circulated through the array as a freeze protection method if the temperature of the collector fluid falls below 35 degrees.

The load pumps for this system operate on a seasonal control. In the summer, cooling is favored and the DHW subsystem is used only after this load is met. In the winter mode, the chiller pumps do not operate and solar energy is only delivered to the DHW loads.

More detailed information about the Gainesville solar energy system and its components can be found in Reference [20].

V.2 System Performance

The performance of the Gainesville system was monitored from January to September, 1985. The total solar insolation and the number of heating and cooling degree days were within two percent of the long term averages for this location. The total energy flows from the period of January through June are shown in Figure V.2. The overall collector efficiency is 24%. Seventy-two percent of the energy collected was delivered to the loads, meeting 80% of the DHW and 100% of the space cooling needs of this facility over the monitoring period. The solar delivered energy corresponds to a net savings of about $1,500.

The low overall collector efficiency was attributed to high night losses from the array. Vitro stated that the average nighttime drop in temperature was near 80 degrees F for the over 1700 gallons of water in the collector.(Reference [20]) This represents a serious loss of energy which could have been avoided by a drainback design. As a results of this cooling, morning operation was delayed until the control set point was met. Typically, operation did not begin until about 10:00 to 11:00 a.m. which the Vitro report attributed to the high night losses. However, there also appeared to be a problem with the differential temperature sensor because the recorded array temperature usually met the control criteria about ten to twenty time steps (about one to two hours) before the pump was initiated. This problem was difficult to asses, however, because the measured array temperature was not the same sensor used for control. No information was available about the location or the accuracy of the actual control sensor

In the Vitro report on the Gainesville system (Reference [20]) the ETC performance is compared to that at Cherokee. It is noted that the overall collector

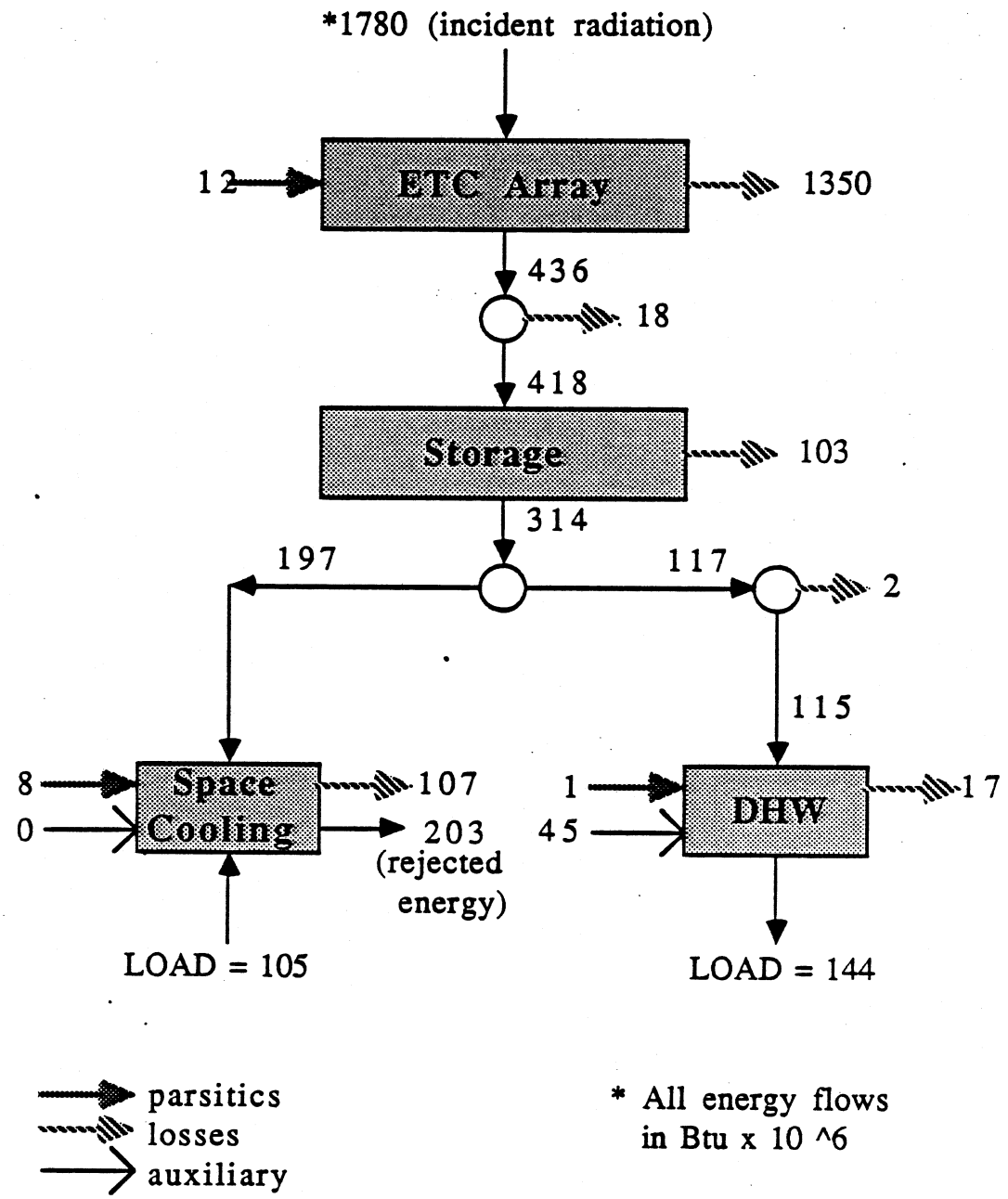

Figure V.2: Gainesville system energy flows from Jan - June 1985 (from Reference [20]).

operational efficiency (efficiency during flow) from March through June was 46% for the Gainesville system and 27% for Cherokee. Vitro attributes this difference to the spacing of the collector tubes despite the use of reflectors; the Gainesville tubes are spaced four inches apart (axis to axis) while six inches are between the Cherokee tubes. With 50% more tube per square foot, the Gainesville array was about 60% more efficient. Because of this behavior, they state that it is apparent the reflectors did not have much of an influence on performance.

The losses from the main storage tank were greater than expected due to poor insulation and thermosiphoning. The heavy tank insulation was cracked and not in good contact with the tank surface. The R value for the tank was reduced from 33 (design specifications) to only 7 hr ft^2 F/Btu. Thermosiphoning regularly occurred as energy was lost from the storage tank through a short connecting pipe and to the DHW preheat tank which was typically about 80 degrees cooler. This was a problem in the summer months when priority was given to space cooling and the DHW solar subsystem was seldom used.

V.3.2 **Collector Subsystem Simulation**

As in Chapter IV, results are presented from simulation with eight different combinations of collector model and parameter inputs. A typical TRNSYS deck for the Gainesville system is listed in Appendix F. For each case, measured versus predicted performance is listed for each of six two week simulations periods. The results of each simulation are again expressed by the percent difference between the total predicted and measured energy collected (Eqn IV.3.1) and by the bias error of the outlet temperature predictions (Eqn IV.3.2).

V.3.1 Initial Simulation

The first simulations run for each period uses the original TRNSYS collector model and DSET laboratory values for the collector test parameters and incidence angle modifiers. The design value for the outlet piping insulation of R=6 was used. These results are presented in Table V.1.

Month	Q measured (total Btu x 10^6)	Q TRNSYS	Bias Error (deg F)	Percent Dif (%)
APR	52.14	47.80	6.2	-8.3
MAY	42.34	42.76	8.0	1.0
JUN	48.72	40.14	5.6	-17.6
JUL	43.85	33.58	7.2	-23.4
AUG	41.09	21.91	16.9	-46.7
SEP	29.37	22.26	9.9	-24.2
SUM	257.51	208.45	---	-19.07

Mean Bias Error = 8.9

Table V.1: Gainesville simulation results using original collector model and design values for $F_R(\tau\alpha)_n$, $F_R U_L$, $K_{\tau\alpha}$, and pipe insulation.

It is immediately obvious that these results do not correspond as well as do those of the initial simulation results for Cherokee. The largest discrepancy is for the month of August. It was found that there were problems with the measured flow rate throughout this month; the pump cycled frequently for no apparent reason and

the recorded flow rates were questionable. There were many time steps when the flow rate was listed as 0.0, although the inlet and outlet temperature readings indicated that there was flow. This caused the simulation results for the zero capacitance model to be much lower than measured values. Steady state conditions were reached each time the pump restarted and the heating of the fluid during the off period was not accounted for. The data was used as TRNSYS input despite these errors to show comparison between the different simulation cases. Other problems found with the Gainesville data will be discussed throughout this chapter.

The simulations were then repeated replacing the design R value for the outlet piping insulation with the effective value of 1.5 hr ft^2 F/Btu which was determined from the system data. Like the Cherokee simulations, there was an insignificant change in the results which are listed in Table V.2.

Month	Q measured (total Btu x 10^6)	Q TRNSYS	Bias Error (deg F)	Percent Dif (%)
APR	52.14	47.79	6.2	-8.3
MAY	42.34	42.76	8.1	1.0
JUN	48.72	40.13	5.6	-3.0
JUL	43.85	33.57	7.3	-10.6
AUG	41.09	21.91	16.9	-46.7
SEP	29.37	22.25	9.8	-24.2
SUM	261.22	208.41	---	-15.47

Mean Bias Error = 8.9

Table V.2: Gainesville simulation results using original collector model, design values for $F_R(\tau\alpha)_n$, F_RU_L, $K_{\tau\alpha}$, and calculated pipe loss factors.

V.3.2 Simulations with New $F_R(\tau\alpha)_n$ and F_RU_L Values

The values for the collector parameters $F_R(\tau\alpha)_n$ and F_RU_L were derived from the system data for each simulation period as was done for the Cherokee system in the previous chapter. To compare the calculated values to the laboratory test results, corrections had to be made for flow rate. For this collector, the laboratory test were run at a flow rate of 10.93 lbm/hr ft2 (115 gpm) while the operating flow rate is 7.5 lbm/hr ft2 (79 gpm). The ratio of the test to use values for the collector parameters is given by:

$$r = \frac{(F_R U_L)_{use}}{(F_R U_L)_{test}} = \frac{(F_R(\tau\alpha)_n)_{use}}{(F_R(\tau\alpha)_n)_{test}}$$

$$= \frac{\frac{\dot{m}C_p}{A_c F' U_L}\left(1 - \exp\left(-A_c F' U_L / \dot{m}C_p\right)\right)_{use}}{\frac{\dot{m}C_p}{A_c F' U_L}\left(1 - \exp\left(-A_c F' U_L / \dot{m}C_p\right)\right)_{test}} \qquad \text{(V.3.1)}$$

where $F'U_L$ is calculated using Eqn III.4.13. The resulting value of r from this equation is 0.98.

Plots of the operating point, $(T_i - T_a)/I_t$, versus efficiency, η, were generated from the data for each period of simulation. Data were only used from time steps when the beam radiation was at or near normal incidence and when flow had been steady for at least an hour, however there was a great deal of scatter in the values. Two examples are shown in Figure V.3 of the resulting plots for the months of June and September. The regression line and the DSET test curve are shown. Table V.3 shows the calculated slope and intercept and the values for standard deviation, σ, and R^2 for each of the months.

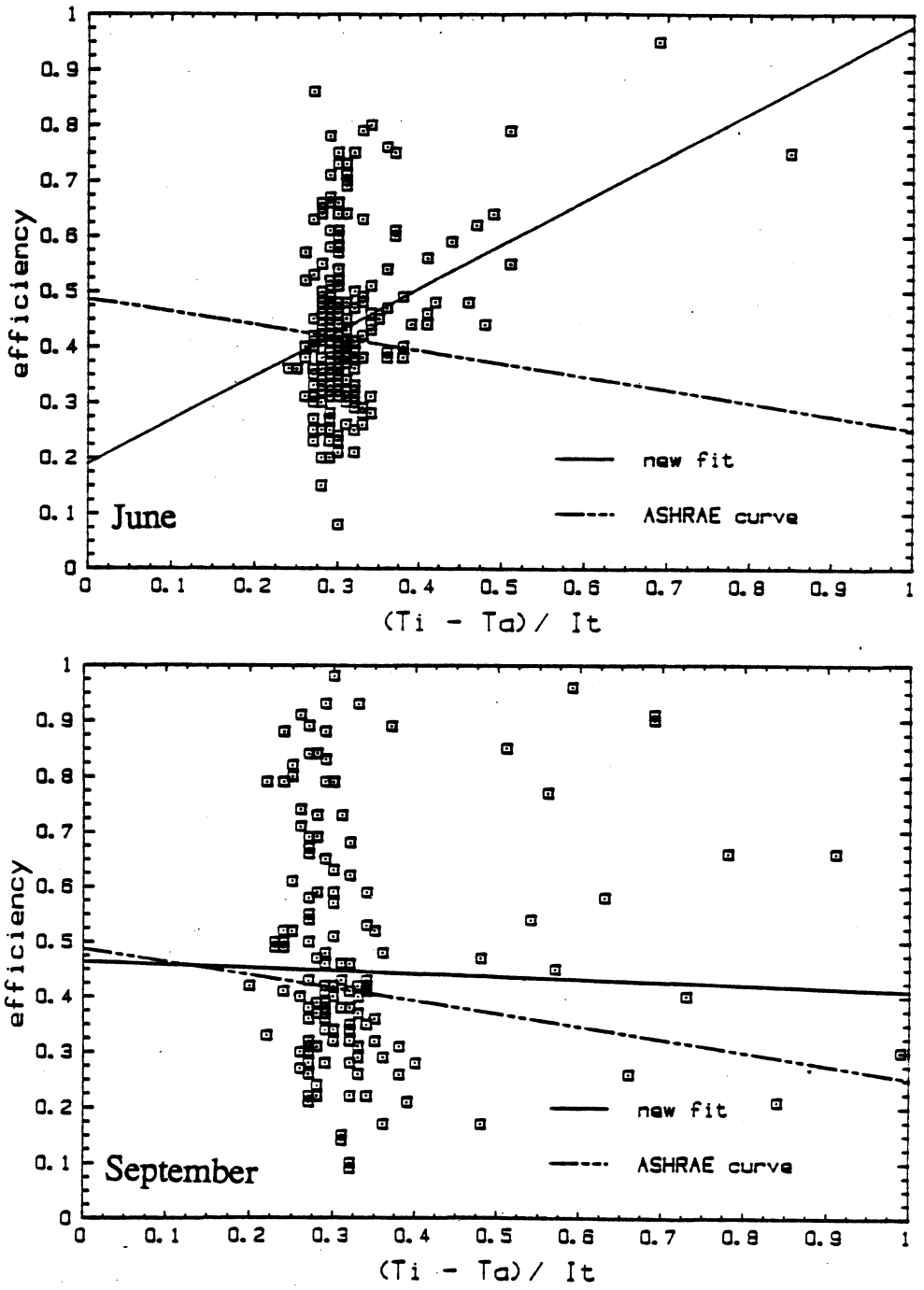

Figure V.3: Generated test curves from system data with radiation at normal incidence.

month	$F_R(\tau\alpha)_n$	$F_R U_L$	σ	R^2
APR	0.182	0.470	0.052	0.260
MAY	0.283	0.190	0.083	0.071
JUN	0.190	0.790	0.040	0.178
JUL	0.249	0.621	0.149	0.290
AUG	0.295	0.403	0.203	0.090
SEP	0.463	0.054	0.211	0.010
AVE	0.277	0.421	0.124	0.149
ASHRAE Test Values (corrected for flow rate)	0.486	-0.220	-----	-----

Table V.3: Calculated values for $F_R(\tau\alpha)_n$ and $F_R U_L$ for each simulation period

The poor results from these curve fits show that the performance of the Gainesville collector is not well characterized by a straight line. The average standard deviation value is 0.125, compared to a value of 0.072 for the Cherokee data. There are many possible reasons for this scatter. Some measurement error is likely, however the magnitude is difficult to estimate. Vitro stated that there were problems with the inlet temperature sensor (Reference [20]) which was replaced in July, although no specific details were given. There were also some problems with poor radiation measurements which were found when the radiation was converted from the tilted surface to the horizontal surface value. The clearness index, K_T, (defined by equation III.3.6) was found to be greater than 1 for about 50 time steps over each two week period, meaning that the measured radiation exceeded the extraterrestrial radiation. This error usually occurred at hours early in the day when

the radiation values were low. This does not have a noticeable effect on the results because the radiation converter substitutes the extraterrestrial value, but this could be indicative of general problems with the radiation pyranometer. The flow measurements used in the efficiency calculations were not as consistent as were the values for Cherokee. The measured flow rate fluctuated over about a 7 gpm range. This could indicate either inconsistent flow or measurement error; both problems would cause scatter in the efficiency plots. There was also the problem with the poor flow measurements for the month of August that were previously mentioned. Because of the many problems associated with the values in Table V.3, no attempts were made to use these parameters as collector inputs.

Instead, an average operational collector efficiency was calculated for each period of simulation data. This value was used as a collector parameter by setting $F_R(\tau\alpha)_n = \eta_{ave}$ and $F_R U_L = 0.0$. This was tried because the values obtained from the regressions were useless parameters to describe the collector efficiency. Also, the calculated curve fits of the more uniform Cherokee data were very close to representing the average efficiency value (refer to section IV.3.2). Table V.4 shows that average efficiencies calculated for each period.

Month	APR	MAY	JUN	JUL	AUG	SEP	ALL DATA
Ave η (%)	42.6	35.2	45.0	47.5	44.7	48.2	43.8

Table V.4: Average operational collector efficiencies for each simulation period.

The simulation results obtained when using these values as collector input are shown in Table V.5. Figure V.4 shows the comparison of accuracy (Q collected percent

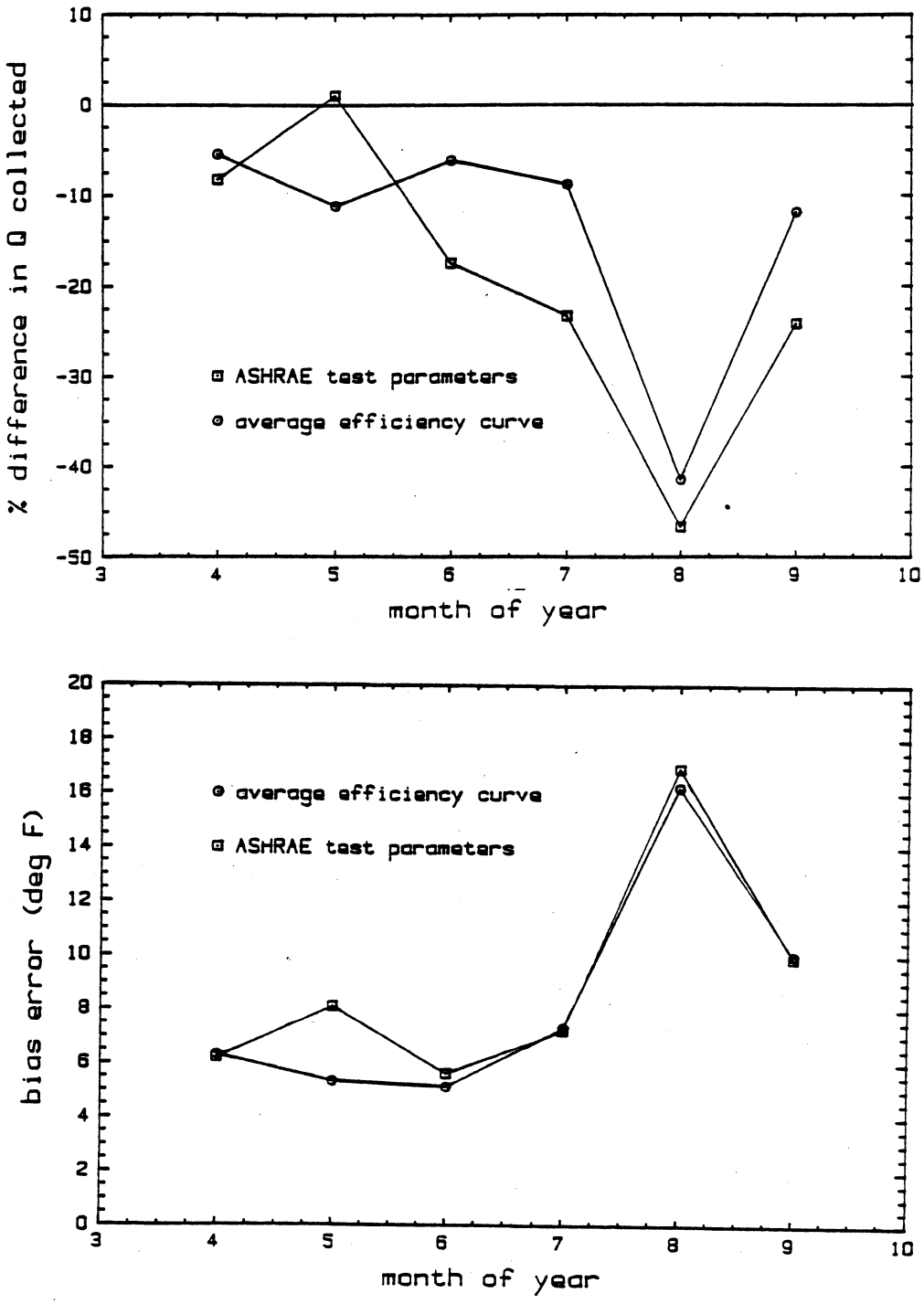

Figure V.4: TRNSYS simulation results using calculated and ASHRAE test parameters.

difference and outlet temperature bias error) from these simulations and the initial simulations which used the laboratory test collector performance parameters.

Month	Q measured (total Btu x 10^6)	Q TRNSYS	Bias Error (deg F)	Percent Dif (%)
APR	52.14	49.29	6.3	-5.5
MAY	42.34	37.57	5.3	-11.3
JUN	48.72	45.72	5.1	-6.2
JUL	43.85	39.92	7.3	-8.9
AUG	41.09	24.05	16.2	-41.5
SEP	29.37	27.87	10.0	-11.6
SUM	257.51	222.42	----	-13.63

Mean Bias Error = 8.4

Table V.5: Gainesville simulation results using original collector model, average efficiency input, and laboratory $K_{\tau\alpha}$ values.

Simulation results improved as expected when using the calculated average efficiency as input for $F_R(\tau\alpha)_n$ and F_RU_L. The only exception is the Q collected percent difference value for May, but these results are misleading. The original low percent difference results from a combination of under prediction early in the day (because the zero capacitance model used does not account for the heating of the array before operation begins) and over prediction throughout the day because the DSET test parameters over predict operational efficiency. The lowered bias error is a better indication of the model improvements. The simulation results for August

still appear very poor, but this is due to the problem with the measured data which were earlier cited. for the reasons earlier cited.

V.3.3 Simulation with New $K_{\tau\alpha}$ Values

The calculation of a new $K_{\tau\alpha}$ was repeated as in Chapter IV. Again, the new values were calculated using equation III.4.22, but in this case, the ASHRAE test values were not substituted. Instead, the values of $F_R(\tau\alpha)_n = 0.438$ and $F_R U_L = 0.0$ which represents the average efficiency calculated from the data. This line was the best indication of the collector efficiency behavior at angles of normal incidence. A third order regression was performed on the more than 4,000 data point and the resulting curve fit is expressed in the following equation.

$$K_{\tau\alpha} = 0.995871 - 0.001962\,\Theta - 0.000042\,\Theta^2 + 0.000001\,\Theta^3 \qquad \text{(V.3.1)}$$

The standard deviation for this is 0.316 and the R^2 value is .033. The resulting values for $K_{\tau\alpha}$ are compared to the laboratory test values in Table V.6 and in Figure V.5.

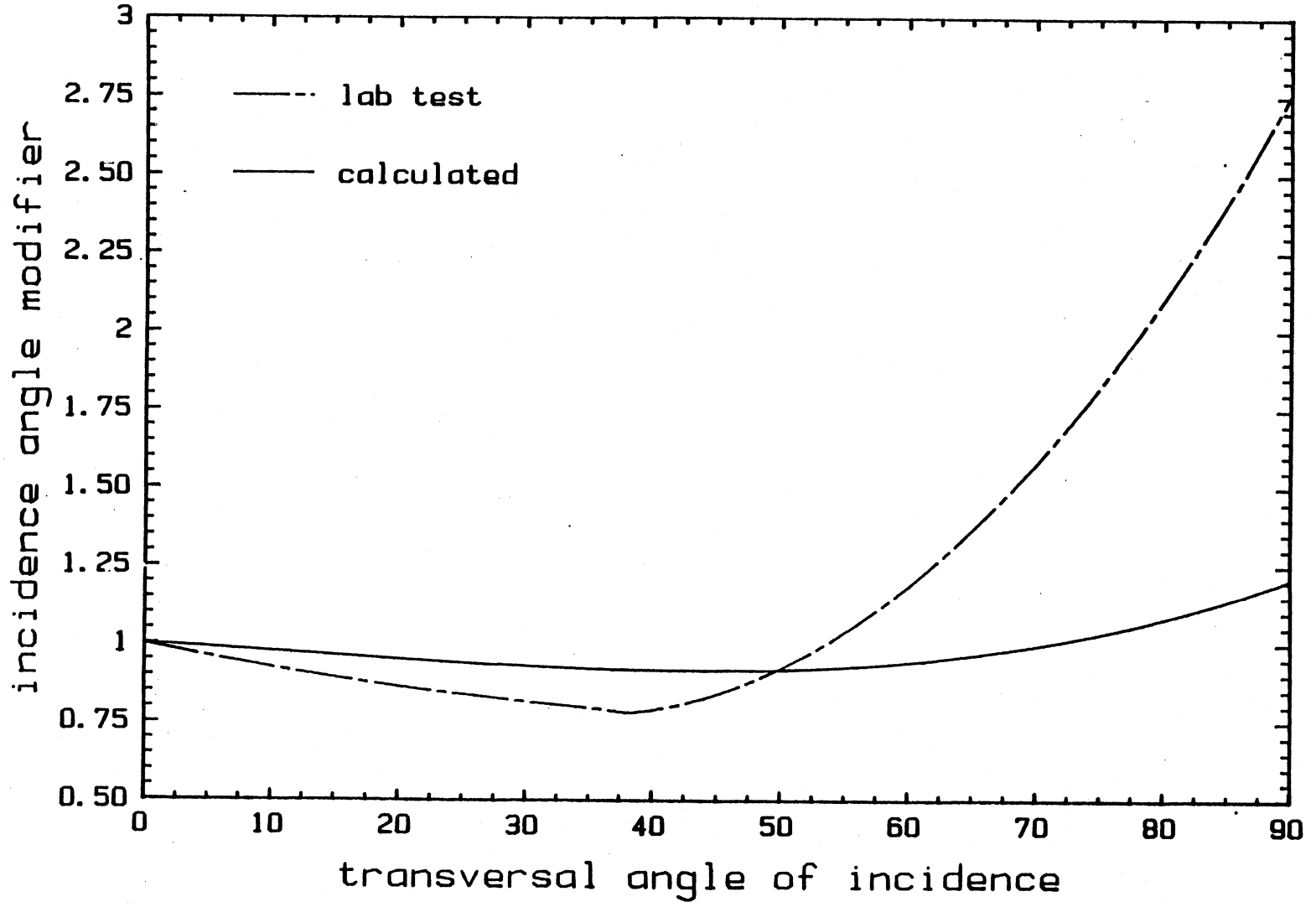

Figure V.5: Transversal incidence angle modifer calculated from all data.

Θt	0	10	20	30	40	50	60	70	80	90
$K_{\tau\alpha}$ Calculated from Data	1.0	1.02	1.04	1.09	1.17	1.26	1.35	1.43	1.48	1.50
$K_{\tau\alpha}$ DSET Lab Test	1.1	.92	.86	.81	.80	.92	1.18	1.58	2.10	2.76

Table V.6: Transversal incidence angle modifier comparison.

The fit for the Gainesville $K_{\tau\alpha}$ values were significantly poorer than the Cherokee data fit; the R^2 values were 0.032 and 0.179, respectively. Inconsistency in the Gainesville performance data was again apparent. The results do show, however that using the average efficiency curve is a good representation of the performance at normal incidence because the fitted $K_{\tau\alpha}$ at $\Theta = 0$ is 1.0. When the laboratory test $F_R(\tau\alpha)_n$ and F_RU_L values were used, the fitted $K_{\tau\alpha}$ at $\Theta = 0$ was 0.94, indicating that the performance was overestimated. This reasoning follows directly from the Hottel-Whillier equation, Eqn. III.4.1.

The new $K_{\tau\alpha}$ values were then used as simulation input along with the performance parameters which represented the monthly average efficiency. The data from the corresponding simulation results are presented in Table V.7.

Month	Q measured (total Btu x 10^6)	Q TRNSYS	Bias Error (deg F)	Percent Dif (%)
APR	52.14	50.84	5.0	-2.5
MAY	42.34	39.68	4.1	-6.3
JUN	48.72	42.54	4.2	-12.7
JUL	43.85	37.37	5.7	-14.8
AUG	41.09	28.99	15.9	-29.4
SEP	29.37	26.82	8.5	-8.7
SUM	257.51	226.24	---	-12.24

Mean Bias Error = 7.2

Table V.7: Gainesville simulation results using original collector model and calculated values for $F_R(\tau\alpha)_n$, F_RU_L, and $K_{\tau\alpha}$.

Consistent improvements in the simulation results are apparent although the error is still relatively high. Compared to the last simulations, the average bias error improved from 8.4 to 7.2 degrees, while the same corrections for the Cherokee simulations resulted in a bias error improvement from 5.7 to 4.6 deg F. The average percent difference improved 1.5 percentage points, but is still high due to the lack of fit for the calculated test curve parameters and incidence angle modifiers.

The simulations were again repeated with no incidence angle modification. These results are presented in Table V.8. Comparison of this data and other simulation results using the original and calculated incidence angle modifier values are shown in Figure V.6.

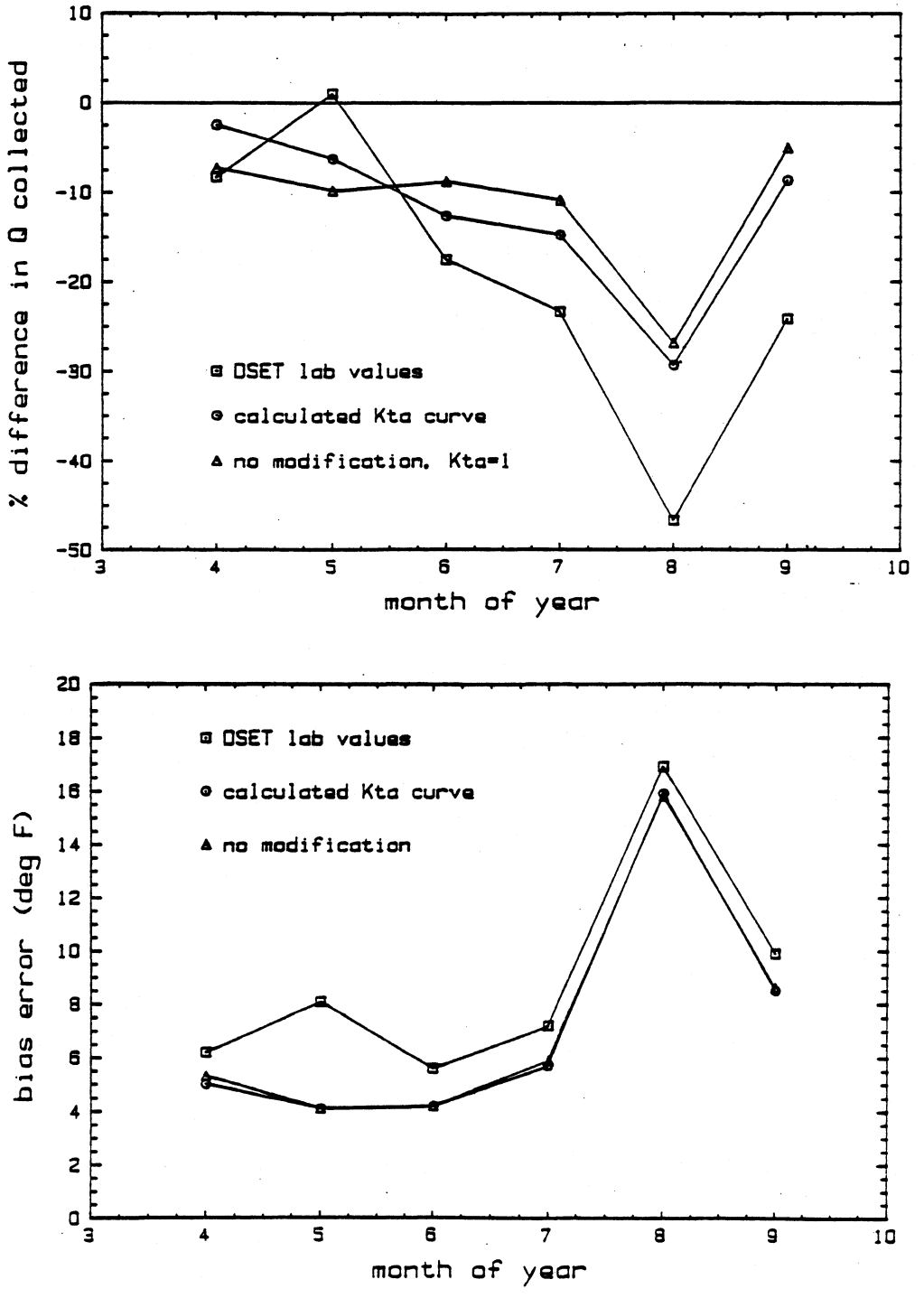

Figure V.6: TRNSYS simulation results using calculated and laboratory values for $K_{\tau\alpha}$ and also no modification.

Month	Q measured (total Btu x 10^6)	Q TRNSYS	Bias Error (deg F)	Percent Dif (%)
APR	52.14	48.32	5.2	-7.3
MAY	42.34	38.15	4.1	-9.9
JUN	48.72	44.41	4.2	-8.8
JUL	43.85	39.08	5.9	-10.9
AUG	41.09	30.05	15.8	-26.7
SEP	29.37	27.87	8.6	-5.1
SUM	257.51	227.88	----	-11.5

Mean Bias Error = 7.3

Table V.8: Gainesville simulation results using original collector model, calculated values for $F_R(\tau\alpha)_n$, F_RU_L, and no incidence angle modification.

These results show very little change from the simulations run with the calculated $K_{\tau\alpha}$ and actually show improvement over results from the simulations using the laboratory values.

V.3.4 Simulation with ETC Capacitance Model

The six simulations were again repeated using the collector model that accounts for capacitance. For the Gainesville system, the non-draining mode was used. The effective capacitance was determined to be 1.6 Btu/ft^2 F. The results for these simulations, which used design values for $F_R(\tau\alpha)_n$, F_RU_L, and $K_{\tau\alpha}$, are presented in Table V.9.

Month	Q measured (total Btu x 10^6)	Q TRNSYS	Bias Error (deg F)	Percent Dif (%)
APR	52.14	49.36	5.6	-5.3
MAY	42.34	44.05	4.2	0.3
JUN	48.72	50.74	4.6	4.2
JUL	43.85	36.58	5.1	-16.6
AUG	41.09	32.31	10.8	-21.4
SEP	29.37	27.69	8.1	-5.7
SUM	257.51	240.73	----	-11.5

Mean Bias Error = 6.4

Table V.9: Gainesville simulation results using capacitance collector model, design values for $F_R(\tau\alpha)_n$, F_RU_L, and $K_{\tau\alpha}$.

Accounting for the capacitance effects alone improves the average monthly value for the percent difference in energy collection by an average of eleven percentage points. The improvement was especially noticeable for the month of August during which there was a lot of pump cycling. The improvement due to capacitance modeling was greater for this system than Cherokee because of the non draining characteristics. The zero capacitance model under predicted temperatures at the beginning of operation as shown in Figure III.3. This is because original model does not account for the heating of the filled array before operation begins.

The simulations were repeated using the capacitance model but with the calculated average efficiency input and the calculated $K_{\tau\alpha}$ values. These simulation results are presented in Table V.10.

Month	Q measured (total Btu x 10^6)	Q TRNSYS	Bias Error (deg F)	Percent Dif (%)
APR	52.14	51.54	2.4	-1.1
MAY	42.34	40.66	2.4	-3.9
JUN	48.72	48.85	2.2	0.3
JUL	43.85	46.09	2.3	5.1
AUG	41.09	31.75	9.4	-15.3
SEP	29.37	28.90	6.1	-1.6
SUM	257.51	249.79	----	-5.1

Mean Bias Error = 4.1

Table V.10: Gainesville simulation results using capacitance collector model and calculated values for $F_R(\tau\alpha)_n$, F_RU_L, and $K_{\tau\alpha}$.

The comparison of the results from the two previous simulations is shown in Figure V.7. By using the calculated values for $F_R(\tau\alpha)_n$, F_RU_L, and $K_{\tau\alpha}$., the overall percent difference improved over six percentage points and the bias error was lowered 2.3 degrees. Again, the improvements were not as drastic as for the Cherokee simulations because the fitted values for the calculated parameters were not as good.

Figure V.7 also shows the comparison between the initial and final simulation. These results show that an average improvement in the percent difference of Q collected of ten percentage points per month is possible by using the capacitance model with the design collector parameters. This and other conclusions will be discussed in Chapter VII.

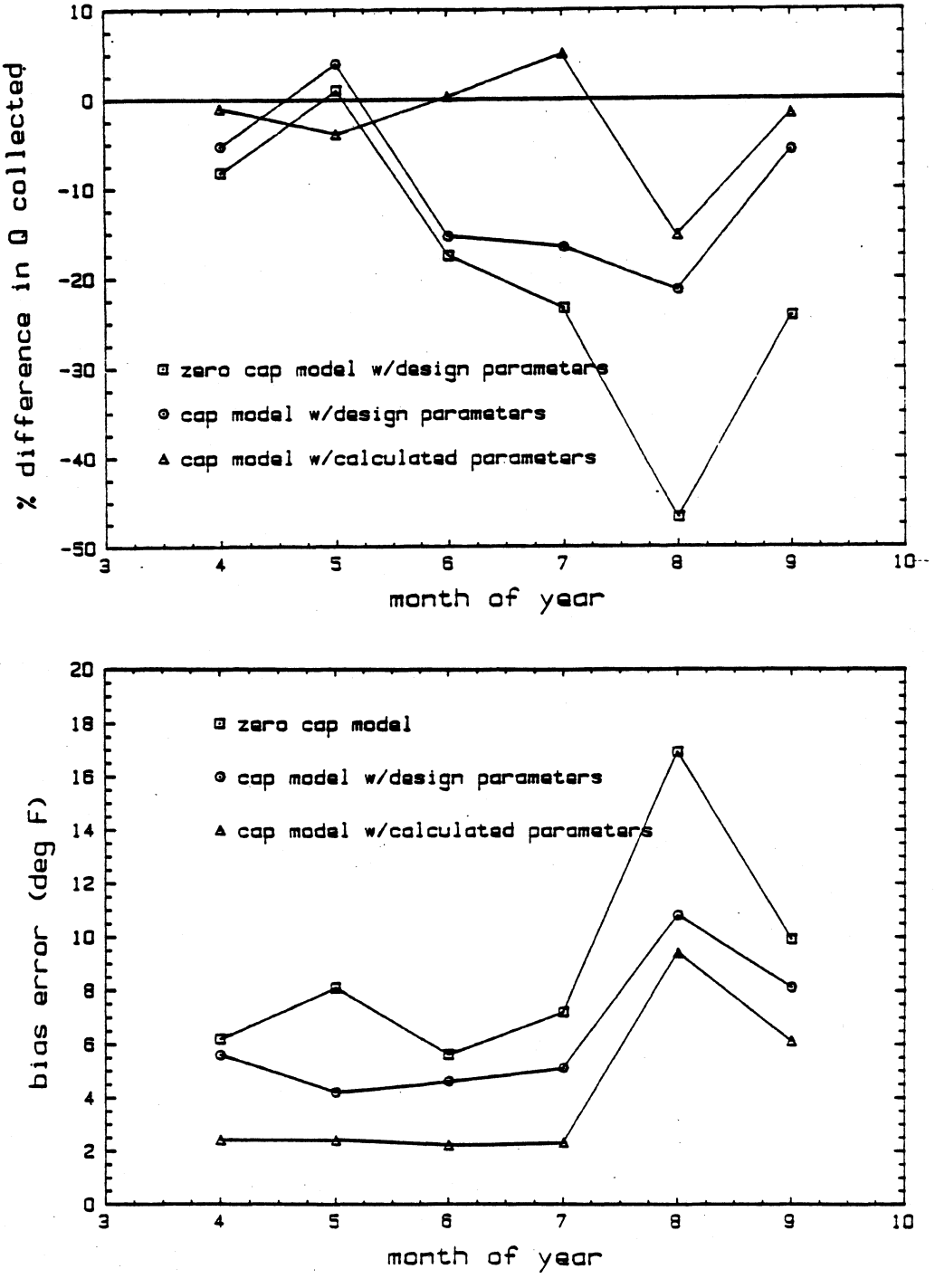

Figure V.7: TRNSYS simulation results using the origonal and capacitance collector models.

CHAPTER VI

Economics of ETCs

This chapter presents a brief overview of the economic analysis of solar heating systems and a comparison of cost of ETCs to traditional flat-plate collectors.

VI.1 Economics of Solar Heating Systems

The basic economic analysis of ETC system is no different than for any type of solar collector. The cost of a solar heating system can be expressed as:

$$C_S = C_A A + C_E \qquad \text{(VI.1.1)}$$

where:

C_A = area weighted costs, \$/ft^2

A = area of collector, ft^2

C_E = area independent equipment costs, \$

The life cycle savings associated with a solar heating system is the difference between the net solar contribution and system's costs over a given period of analysis. As given in Reference [16], this can be expressed as:

$$LCS = P_1 C_F L F - P_2 (C_A A + C_E) \quad \text{(VI.1.2)}$$

where:

C_F = cost of fuel, \$/Btu

L = heating load, Btu

F = fraction of the load met by the solar contribution

and P_1 is the ratio of life cycle fuel cost savings to the first year savings and P_2 is the ratio of the life cycle expenditures due to additional capital investment to the initial investment. For a non-income producing system, assuming that no money is borrowed for the initial investment, these parameters are defined as:

$$P_1 = PWF (N, i_f, d) = \sum_{j=1}^{N} \frac{(1 + i_f)^{j-1}}{(1 + d)^j} \quad \text{(VI.1.3)}$$

$$P_2 = 1 + [M_S + tx (1-tx) PWF (N,i,d) - RS / (1+d)^N \quad \text{(VI.1.4)}$$

where:

PWF = present worth factor

N = number of years of analysis

i_f = fuel inflation rate

d = market discount rate

M_S = ratio of first year miscellaneous costs to initial investment

tx = property tax rate based on assesed value

tx = effective income tax rate

RS = ratio of resale value at the end analysis period to initial investment.

For a given collector application, there exists an optimum where an increase of collector area to achieve a higher solar fraction decreases the overall economic benefit of the system. This area is determined by setting the first derivative of Eqn. VI.1.1 equal to zero and finding the area that satisfies the equation:

$$\frac{\partial F}{\partial A_C} = \frac{P_2 C_A}{P_1 C_f L} \qquad \text{(VI.1.5)}$$

This relationship is illustrated in Figure VI.1 which shows a typical curve of solar fraction versus collector area.

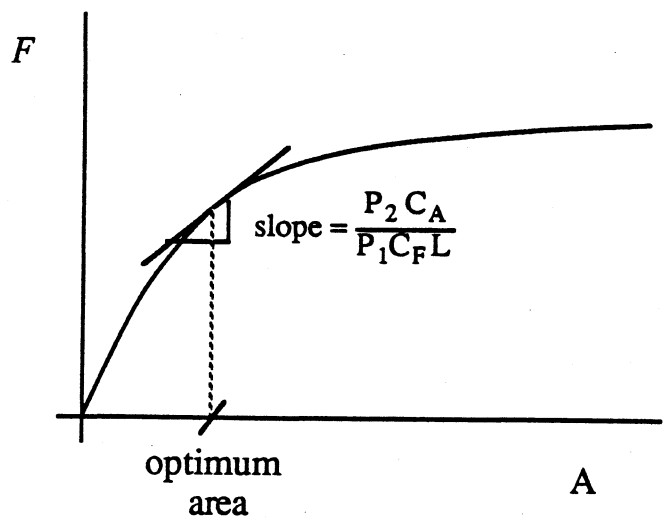

Figure VI.1: Optimum area for a typical area versus solar fraction curve.

VI.2 Cost Comparison of ETCs to Flat-Plate Collectors

An economic comparison of ETCs to flat-plate collector was made using the F-CHART solar design program (Reference [21]). As an example, an F-Chart model of the Cherokee system was made. The program was run using typical meteorological data for Asheville N.C. (about 35 miles from Cherokee) and collector parameters for both the SUNPACK ETC and a typical flat-plate collector. The following annual solar fractions were obtained: $F_{ETC} = 0.13$, $F_{FP} = 0.09$.

To compare the economic performance of the two system, the life cycle savings, as defined in Eqn. VI.1.2, are set equal and the following equation is obtained assuming the cost of fuel is the same for both systems:

$$F_{ETC} - F_{FP} = \frac{P_2}{P_1 C_F L}\left(C_{S,ETC} - C_{S,FP}\right) \qquad \text{(VI.2.1)}$$

This equation gives a general form for economic comparison of two different collector types. For this example, the following assumptions are made: equal equipment costs for both systems, 20 year analysis, 8% market discount rate, 6% fuel inflation rate, 4% general inflation rate, 100% resale value, no property tax, 1.5% of investment for insurance costs, fuel cost of \$5.50/1,000 ft^3 of natural gas, and an annual load of 6.05×10^9 Btu. Based on these values and the Cherokee system parameters, Eqn VI.2.1 reduced to:

$$F_{ETC} - F_{FP} = .00254\left(C_{A,ETC} - C_{A,FP}\right)$$

Substituting the solar fractions calculated by F-Chart for this example, the difference in price per square foot for an equal life cycle savings in determined to be $15.75. This means that for this applications, ETCs would be more economical if they could be bought for less than $15.75 per square foot over the price of flat-plate collectors. Many assumption were made in this example, but the same analysis could be applied to any comparison of collector types.

Average costs for both collector types were recently reported by the Energy Information Center of DOE (Reference [22]). For the total equipment shipments in 1985, the average cost for ETCs was $23.39 / ft^2 while the average for flat-plate collectors was $10.43 / ft^2. These costs are for the collectors alone and do not include installation. Based on this difference of $12.96 , ETCs would be more economical for the example presented, given the assumed economic parameters.

Information about the cost comparisons of ETCs and flat-plate collector systems was also available from a Vitro summary of the SFBP sites (Reference [23]). In this report, the total system cost in $ / ft^2 was listed for ever 20 systems. These figures included all of the solar heating system costs and miscellaneous expenses such as equipment costs, monitoring expenses, maintenance and installation. The average system cost for flat-plate collectors systems was $76.27 / ft^2 while the ETC systems averaged $78.88 / ft^2. This information indicates that although the ETC panels may be twice as expensive as flat-plate collectors, the overall system costs vary very little. The equipment costs associated with ETCs are lower because of a number of economic benefits associated with using the collector

with a higher overall efficiency. This cascading effect is shown in Figure VI.2. Given the lowered area independent cost for ETCs, the economic advantage is even greater than predicted in the last example.

Equation VI.2.1 gives a simple method for comparing the economic benefits of different collector types for a given application. In the example given, ETC systems were found to be a better choice, however a number of assumptions were made. Each solar heating application should be analyzed on an individual basis to compare the economics merits of the different collector types.

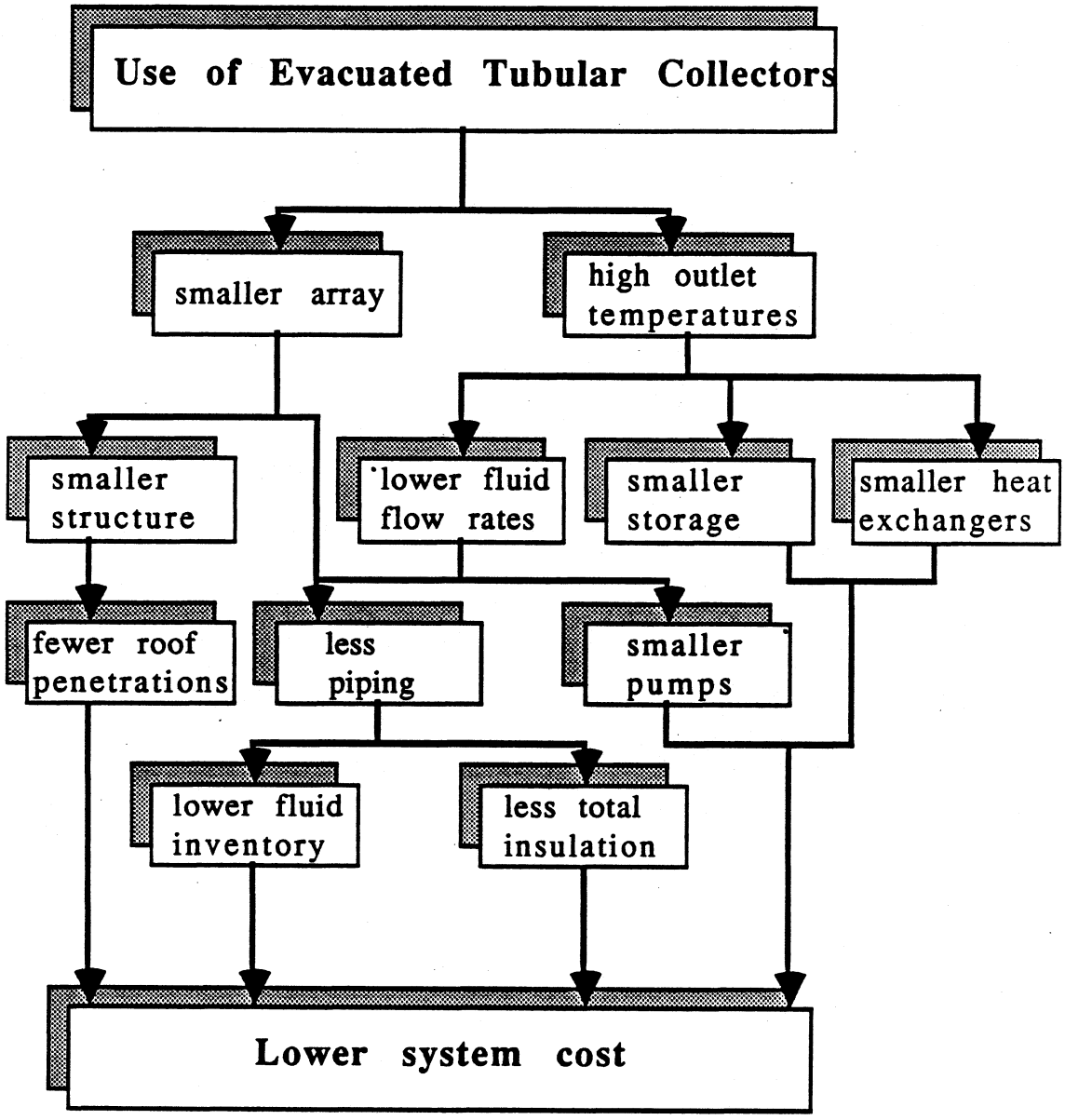

Figure VI.2: Cascading economic benefits of using ETC systems (from Reference [24]).

CHAPTER VII

Conclusions

This chapter compares the various simulation results for the Gainesville and Cherokee systems. Conclusions are drawn from the analysis presented in the previous chapters. Recommendations for further study are also given.

VII.1 Simulation Results

VII.1.1 Comparison of Cherokee Simulation Results

The TRNSYS results for the Cherokee system are summarized in Table VII.1 which presents the Q collected percent difference and outlet temperature bias error for simulated versus measured performance. The inputs and collector model used correspond to the following cases:

1. Original collector model, design values for $F_R(\tau\alpha)_n$, F_RU_L, $K_{\tau\alpha}$, and pipe losses.
2. Original collector model, design values for $F_R(\tau\alpha)_n$, F_RU_L, $K_{\tau\alpha}$, and calculated value for pipe losses.
3. Original collector model, design values for $K_{\tau\alpha}$, and calculated values for $F_R(\tau\alpha)_n$, F_RU_L.

simulation \ month		JAN	FEB	MAR	APR	MAY	JUN
1	%Δ	-12.5	-3.6	-8.0	-14.8	-14.4	-18.2
	Bias Error	4.6	5.0	5.1	6.4	6.0	7.4
2	%Δ	-12.8	-3.6	-8.6	-14.8	-14.3	-18.3
	Bias Error	4.7	5.0	5.1	6.4	6.0	7.4
3	%Δ	-9.1	1.2	-5.4	-7.3	-4.0	-7.5
	Bias Error	4.5	4.7	4.4	6.1	5.2	7.0
4	%Δ	4.4	3.4	-2.5	0.3	0.8	-1.7
	Bias Error	3.8	4.3	3.6	4.9	4.8	6.6
5	%Δ	-6.6	1.3	-8.5	-12.5	-12.4	-11.9
	Bias Error	4.7	4.9	4.3	5.6	5.3	7.0
6	%Δ	-4.8	-3.7	-4.3	-6.0	-3.6	-8.5
	Bias Error	3.4	3.8	4.5	5.3	4.2	5.5
7	%Δ	-2.0	-2.1	-2.7	-5.8	-3.6	-4.7
	Bias Error	2.1	2.7	2.8	3.8	3.0	4.6
8	%Δ	1.3	2.7	0.7	1.7	-3.5	-1.2
	Bias Error	1.9	2.1	1.9	3.2	2.9	2.5

Table VII.1 : Summary of results from Cherokee simulations.

4. Original collector model, calculated values for $F_R(\tau\alpha)_n$, F_RU_L, and $K_{\tau\alpha}$.
5. Original collector model, calculated values for $F_R(\tau\alpha)_n$, F_RU_L, and no incidence angle modification ($K_{\tau\alpha}$=1).
6. Capacitance collector model, design values for $F_R(\tau\alpha)_n$, F_RU_L, and $K_{\tau\alpha}$.
7. Capacitance collector model, design values for $F_R(\tau\alpha)_n$, F_RU_L, and calculated values for $K_{\tau\alpha}$.
8. Capacitance collector model, calculated values for $F_R(\tau\alpha)_n$, F_RU_L, and $K_{\tau\alpha}$.

The results from these simulations cases are discussed in Section VII.2

VII.1.2 Comparison of Gainesville Simulation Results

The simulation results for the Gainesville system are presented in Table VII.2. The combinations of inputs and collector models used for each case are listed below:

1. Original collector model, design values for $F_R(\tau\alpha)_n$, F_RU_L, $K_{\tau\alpha}$, and pipe losses.
2. Original collector model, design values for $F_R(\tau\alpha)_n$, F_RU_L, $K_{\tau\alpha}$, and calculated value for pipe losses.

simulation \ month		APR	MAY	JUN	JUL	AUG	SEP
1	%Δ	-8.3	1.0	-17.6	-23.4	-46.7	-24.2
	Bias Error	6.2	8.1	5.6	7.2	16.9	9.9
2	%Δ	-8.3	1.0	-17.6	-23.4	-46.7	-24.2
	Bias Error	6.2	6.0	5.6	7.3	16.9	9.8
3	%Δ	-5.5	-11.3	-6.2	-8.9	-41.5	-11.9
	Bias Error	6.3	5.3	5.1	7.3	16.2	10.0
4	%Δ	-2.5	-6.3	-12.7	-14.8	-29.4	-8.7
	Bias Error	5.0	4.1	4.2	5.7	15.9	8.5
5	%Δ	-7.3	-9.9	-8.8	-10.9	-26.9	-5.1
	Bias Error	5.3	4.1	4.2	5.9	15.8	8.6
6	%Δ	-5.3	4.0	-15.4	-16.6	-21.4	-5.7
	Bias Error	5.6	4.2	4.6	5.1	10.8	8.1
7	%Δ	-1.1	-3.9	0.3	5.1	-15.3	-1.6
	Bias Error	2.4	2.4	2.2	2.3	9.4	6.1

Table VII.2: Summary of results from Gainesville simulations.

3. Original collector model, design values for $K_{\tau\alpha}$, and calculated values for $F_R(\tau\alpha)_n$, $F_R U_L$ (representing average operational efficiency).
4. Original collector model, calculated values for $F_R(\tau\alpha)_n$, $F_R U_L$, and $K_{\tau\alpha}$.
5. Original collector model, calculated values for $F_R(\tau\alpha)_n$, $F_R U_L$, and no incidence angle modification ($K_{\tau\alpha}$=1).
6. Capacitance collector model, design values for $F_R(\tau\alpha)_n$, $F_R U_L$, and $K_{\tau\alpha}$.
7. Capacitance collector model, calculated values for $F_R(\tau\alpha)_n$, $F_R U_L$, and $K_{\tau\alpha}$.

The results from these simulations cases are discussed in the following section.

VII.2 Conclusions

The following conclusions are drawn from the results of this study.

VII.2.1 Usefulness of the SFBP Quality Site Data

• The extensive instrumentation of the SFBP Quality monitoring sites provides a means for analysis of many components from various types of solar heating systems. The small time steps used in data acquisition are especially helpful when using the data as input to obtain quality simulation results.

• The lack of documentation of the monitoring presents problems when modeling systems. While there is sufficient information available about the individual sensors, no information is given about their specific location. Major system failures were generally well documented in the Vitro reports, but problems with individual sensors were not usually described. Most difficulties were discovered while visually screening the measured data which was very tedious.

• The number of gaps in the data also presents a problem when using the data as simulation input, specifically for TRNSYS which requires data supplies at constant time intervals. It was not difficult to fill the many small data gaps with interpolated data, but users of the data should be aware of this problem.

• Overall, the quantity of the data collected in the SFBP quality monitoring program provides a means for verification of a variety of analytical models for solar system components. However, care must be taken in the use and interpretation of these measurements and it is suggested that all data be visually screened before use.

VII.2.2 Use of ASHRAE Collector Parameters $F_R(\tau\alpha)_n$ and $F_R U_L$ for ETC Simulation

• In general, the ASHRAE test curve (η vs. $(T_i - T_a)/I_t$) intercept $F_R(\tau\alpha)_n$ appears to be an adequate estimation for the actual performance of both systems studied. The laboratory determined $F_R U_L$, however is too high and tends to over estimate losses at high operating points.

• The monthly regression of the calculated test curve data for the Cherokee system supports the above conclusions. However, it is shown that the curve fit of the efficiency versus operating point data has a very low slope and is close to simply

representing the average efficiency of the collector.

• Similar regressions for the Gainesville system were not conclusive due to the wide scatter of the data. This problem can be attributed in part to sensor error, but also shows that the efficiency does not follow a strictly linear behavior. The monthly average efficiency was determined to be the only practical means of describing the collector performance based on the measured data.

• Simulation with the performance parameters as determined from the data resulting in the following average monthly improvements over initial simulations:

	Q collected Δ%	T out Bias Error
Cherokee	6 %	.5 deg F
Gainesville	2 %	.5 deg F

Recall that the accuracy (due to the sensor limitations) for energy measurements is +/- 4% and the temperature measurements are +/- 1 degree F.

• Because the above values do not show significant improvement, it is determined that the ASHRAE parameters are suitable for simulation input. No better estimations are available for design phase simulations. Based on the performance of these two collectors, however, it was found that the operational losses were less than predicted in the laboratory test.

VII.2.3 Use of the DSET Laboratory $K_{\tau\alpha}$ Curve for ETC Simulation Input

• The laboratory test values for the transversal incidence angle modifier for the SUNPACK ETC were found to be unsatisfactory for simulation input for both of the systems studied.

• The $K_{\tau\alpha}$ curves generated form the measured operational data are presented in Figure IV.5 and V.5. In general, there was much less angular dependence than predicted.

• The Cherokee $K_{\tau\alpha}$ values were higher than predicted for the incidence angles of 10 - 60 degrees which occur during hours of significant energy collection. The $K_{\tau\alpha}$ values was much lower than predicted for angles over 70 degrees, but this had little effect on the results.

• The new curve for the Gainesville data was closer to the DSET Laboratory curve for angles up to 50 degrees, but the values were still greater than predicted. The values for angles above 50 degrees were also much lower than for the test case.

• Simulation with the incidence angle modifiers as determined from the data resulting in the following monthly average improvements over simulations using laboratory values:

	Q collected Δ%	T out Bias Error
Cherokee	9.7 %	1.1 deg F
Gainesville	7 %	1.8 deg F

• While these improvements are significant it is important to note that the results were determined using the measured operational data. This information is obviously not available when design simulations for a system are performed.

• These results show the problems associated with using laboratory determined incidence angle modifiers to represent field performance. This was especially difficult because there was little documentation accompanying the laboratory results about the conditions of the test. It appears that more efficient reflectors were used in the laboratory than in actual operation because the $K_{\tau\alpha}$ above 70 degrees was much lower than predicted. It also appears that there may have been

differences in the tube spacing, but no specific information was available.

• When no incidence angle modification was used, the following improvements over initial simulation using the laboratory $K_{\tau\alpha}$ values were achieved:

	Q collected Δ%	T out Bias Error
Cherokee	3 %	.5 deg F
Gainesville	8.7 %	1.6 deg F

• Based on the results for the collectors studied, it appears that it is better to use no incidence angle modification, i.e. $K_{\tau\alpha} = 1$ for all angles, when specific information about the test conditions and exact collector geometry is not known.

VII.2.4 Use of the Capacitance Model for ETC Simulation

• Use of the capacitance model with design values for the collector parameters resulting in the following monthly average improvements over simulation predictions using the traditional TRNSYS collector model:

	Q collected Δ%	T out Bias Error
Cherokee	7 %	1.3 deg F
Gainesville	9%	2.5 deg F

• Some of the improvements resulted from better modeling of the initial daily operation for both of the systems. The new model accounted for the filling of the Cherokee array and for the morning heating of the Gainesville collector.

• Further improvement results from better temperature tracking throughout the day for both systems because the capacitance effects were accounted for.

• Improvements for the Gainesville system were slightly greater due to the

non-draining collector design.

• From the simulation results for the Gainesville and Cherokee collectors, it is evident that the capacitance model is needed in order to reproduce measured performance. In general, it is concluded that the capacitance model should be used to best simulate ETCs.

VII.2.5 General Comments on ETC System Design

• Unforeseen thermal losses from the storage subsystem affected the performance of both of the systems studied. Tank losses were especially great and could have been avoided by proper fitting insulation. Thermosiphoning was a significant problem in the Gainesville system and could have been remidied design modifications.

• Overnight collector losses were also significant for the Gainesville system. It is apparent that a drain back collector is a better design for ETC arrays which hold a large volume of working fluid.

• The DHW preheat loop was not necessary for either of the systems because of design load over estimation. In both cases, performance could be improved by replumbing of the flow until demand increases enough to warrant the use of the pre-heat loop.

VII.3.6 Economics of ETCs

• Although ETC panel cost significantly more per square foot than flat-plate collectors, the total system cost are comparable.

• ETCs were an economically favorable choice for the example given in Section VII.2, but each application should be evaluated on an individual basis. Equation VII.2.1 gives a general form for economic comparison of different collector types for a given system.

VII.4 **Recommendations for Further Study**

The following are recommendations for future work.

• The parameterization of ETC efficiency should be further investigated. Incorporating the effects of temperature dependent losses may improve the model.

• The computational penalty when using the multi-node collector model should be studied to see if it is significant for long term TRNSYS studies.

Appendices

APPENDIX A - This appendix contains the TRNSYS subroutine FORTRAN code for the "Radiation Converter" as described in Section III.3.

```
      SUBROUTINE TYPE20 (TIME, XIN,OUT,T,DTDT,PAR,INFO)
C
C  TRNSYS Subroutine, RADIATION CONVERTER
C
C  This subroutine 'untilts' radiation data measured on
C  the tilted surface to the horizontal surface value
C  needed for input into the TRNSYS radiation processor.
C
C  Ann L. Barrett,  1987
C
      REAL LAT, IT, IO, I, IT2, KT
      DIMENSION PAR(20), XIN(20), OUT(20), INFO(10)
      COMMON /SIM/ DELT
      DATA PI/3.1415927/
      NP=5
      NI=2
      INFO(6)=1
C
C  Set parameters and convert angles to radians.
C  Parameters are:
C    1. day number for beginning of simmulation
C    2. latitude
C    3. collector slope
C    4. ground reflectance
C    5. time shift
C
      DAY=PAR(1)
      LAT=PAR(2)
      LAT=LAT*PI/180.
      BETA=PAR(3)
      BETA=BETA*PI/180.
      RHO=PAR(4)
      SHIFT=PAR(5)
C
C  Set inputs.
C  Inputs are:
C    1. measured tilted surface radiation value
```

```
C   2. etraterrestrial radiation value radiation processor
C
      IT=XIN(1)
      IO=XIN(2)
C
C These equations can be used to calculated Io
C (etraterrestrial radiation), but for small time
C steps is is more efficient to read in the value
C from the last call of the radiation processor.
C
C       B=360.*(DAY-81.)/364.*PI/180.
C       DTIME=(4*(SHIFT)+9.87*SIN(2.*B)-7.53*COS(B)-1.5*SIN(B))/60.
C      IND=TIME/24
C      H=TIME-IND*24 + DTIME
C       W=(H-12.)*15.*PI/180.
C       W2=W+DELT*15.*PI/180.
C       IO=12.*3600.GSC*(1.+.033*COS(DAY*PI*2/365.242))
C      & *(COS(LAT)*COS(DEC)*(SIN(W2)-SIN(W))+(W2-W)
C      & *SIN(LAT)*SIN(DEC))
C       IO=IO/1055.06*.0929034/DELT
C
C Calculate solar position angles and RB.
C
       DEC=23.45*SIN(360.*(284.+DAY)*PI/365./180.)*PI/180.
      COSTH=COS(LAT-BETA)*COS(DEC)*COS(W)+SIN(LAT-BETA)
     &  *SIN(DEC)
      THETA=ACOS(COSTH)*180./PI
      COSTHZ=COS(LAT)*COS(DEC)*COS(W)+SIN(LAT)*SIN(DEC)
      THETAZ=ACOS(COSTHZ)*180./PI
      RB=COSTH/COSTHZ
C
C Exit for low radiation, the correction is negligible.
C
      IF (IO.LT.10.) THEN
        I=IT
        GOTO 60
      ENDIF
C
```

```
C Exit if there is no measured radiation.
C
     IF (IT.LE.0) THEN
       I=IT
       GOTO 60
     ENDIF
C
C Begin with an initial guess for KT by estimating R=RB,
C step down the guess by 50% to begin with a low value
C into the interation process.
C
     KT=IT/RB/IO*.5
C
C Begin the main iteration loop.
C
20   CONTINUE
C
C Exit loop and signal error if iterations exceed 200.
C
     IF (J.GE.200) GOTO 40
C
C Calculate I (horizontal surface radiation)
C using current KT.
C
     I=KT*IO
C
C Use the Erbs correlation to calculate the other
C components and the corresponding new It value.
C
     IF(KT.GT.0.8) THEN
       ID=.165*I
     ELSE IF(KT.GE.0.22) THEN
       ID=I*(.9511-.1604*KT+4.388*KT*KT-16.638*(KT**3)
    &    +12.336*(KT**4))
     ELSE
       ID=I*(1.-.09*KT)
     ENDIF
```

```
      IB=I-ID
      IT2=IB*RB+ID*(1.+COS(BETA))/2.+RHO*I*(1.-COS(BETA))/2.
C
C  Check the difference of the measured and calculated It.
C
      DEL=ABS(IT2-IT)
C
C  Exit if there is convergence.
C
      IF (DEL.LT.1.) GOTO 60
C
C  Exit and signal error if there is no convergence
C  for this time step.
C
      CHECK=DEL-DELHOLD
      DELHOLD=DEL
       IF (CHECK.GT.0.AND.J.GT.2) GOTO 50
C
C  Re-estimate KT according to error.
C
      IF (DEL.GT. 10) THEN
        KT=KT+.05
        J=J+1
       GOTO 20
      ELSE IF (DEL.GT. 5) THEN
        KT=KT+.01
        IF (KT.GT.1.) GOTO 25
        J=J+1
       GOTO 20
      ELSE IF (DEL.GT. 1) THEN
        KT=KT+.001
        IF (KT.GT.1.) GOTO 25
        J=J+1
       GOTO 20
      ENDIF
C
C  Exit iteration if KT=1, clear day.
C
```

```
25   I=IO
     GOTO 60
C
40   WRITE (*,*)'Radiation converter error at time =',TIME
     write (*,*)' Too many interations'
     I=IT
     GOTO 60
50   WRITE (*,*)'Radiation converter error at time =',TIME
     write (*,*)' No convergence'
     I=IT
     GOTO 60
C
C Set output - horizontal surface total radiation
C
60     OUT(1)=I
C
     RETURN
     END
```

APPENDIX B - This appendix contains the FORTRAN program written to generate collector test curve points from experimental data.

```
      PROGRAM TESTCRV
C
C
C FORTRAN Program TESTCRV
C
C This program calculates the instantaneous values of
C efficiency (n) and operating point ((Ti-Ta)/It) to
C plot collector test curves from experimental data.
C The points are then fit with a first order linear
C regression with an additional program to find the
C values of FR(ta)n and FRUL
C
C Ann L. Barrett,  1987
C
      REAL N, KTA, MIN, MO
C
C Begin main calculation loop
C
10    CONTINUE
      READ(10,18,END=20) MO, D, HR, MIN, TA, RAD, FLOW, TI, TO
18      FORMAT (T8,F3.0,T11,F2.0,T18,F3.0,T21,F2.0,T31,F6.2,T41,
     +        F6.2,T51,F6.2,T61,F6.2,T71,F6.2)
C
C Find day number
C
      D=D+(MO-1)*30.
C
C Average values for 1 hour if desired
C
C     IF (HR.EQ.HRHOLD) THEN
C       I=I+1
C       SRAD=SRAD+RAD
C       STA=STA+TA
C       SFLOW=SFLOW+FLOW
C       IF (FLOW.EQ.0) SFLOW=0.
C       STI=STI+TI
```

```
C      STO=STO+TO
C    ELSE
C      IF (I.EQ.0) GOTO 15
C      RAD=SRAD/REAL(I)
C      TA=STA/REAL(I)
C      FLOW=SFLOW/REAL(I)
C      TI=STI/REAL(I)
C      TO=STO/REAL(I)
C      SRAD=0.
C      STA=0.
C      SFLOW=0.
C      STI=0.
C      STO=0.
C      I=0
C
C    HRJ=HRHOLD
      HRJ=HR+MIN/60.
C
C Find angle of incidence to determine if
C radiation is near normal
C
     CALL FINDTHETA (D,HRJ,THETAT)
C
C Calculate efficiency and operating point
C Exit loop if incidence angle is greater than 10 degress
C or no energy is collected
C
     QU=(FLOW*8.31*60.)*1.0*(TO-TI)
     QC=RAD*4429.
     IF (QU.LE.0..OR.QC.LE.0.) GOTO 15
     IF (THETAT.GT.10.) GOTO 15
     N=QU/QC
     X=(TI-TA)/RAD
     IF (X.LT..01.OR.X.GT.1.0) GOTO 15
     IF (N.GT.1.) GOTO 15
     K=K+1
     WRITE (20,16) X,N,HRJ,THETAT,K
```

```
16    FORMAT (T10,F4.2,T20,F4.2,T30,F5.2,T40,F5.2,T50,I4)
15   CONTINUE
C
C    HRHOLD=HR
     GOTO 10
20   CONTINUE
     STOP
     END
C
C
C
     SUBROUTINE FINDTHETA (D,HR,THETAT)
C
C FORTRAN Subroutine FINDTHETA
C
C This subroute calculated the transversal angle of
C incidence for a given day and hour
C
C Ann L. Barrett,  1987
C
C Input values for collector orientation and location
C
     PI=3.1416
     BET=35.*PI/180.
     PHI=34.9*PI/180.
     GAM=-8.*PI/180.
C
C Calculate time shift
C
     DEL=23.45*SIN(360.*(284+D)*PI/365./180.)*PI/180.
     B=360.*(D-81.)/364.
     B=B*PI/180.
     E=9.87*SIN(2*B)-7.53*COS(B)-1.5*SIN(B)
     SHR=HR +E/60. +4*(90-83.12)/60.
     OME=(SHR-12.)*15.*PI/180.
C
C Calculate all angle relations
```

```
C
      COSTHE=SIN(DEL)*SIN(PHI)*COS(BET)-SIN(DEL)*SIN(BET)*COS(PHI)
     +*COS(GAM)+COS(DEL)*COS(PHI)*COS(BET)*COS(OME) +
      COS(DEL)*SIN(PHI)
     + *SIN(BET)*COS(GAM)*COS(OME)
     +COS(DEL)*SIN(BET)*SIN(GAM)*SIN(OME)
       IF (COSTHE.GT.1.) COSTHE=1.
       IF (COSTHE.LT.-1.) COSTHE=-1.
       THETA=ACOS(COSTHE)
C
       COSTHEZ=COS(DEL)*COS(PHI)*COS(OME)+SIN(DEL)*SIN(PHI)
       IF (COSTHEZ.GT.1.) COSTHEZ=1.
       IF (COSTHEZ.LT.-1.) COSTHEZ=-1.
       THETAZ=ACOS(COSTHEZ)
C
       SINGAMS=COS(DEL)*SIN(OME)/SIN(THETAZ)
       IF (SINGAMS.GT.1.) SINGAMS=1.
       IF (SINGAMS.LT.-1.) SINGAMS=-1.
       GAMS=ASIN(SINGAMS)
C
       TANTHETAT=SIN(THETAZ)*SIN(GAM-GAMS)/COS(THETA)
       THETAT=ATAN(TANTHETAT)
       THETAT=ABS(THETAT*180./PI)
       THETA=THETA*180./PI
       GAMS=GAMS*180./PI
       IF (THETA.GT.90.) THETAT=0.
C
       RETURN
       END
```

APPENDIX C - This appendix contains the TRNSYS subroutine FORTRAN code for the "Capacitance Collector Model" as described in Section III.4.2.

```
      SUBROUTINE TYPE1(TIME,XIN,OUT,T,DTDT,PAR,INFO)C
C
C TRNSYS Suboutine, SOALR COLLECTOR MODEL
C
C This subroutine simulates a solar collector
C and  includes the effects of capaciatnce and
C collector filling.
C
C Ann L. Barrett, 1987  (Adapted from J.P. Kummer, 1986)
C
      IMPLICIT REAL M
      INTEGER CMODE,EMODE,OMODE, GAMMA
      DIMENSION PAR(25),XIN(15),OUT(20),INFO(10)
      DIMENSION TM(200), Y(2)
      COMMON/SIM/TIMEO,TFINAL,DELT
      COMMON/STORE/NSTORE,IAV,S(5000)
      COMMON/LUNITS/LUR/LUW/IFORM
      DATA IUNIT/0/,RDCONV/0.017453/,PI/3.1415927/,SQRT2/1.41421356/,
     .   NDELT/9/
      TAUALF(THETA)=1.-B0*(1./AMAX1(0.5,COS(THETA*RDCONV))-1.)
     & - (1.-B0)*(AMAX1(60.,THETA)-60.)/30.
C
      IF(INFO(7).GT.-1) GOTO 5
C
C First call os simulation
C
      INFO(6)=3
      CMODE=INT(PAR(1)+0.1)
      OMODE=INT(PAR(11)+0.1)
      NP=18
      NI=11
      NODES=PAR(14)
      INFO(10)=2*NODES+2
C
1     CALL TYPECK(1,INFO,NI,NP,0)
```

```
C
      ISTORE=INFO(10)
      DO I=1,NODES
        S(ISTORE+NODES+I)=PAR(17)
      ENDDO
      S(ISTORE+2*NODES+1)=PAR(16)
C
5     IF(INFO(1) .EQ. IUNIT) GOTO 50
      IUNIT=INFO(1)
C
C  Set Parameters
C
      CMODE=INT(PAR(1)+0.1)
      NS=INT(PAR(2)+0.1)
      XNS=FLOAT(NS)
      A=PAR(3)
      AN=A/NODES
      CPC=PAR(4)
      EMODE=INT(PAR(5)+0.1)
      GTEST=PAR(6)
      FRTAN=PAR(7)
      FRUL=PAR(8)
      EFFEC=PAR(9)
      CPF=PAR(10)
      IF(EFFEC.LE.0.) CPF=CPC
      FPUL=-GTEST*CPC*ALOG(1.-FRUL/GTEST/CPC)
      RTEST=GTEST*CPC*(1.-EXP(-FPUL/GTEST/CPC))
      FPFR=1./(GTEST*CPC/FPUL*(1.-EXP(-FPUL/GTEST/CPC)))
      LU2=INT(PAR(12)+0.1)
      NX2=INT(PAR(13)+0.1)
      NODES=PAR(14)
      CAPE=PAR(15)
      MASVOL=PAR(16)
      DRAIN=PAR(18)
      CAPW=MASVOL*CPC/A
      CAPNW=CAPE-CAPW
      IF (CAPNW.LT.0) PRINT*, 'CAPNW ERROR'
50    ISTORE=INFO(10)
```

```
      IF (INFO(7).GT.0) GOTO 60
      DO I=1, NODES+1
        S(ISTORE+I-1)=S(ISTORE+NODES+I)
      ENDDO
C
C Inputs
C
60    TIN=XIN(1)
      MIN=XIN(2)
      FLWF=XIN(3)
      TA=XIN(4)
      GT=XIN(5)
      GDT=XIN(6)
      THETA=XIN(7)
      THETAZ=XIN(8)
      SAZM=XIN(9)
      SLP=XIN(10)
      AZMTH=XIN(11)
      IF(INFO(7).GT.0) GOTO 100
C
C Determine incidence angle modifier, once each timestep
C
      IF(GT .GT. 0. .AND. THETA .LT. 90.) GOTO 80
C
C No radiation
C
      XKAT=0.
      GOTO 100
C
80    IF(THETAZ.LT.90.) GO TO 82
      XKAT=0.
      GO TO 100
C     Beam
82    TANTT=SIN(THETAZ*RDCONV)*SIN(ABS(AZMTH-SAZM)*RDCONV)

     . /COS(THETA*RDCONV)
      THETAT=ATAN(TANTT)/RDCONV
```

```
      TANALF=TAN(THETAZ*RDCONV)*COS((AZMTH-SAZM)*RDCONV)
      THETAL=ABS(ATAN(TANALF)/RDCONV-SLP)
      CALL DATA(LU2,1,NX2,2,THETAL,Y,INFO)
      XKATB=Y(1)
      CALL DATA(LU2,1,NX2,2,THETAT,Y,INFO)
      XKATB=XKATB*Y(2)
      IF(OUT(20).GT.0.) GO TO 85
      XKATD2=0.
      DDELT=PI/2./FLOAT(NDELT)
      DO 84 I=1,NDELT
      XKATD1=0.
      SAZM=FLOAT(I-1)*DDELT+DDELT/2.
      DO 83 J=1,NDELT
      THETA=FLOAT(J-1)*DDELT+DDELT/2.
      SINTT=SIN(THETA)
      COSTT=COS(THETA)
      TANTT=SINTT/COSTT
      THETAT=ATAN(TANTT*SIN(SAZM))/RDCONV
      THETAL=ATAN(TANTT*COS(SAZM))/RDCONV
      CALL DATA(LU2,1,NX2,2,THETAL,Y,INFO)
      XKATD=Y(1)
      CALL DATA(LU2,1,NX2,2,THETAT,Y,INFO)
      XKATD=XKATD*Y(2)
   83 XKATD1=XKATD1+XKATD*COSTT*SINTT*DDELT
   84 XKATD2=XKATD2+XKATD1*DDELT
      XKATD=4.*XKATD2/PI
      OUT(20)=XKATD
   85 XKATD=OUT(20)
      XKAT=(XKATB*(GT-GDT)+XKATD*GDT)/GT
      GO TO 100
   90 EFFD=44.86-0.0716*THETAC+0.00512*THETAC*THETAC
     . -0.00002798*THETAC*THETAC*THETAC
      COSSLP=COS(SLP*RDCONV)
      CR=OUT(14)
      GO TO (91,92) ,IAXIS
C Horizontal axis
   91 FSKY=(1./CR+AMIN1(1./CR,COSSLP))/2.
      FGND=(AMAX1(1./CR,COSSLP)-COSSLP)/2.
```

```
      TANALF=TAN(THETAZ*RDCONV)*COS((AZMTH-SAZM)*RDCONV)
      THETAP=ABS(ATAN(TANALF)/RDCONV-SLP)
      GO TO 95
C  Sloped axis
92    FSKY=(1.+COSSLP)/CR/2.
      FGND=(1.-COSSLP)/CR/2.
      TANTP=SIN(THETAZ*RDCONV)*SIN(ABS(AZMTH-SAZM)*RDCONV)
     . /COS(THETA*RDCONV)
      THETAP=ATAN(TANTP)/RDCONV
C  Check for sun within acceptance angle
95    FB=0.
      IF(THETAP.LE.THETAC) FB=1.
      XKATB=TALF(NG,THETA,XKL,RI,ALF,RHOD)/TALN
      XKATB=XKATB*FB
      XKATD=TALF(NG,EFFD,XKL,RI,ALF,RHOD)/TALN
      GB=GT-GD*(1.+COSSLP)/2.-RHO*GH*(1.-COSSLP)/2.
      GDT=GD*FSKY+RHO*GH*FGND
      XKAT=(XKATB*GB+XKATD*GDT)/GT
C
C  Thermal perfromance
C
100   IF (INFO(7).LE.0) OUT(17)=XKAT
      MASBEG=MASEND
      IF (MIN.EQ.0) KOUNT=KOUNT+1
      IF (KOUNT.GT.50)  MASBEG=0.
      IF (MIN.NE.0) KOUNT=0
      CAP=CAPNW+MASBEG*CPC/A
      IF (DRAIN.EQ.0.) CAP=CAPE
      IF (MIN .GT. 0.) GOTO 110
      QU=0.
      TTOTAL=0.
      SOLAR=XKAT*GT
      AA=-FPUL/CAP
      BB=(FRTAN*FPFR*SOLAR+FPUL*TA)/CAP
      DO  I=1,NODES
       TM1=S(ISTORE+I-1)
       CALL DIFFEQ(TIME,AA,BB,TM1,TM(I),TMBAR)
```

```
      S(ISTORE+NODES+I)=TM(I)
      TTOTAL=TTOTAL+TMBAR
     ENDDO
     TOAVE=TMBAR
     MOUT=0.
     GOTO 300
C
C  Flow into collector
C
110  MOUT=MIN
     IF (DRAIN.EQ.0) GOTO 120
     MASEND=MIN*DELT+MASBEG
     IF (MASEND.GT.MASVOL) MASEND=MASVOL
     IF (ABS(MASBEG-MASVOL) .LT. .001) GO TO 120
      TTOTAL=0.
      DO  I=1,NODES
       TTOTAL=TTOTAL+S(ISTORE+I-1)
      ENDDO
      TTOTAV=TTOTAL/NODES
      CAP=MASEND*CPC/A+CAPNW
      IF (DRAIN.EQ.0) CAP=CAPE
      TMIX=((MASEND-MASBEG)*CPC*TIN/A+MASBEG*CPC*TTOTAV/A
     .     +CAPNW*TTOTAV)/CAP
      TIMFIL=(MASEND-MASBEG)/MIN
      SOLAR=XKAT*GT
      AA=-FPUL/CAP
      BB=(FRTAN*FPFR*SOLAR+FPUL*TA)/CAP
      DO I=1,NODES
        TM1=TMIX
        CALL DIFFEQ(TIME,AA,BB,TM1,TM(I),TMBAR)
        S(ISTORE+NODES+I)=TM(I)
      ENDDO
      TOAVE=TMBAR
      MOUT=AMAX1((MIN*DELT+MASBEG-MASVOL)/DELT,0.)
      IF (DRAIN.EQ.1) MOUT=0.
      QU=0.
      IF (MOUT .EQ. 0.) GO TO 300
```

```
C
C Collector filled
C
120  MOUT=MIN
     FLWC=MOUT
     CAP=CAPE
     SOLAR=XKAT*GT
     AA=-((FPUL+FLWC*CPC/AN)/CAP)
     TTOTAL=0.
     DO 150 I=1,NODES
       TM1=TM(I)
         IF(I .EQ. 1) THEN
          TIND=TIN
         ELSE
          TIND=TMBAR
         END IF
       BB=(FRTAN*FPFR*SOLAR+FPUL*TA+FLWC*CPC/AN*TIND)/CAP
       CALL DIFFEQ(TIME,AA,BB,TM1,TM(I),TMBAR)
      TTOTAL=TTOTAL+TM(I)
      S(ISTORE+NODES+I)=TM(I)
150  CONTINUE
     TMEAN=TTOTAL/NODES
     TOAVE=TMBAR
     QU=FLWC*CPC*(TOAVE-TIN)
C
C Outputs
C
300  S(ISTORE+2*NODES+1)=MASEND
     IF (TOAVE.LT.TIN) TOAVE=TIN
     OUT(1)=TOAVE
     OUT(2)=MOUT
     OUT(3)=QU
C
     RETURN
     END
C
C
C
```

```
C  TRNSYS Suboutine, DIFFERENTIAL EQUATION SOLVER 2
C
C  This subroutine is a modified verions of the TRNSYS
C  differential equation solver which can solve for periods
C  other than a full time step
C
C  J.P. Kummer, 1986
C
      SUBROUTINE DIFF2(TIME,DELT2,AA,BB,TI,TF,TBAR)
      COMMON /SIM/ TIMEO,TFINAL,DELT
C
      IF(TIME .GT. TIMEO) GO TO 10
C  Maintain initial conditions at time 0
      TF = TI
      TBAR = TI
      RETURN
10    IF(ABS(AA) .GT. 0.) GO TO 20
C  Linear solution to differential equation
      TF = BB*DELT2 + TI
      TBAR = (TF + TI)/2.
      RETURN
C  Exponential solution to differential solution
20    TF = (TI + BB/AA)*EXP(AA*DELT2) - BB/AA
      TBAR = (TI + BB/AA)/AA/DELT2*(EXP(AA*DELT2) - 1.) - BB/AA
      RETURN
      END
```

APPENDIX D - This appendix contains the FORTRAN program written to calculate $K_{\tau\alpha}$ as a function of transversal incidence angle from experimental data.

```
      PROGRAM FINDIAM
C
C  FORTRAN Program FINDIAM
C
C  This program calculates the effective trnasversal
C  incidence angle modifier from measured data.  The
C  values are then fit with a third order regression
C  using an additional program
C
C  Ann L. Barrett,  1987
C
      REAL N, KTA,MIN, N2, MON
      OPEN
(10,FILE='[BARRETT.CIH.DAT]ALL.DAT',STATUS='UNKNOWN')
      OPEN (20,FILE='[BARRETT.CIH]ALLIAM.DAT',STATUS='UNKNOWN')
      FRTA=.391
      FRUL=.224
C
C  Begin main calculation loop
C
10    CONTINUE
      READ(10,15,END=20) MON,D,HR,MIN,CH19,CH2,CH6,CH20,CH23
C                    T AMB, RAD, FLOW, T IN, T OUT
      K=K+1
15     FORMAT (T9,F3.0,T11,F3.0,T18,F3.0,T21,F3.0,T32,F5.2,T41,F6.2,
     +T52,F5.2,T61,F6.2,T71,F6.2)
C
C  Omit data from first hour to avoid transient problems
C
      IF (CH6.EQ.0.) OFF=OFF+1
      IF (CH6.NE.0.AND.OFF.GT.50.) THEN
        DO I=1,11
         READ(10,15,END=20) MON,D,HR,MIN,CH19,CH2,CH6,CH20,CH23
        ENDDO
        OFF=0.
```

```
      ENDIF
C
C  Calculate day, hour and incidence angle
C
      HR=HR+MIN/60.
      IF (MON.GT.12) MON=MON/10.
      D=D+(MON-1)*30
      CALL FINDTHETA (D,HR,THETAT)
C
C  Calculate efficiency and  determine Kta
C  from Hottel-Whillier Equation
C
      QU=(CH6*8.31*60)*1.0*(CH23-CH20)
      IF (QU.LT.0.) QU=0.
      QC=CH2*4429.
      N=0.
      IF (QU.GT.0..AND.QC.GT.0.) THEN
       N=QU/QC
       KTA=(N+FRUL*(CH20-CH19)/CH2)/FRTA
       IF (KTA.LT.4..AND.KTA.GT..8) WRITE (20,6) THETAT,KTA,HR
6       FORMAT (T10,F6.2,T20,F6.2,T30,F6.2)
      ENDIF
C
      GOTO 10
C
20    CONTINUE
      STOP
      END
```

APPENDIX E - This appendix contains a typical deck listing for the Cherokee collector simulation using the origonal collector model.

```
*-------------------------------------------------
* TRNSYS DECK CIHH
* COLLECTOR MODEL FOR THE CHEROKEE INDIAN
*    HOSPITAL SOLAR ENERGY SYSTEM
* COMPARES ACTUAL AND PREDICTED T OUT
* 5 1/3 MINUTE INTERVALS
* ZERO CAPACITANCE
*-------------------------------------------------
* ANN BARRETT,  1097
*-------------------------------------------------
*
SIMULATION 3600  3936  .08889

TOL  -.01  -.01

LIMITS 100 4

NOLIST
*-------------------------------------------------
UNIT 2  TYPE 9  DATA READER

PARAMETERS 19
* #VAL   DT       FLOW CONVERSION              LU  FORMAT
  5  .088889  -1 1 0  -2 1 0  -3 500.4 0  -4 1 0  -5 1 0  10  1
(T32,F5.2,T41,F6.2,T52,F5.2,T61,F6.2,T71,F6.2)

*-------------------------------------------------
UNIT 3  TYPE 15  ALGEBRA CONVERTER

PARAMETERS 5
 -11  -1 .08889 1 -4
INPUTS 1
 9,1
 0.0
*-------------------------------------------------
UNIT 9  TYPE 20  RADIATION UNTILTER
```

```
PARAMETERS 5
* DAY  LAT SLOPE  RHO   SHIFT
  151  35.4 34.   .2   6.88
INPUTS 1
* IT   IO
  2,2   4,1
  0,0   0,0
*--------------------------------------------------
UNIT 4  TYPE 16  RADIATION PROCESSOR

PARAMETERS 6
* ERBS  FIXED  DAY  LAT  SOLAR C  SHIFT
   3     1    151  35.4  428.    6.88
INPUTS 6
* I  TD1  TD2  RHO  SLOPE  AZIMUTH
 3,1  2,19  2,20  0,0   0,0   0,0
  0.  0.   0.  .2     34.   -8.

*--------------------------------------------------
UNIT 5  TYPE 31  PIPE

PARAMETERS 6
* DIA  LENGTH  U  RHO  CP  TI
 .42    800    0 62.42 1   60
INPUTS 3
* T IN  FLOW  T AMB
   2,4   2,3   2,1
   0     0     0
*--------------------------------------------------
UNIT 6  TYPE 1  SOLAR COLLECTOR

PARAMETERS 13
*MODE NO AREA CPW EFF GTEST FRTA FRUL HX CPW IAM  LU  ANG
  1   1 4429. 1   1  5.1   .391 .224 -1  1   4   20   10
INPUTS 11
* TIN FLOW FLOW TAMB  IT   ID   THETA  THETAZ  GAMS  BETA  GAM
  5,1  5,2  0,0  2,1  2,2  4,8   4,9    4,2     4,3   4,10  0,0
```

```
  0  0  0  0  0  0  0  0  0  34  -8.

*-------------------------------------------------
UNIT 7  TYPE 31  PIPE

PARAMETERS 6
* DIA  LENGTH  U  RHO  CP  T I
 .4167  20  3.345  62.42  1  40

INPUTS 3
* T IN  FLOW  T AMB
  6,1  6,2  2,1
  0  0  0

*-------------------------------------------------

UNIT 8  TYPE 28  OUTPUT

PARAMETERS 23
*DT  TON TOFF LU MODE  OPERATORS
.08889  3600  3936 30 2 -11 -2 2 -4 -12 -2 2 -4 -13 -2 2 -4 -14 -2 2 -4 -15 -4

INPUTS 5
7,1  2,5  5,1  5,2  6,3

LABELS 5
T_PRE  T_ACT  T_IN  FLOW  Q_COL

*-------------------------------------------------

END
```

APPENDIX F - This appendix contains a typical deck listing for the Gainesville collector simulation using the capacitance collector model.

```
*-------------------------------------------------------
* TRNSYS DECK GNVG
* COLLECTOR MODEL FOR THE GAINESVILLE JOB
*    CORPS CENTER SOLAR ENERGY SYSTEM
* COMPAREs ACTUAL AND PREDICTED T OUT
* 5 1/3 MINUTE INTERVALS
* USES NEW TYPE1 TO MODEL CAPACITANCE AND FILLING
*-------------------------------------------------------
* ANN BARRETT,  1987
*-------------------------------------------------------
*
SIMULATION 5058 6144  .08889

TOL  -.01  -.01

LIMITS 100 4

CONSTANTS DAY=243

NOLIST
*-------------------------------------------------------
UNIT 2  TYPE 9  DATA READER

PARAMETERS 19
* #VAL  DT    IT    TA    FLOW    T IN  T OUT LU  FORMAT
  5  .088889  -1 1 0  2 1 0  -3 500.4 0  4 1 0  5 1 0  10   1
(T15,F6.2,T26,F5.2,T36,F5.2,T45,F6.2,T55,F6.2)
*-------------------------------------------------------
UNIT 3  TYPE 15  ALGEBRA CONVERTER

PARAMETERS 5
 -11  -1 .08889 1 -4
INPUTS 1
 9,1
 0.0
*-------------------------------------------------------
UNIT 9  TYPE 20  RADIATION UNTILTER
```

```
PARAMETERS 5
* DAY  LAT SLOPE  RHO   SHIFT
  DAY  35.4 34.   .2   6.88
INPUTS 1
* IT   IO
  2,1   4,1
  0,0   0,0
*--------------------------------------------------------
UNIT 4  TYPE 16  RADIATION PROCESSOR

PARAMETERS 6
* ERBS  FIXED  DAY  LAT  SOLAR C  SHIFT
   3     1    DAY  29.8  428.    7.3
INPUTS 6
* I  TD1   TD2   RHO   SLOPE  AZIMUTH
 3,1  2,19   2,20   0,0    0,0    0,0
  0.   0.    0.   .2      25.     0
*--------------------------------------------------------
UNIT 5  TYPE 31  PIPE
PARAMETERS 6
*  DIA  LENGTH  U  RHO  CP  TI
   .42   300   0  62.42  1   60
INPUTS 3
*  T IN  FLOW  T AMB
   10,1   2,3   2,2
   0     0     0
*--------------------------------------------------------
UNIT 6  TYPE 1  SOLAR COLLECTOR

PARAMETERS 18
*MODE NO AREA CPW EFF GTEST FRTA FRUL HX CPW IAM  LU  ANG
NOD CAPE MVOL TEMP D
  1  1  5261. 1  1  10.96 .496  .224  -1  1  4  20  10  200 1.6 5000  73  0

INPUTS 11
* TIN FLOW FLOW TAMB  IT  ID  THETA  THETAZ  GAMS  BETA  GAM
  5,1  5,2  0,0  2,2  2,1  4,8  4,9   4,2    4,3   4,10  0,0
```

```
  0  0  0  0  0  0  0  0  0  25  0
*-------------------------------------------------
UNIT 7  TYPE 31  PIPE

PARAMETERS 6
* DIA  LENGTH  U  RHO  CP  T I
.5  20  .42  62.42  1  73

INPUTS 3
* T IN  FLOW  T AMB
 6,1  6,2  2,2
 0  0  0
*-------------------------------------------------

UNIT 8  TYPE 28  OUTPUT

PARAMETERS 23
*DT  TON TOFF LU MODE  OPERATORS
.08889  5080 6144  30 2 -11 -2 2 -4 -12 -2 2 -4 -13 -2 2 -4 -14 -2 2 -4 -15 -4

INPUTS 5
 7,1  2,5  5,1  7,2  6,3

LABELS 5
T_PRE  T_ACT  T_IN  FLOW  Q_COL

*-------------------------------------------------

END
```

References

REFERENCES CITED -

1.) Rabl, A., Active Solar Collectors and Their Applications, Oxford University Press, New York, (1985).

2.) Duff, W.S., *et al*, "Detailed Modeling of Evacuated Collector Systems", IEA Task VI Report, (1985).

3.) Speyer, E., "Solar Energy Collection With Evacuated Tubes", A.S.M.E. Journal of Engineering for Power 86, pp. 270-276, (1985).

4.) McIntire, W.R., "Factored Approximation for Biaxial Incidence Angle Modifiers", Solar Energy 29, pp. 315-322, (1982).

5.) McIntire, W.R., and Reed, K., "Incidence Angle Modifiers for Evacuated Tube Collectors", ISES Annual Meeting Proceedings, pp. 282-284, (1981).

6.) McIntire, W.R., and Reed, K., "Optical Relationships for Optically Non-Symmetric Solar Collectors", Solar Energy 31, pp. 405-410, (1983).

7.) Rabl, A., "A Note on the Optics of Glass Tubes", Solar Energy 19, p. 215, (1977)

8.) Snail, K.A., O'Gallager, J.J., and Winston, R., "A Stationary Evacuated Collector with an Integrated Concentrator", Solar Energy 33, pp. 441-449, (1984).

9.) Snail, K.A., O'Gallager, J.J., and Winston, R., "A New Evacuated CPC Tube", Solar Energy 29, pp. 575-577, (1982).

10.) Winston, R., and O'Gallager, J.J., "Development of Compound Parabolic Concentrators for Solar Energy", International Journal of Ambient Energy 4, pp. 171-185, (1984).

11.) Guisan, O., *et al*, "Characterization of Evacuated Collectors, Arrays, and Subsystems", IEA Task VI Report, (1986).

12.) Gemmell, W.L., *et al*, "Detailed Modeling of Evacuated Collector Systems", IEA Task VI Report, (1985).

13.) Klein, S.A., *et al*, TRNSYS 12.1 User's Manual, University of Wisconsin - Madison, Solar Energy Laboratory, Engineering Experimental Station Report 38-12, (1983).

14.) "American Society of Heating Refrigeration, and Air Conditioning Engineers, ASHRAE Standard 93-77, Methods of Testing to Determine the Thermal Performance of Solar Collectors", (1977).

15.) Logee, T.L., and Kendall, P.W., "Actual Versus Design Performance of Solar Systems in the National Solar Data Network", Vitro Corporation Report, (1984).

16.) Duffie, J.A., and Beckman, W.A., Solar Engineering of Thermal Processes, John Wiley and Sons, New York, (1980).

17.) Kummer, J.P., "Thermal Performance of Three Freeze Protection Methods as Applied to a Large Solar Energy Systems", M.S. Thesis, University of Wisconsin - Madison, Solar Energy Laboratory, (1986).

18.) Robbin, J.S., *et al*, "Owens Illinois SUNPACK Thermal Performance Test Report", DSET Laboratory Report, (1980).

19.) Raymond, M.G., "Quality Site Seasonal Report, Cherokee Indian Hospital - SFBP #4058" Vitro Corporation Report, (1986).

20.) Raymond, M.G., "Quality Site Seasonal Report, Gainesville Job Corps Center - SFBP #5009" Vitro Corporation Report, (1986).

21.) F-Chart User's Manual, University of Wisconsin - Madison, Solar Energy Laboratory, Engineering Experimental Station Report 50, (1985).

22.) "Solar Equipment Cost Comparisons", International Solar Energy Intelligence Report, p. 329, October 27, 1987.

23.) Marlatt, W.P., ETEC of Rockwell International, Inc., correspondence of 12/1/86

24.) Duff, W.S., "Draft Material for the ETEC Design Manual ETC Sections", (1985).

ADDITIONAL REFERENCES -

"Active Solar Heating Systems Design Manual", ETEC Report, (1987).

Chandrashekar, M., *et al*, "Data Collection and Performance Specifications for Solar Energy Projects", IEA Task VI Report, (1985)

Erbs, D.G., "Models and Applications for Weather Statistics Related to Building Heating and Cooling Loads", Ph.D. Thesis, University of Wisconsin - Madison, Solar Energy Laboratory, (1984).

Francetis, J.S., "Acceptance Test Report - SFBP #5009, Gainesville Job Corps Center", ETEC Report, (1984).

Garg, H.P., Advances in Solar Energy, D. Reidel Publishing Company, Boston, pp. 57-60, 111-112, (1987).

Godolphine, D., "Rising Hopes for Vacuum Tube Collectors", Solar Age, pp. 31-35, June 1985.

Hillig, O.R., and Pekrul, P.J., "An Overview of the Solar in Federal Buildings Demonstration Program (SFBP)", ETEC Report, (1983).

Luick, D.K., "Analysis of Performance Data and Computer Modeling of Solar Energy Systems", M.S. Thesis, University of Wisconsin - Madison, Solar Energy Laboratory, (1987).

Marlatt, W.P., ETEC of Rockwell International, Inc., personal communications, 1986-87.

Osisik, M.N., Heat Transfer, A Basis Approach, McGraw-Hill, New York, (1985).

Paradise, D.R., "Acceptance Test Report - SFBP #4058, Cherokee Indian Hospital", ETEC Report, (1983).

Pollack, E., Vitro Corporation, personal communications, 1987.

Raymond, M.G., Vitro Corporation, personal communications, 1987.

Solar Products Specification Guide, Solar Vision, Inc., (1983).